AD-A178 630 EFFECTS OF CUTOUT ORIENTATIONS ON NATURAL FREQUENCIES AND MODE SHAPES OF..(U) AIR FORCE INST OF TECH WRIGHT-PATTERSON AFB OH SCHOOL OF ENGI.. G J CYR 1/2

UNCLASSIFIED DEC 86 AFIT/GAE/AA/86D-3 F/G 11/4 NL

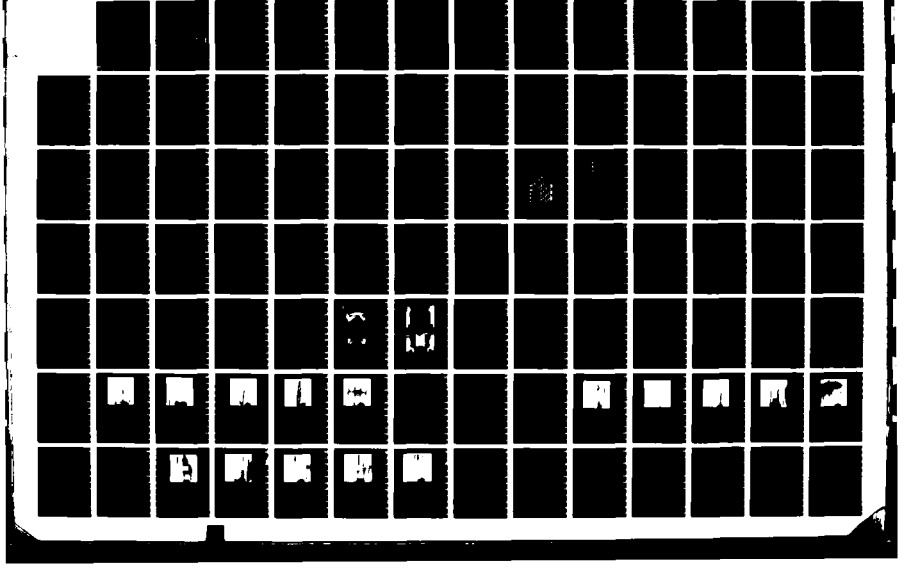

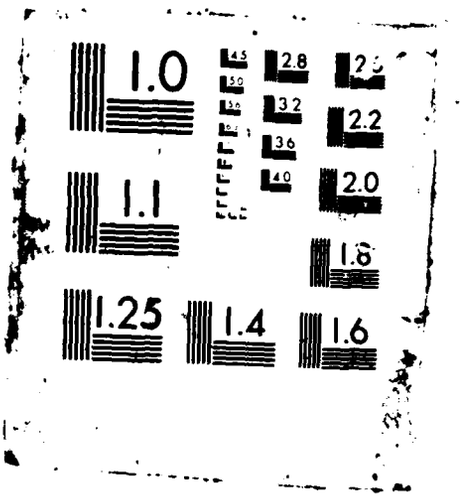
1.0
1.1
1.25
1.4
1.6
2.8
3.2
3.6
2.2
2.0
1.8


# EFFECTS OF CUTOUT ORIENTATION ON NATURAL FREQUENCIES AND MODE SHAPES OF CURVED RECTANGULAR COMPOSITE PANELS

THESIS

Garry J Cyr
Captain, USAF

AFIT/GAE/AA/86D-3





DEPARTMENT OF THE AIR FORCE
AIR UNIVERSITY
AIR FORCE INSTITUTE OF TECHNOLOGY

Wright-Patterson Air Force Base, Ohio

(1)

# EFFECTS OF CUTOUT ORIENTATION ON NATURAL FREQUENCIES AND MODE SHAPES OF CURVED RECTANGULAR COMPOSITE PANELS

**THESIS**

Garry J Cyr
Captain, USAF

**AFIT/GAE/AA/86D-3**

AFIT/GAE/AA/86D-3

# EFFECTS OF CUTOUT ORIENTATIONS ON NATURAL FREQUENCIES AND MODE SHAPES OF CURVED RECTANGULAR COMPOSITE PANELS

THESIS

Presented to the Faculty of the School of
Engineering of the Air Force Institute of Technology
Air University
In Partial Fulfillment of the
Requirements for the Degree of
Master of Science in Aeronautical Engineering

Garry J. Cyr, B.S.
Captain, USAF

December 1986



Approved for public release; distribution unlimited

## Acknowledgements

Most of all, I want to thank my wife Susan for her understanding, patience and support during this graduate program. I want to thank my sons, David, Matt and Adam for "understanding" when Dad had to study. If it wasn't for my family's backing, I could not have completed this thesis and graduate program.

My deepest respects and sincerest thanks to Dr Ron Hinrichsen, my thesis advisor, whose many hours of tutoring, unending advice and computer wisdom made this thesis a success. I would like to thank Lt David Felker for his quick response in making the composite panels. Lastly but not leastly, I want to thank the technicians Jay Anderson and Leroy Cannon for their expertise with the equipment.

Commodore 64;Font Master II;Panasonic KX-P1091

## Table of Contents


| | | Page |
|---|---|---|
| Acknowledgements | | ii |
| List of Figures | | v |
| List of Tables | | viii |
| Abstract | | ix |
| I. | Introduction | 1 |
| | Background | 1 |
| | Approach | 2 |
| II. | Theory | 4 |
| | Finite Element Method/STAGSC-1 | 4 |
| | Element Formulation | 19 |
| | Holographic Interferometry | 22 |
| III. | Panel Characteristics | 27 |
| | Cutout Technique | 30 |
| IV. | Finite Element Analysis | 35 |
| | Element Selection | 35 |
| | Panel Modelling | 44 |
| | The Solid, 0° & 90° Panels | 44 |
| | The +45° & -45° Panels | 46 |
| V. | Holographic Analysis | 48 |
| | Test Fixture | 48 |
| | Holographic Technique | 52 |
| VI. | Results and Discussion | 55 |
| | The Solid Panel | 56 |
| | The 0° Panel | 65 |
| | The 90° Panel | 72 |
| | The +45° Panel | 80 |
| | The -45° Panel | 96 |
| | Cutout Effects | 103 |
| VII. | Conclusions | 113 |

VIII. Recommendations..... 115

Bibliography..... 116

Appendix A: Curing Cycle for Gr-Ep..... 118

Appendix B: Sample STAGSC-1 Input File..... 120

Appendix C: Holographic Technique..... 124

Appendix D: Certificate of Analysis..... 129

Appendix E: Equipment List..... 131

VITA..... 132

## List of Figures


| Figure | | Page |
|---|---|---|
| 1. | Geometry of Deformation in X-Z Plane..... | 5 |
| 2. | Coordinate System for Panel..... | 9 |
| 3. | Principle Axis and Fiber Direction..... | 12 |
| 4. | In-Plane Forces on Laminate..... | 14 |
| 5. | Moments on Laminate..... | 14 |
| 6. | Geometry of N-Layered Laminate..... | 15 |
| 7. | Holographic Test Setup..... | 22 |
| 8. | Constructive & Destructive Interference Effects on Light Intensity..... | 23 |
| 9. | Fringe Pattern Formation on Plate..... | 24 |
| 10. | Reconstructed Wave Formation..... | 25 |
| 11. | Panel 1 Thickness Variations..... | 28 |
| 12. | Panel 2 Thickness Variations..... | 28 |
| 13. | Panel 3 Thickness Variations..... | 28 |
| 14. | Panel 4 Thickness Variations..... | 28 |
| 15. | Panel 5 Thickness Variations..... | 29 |
| 16. | Cutout Orientations..... | 30 |
| 17. | Cutting Fixture..... | 32 |
| 18. | Router Baseplate..... | 33 |
| 19. | Flat Elements for Curved Shell Analysis..... | 35 |
| 20. | 320 Triangular Plate Element..... | 36 |
| 21. | 322 Triangular Plate Element..... | 36 |
| 22. | 410 Quadrilateral Plate Element..... | 37 |
| 22A. | 411 Quadrilateral Plate Element..... | 38 |

23. 420 Quadrilateral Plate Element..... 39

24. 422 Quadrilateral Plate Element..... 40

25. Solid Panel 25 x 25 Mesh..... 45

26A. Test Fixture..... 49

26B. Test Fixture..... 50

27. Block Diagram of Equipment Configuration..... 53

28. Optical Setup..... 54

29. Solid Panel--Mode 1..... 59

30. Solid Panel--Mode 2..... 60

31. Solid Panel--Mode 3..... 61

32. Solid Panel--Mode 4..... 62

33. Solid Panel--Mode 5..... 63

34. Mode 3 $[0/45/-45/90]_s$..... 64

35. Mode 4 $[0/45/-45/90]_s$..... 64

36. 0° Panel 25 x 25 Mesh..... 66

37. 0° Panel--Mode 1..... 67

38. 0° Panel--Mode 2..... 68

39. 0° Panel--Mode 3..... 69

40. 0° Panel--Mode 4..... 70

41. 0° Panel--Mode 5..... 71

42. 90° Panel 25 x 25 Mesh..... 73

43. 90° Panel--Mode 1..... 74

44. 90° Panel--Mode 2..... 75

45. 90° Panel--Mode 3..... 76

46. 90° Panel--Mode 4..... 77

47. 90° Panel--Mode 5..... 78

48. 45° Mesh..... 81
49. 45° Mesh 320-420 Elements..... 82
50. 45° Mesh Triangles Removed..... 84
51. Complex 45° Mesh..... 86
52. Final Mesh 410 Elements..... 88
53. +45° Cutout 320-410 Elements..... 89
54. +45° Panel--Mode 1..... 91
55. +45° Panel--Mode 2..... 92
56. +45° Panel--Mode 3..... 93
57. +45° Panel--Mode 4..... 94
58. +45° Panel--Mode 4..... 95
59. -45° Cutout 320-410 Elements..... 96
60. -45° Panel--Mode 1..... 98
61. -45° Panel--Mode 2..... 99
62. -45° Panel--Mode 3..... 100
63. -45° Panel--Mode 4..... 101
64. -45° Panel--Mode 5..... 102
65. Cutout Orientation vs Frequency..... 104
66. Cutout Size vs Frequency..... 109
67. Cutout Size vs Frequency..... 110
68. Equivalent Stiffness vs Cutout Size..... 111
69. Mode Switch Region for Mode 1..... 112

## List of Tables


| Table | | Page |
|---|---|---|
| 1. | Panel Material Properties..... | 27 |
| 2. | Solid Panel Results..... | 57 |
| 3. | 0° Panel Results..... | 65 |
| 4. | 90° Panel Results..... | 72 |
| 5. | 45° Mesh 320-410 Elements..... | 81 |
| 6. | 45° Mesh 320-420 Elements..... | 83 |
| 7. | Complex 45° Mesh..... | 87 |
| 8. | Final Mesh 410 Elements..... | 88 |
| 9. | +45° Mesh 320-410 Elements..... | 90 |
| 10. | -45° Mesh 320-410 Elements..... | 97 |

## ABSTRACT

STAGSC-1, a finite element code, and holographic interferometry were used to analyze the effects of cutout orientation (0°, +45°, -45° and 90°) on the first five natural frequencies and mode shapes of a curved Gr-Ep panel. The clamped-clamped panels had a quasi-isotropic layup $[0, -45, 45, 90]_s$ and measured 12 inch high with a 12 inch chord.

When the finite element code was compared to the time averaged holograms, the two techniques showed close correlation of both the natural frequencies and mode shapes. It was found that the 0° cutout orientation had a significant effect on the panel stiffness while the other cutout orientations did not adversely effect the stiffness. It was also found that if a large number of elements in the finite element mesh are oriented at an angle other than 0° or 90°, then the STAGSC-1 model is artificially stiffened.

# I. INTRODUCTION

## Background

Each succeeding generation of aircraft continually demands more and more from the stuctures and materials from which they are built. Composite materials are becoming more important in meeting the requirements for lighter weight and higher strength. As these demands increase, it is necessary to completely understand the static and dynamic characteristics of the composite. Since the curved composite shell is extremely applicable to military aerospace structures, the likelihood of the composite sustaining damage that must be repaired increases as more and more of the structure is constructed with composites. The dynamic characteristics of the curved composite with a cutout must be fully understood so that the composite is properly repaired.

Numerous studies examining mode shapes and natural frequencies have been conducted with flat plates. In 1970, Monahan [12] showed the effects of square cutouts on the mode shapes and natural frequencies of a clamped 7x10 inch rectangular plate. Monahan applied a finite element program to predict the natural frequencies and mode shapes of the flat plates and then verified the results by performing

holographic analysis. In 1976, Rajamani and Prabhakaran [9], investigated the effects of rectangular cutouts on the natural frequencies of clamped-clamped flat composite plates. By varying the fiber orientation, Rajamani and Prabhakaran were able to show that there is a tendency for the modes to interchange or switch (symmetric to anti-symmetric and vice versa) with large cutouts for all modulus ratios except for unidirectional Gr-Ep with a fiber orientation of 45 degrees.

In 1985, Walley [3] showed the effects of cutout size (2x2, 2x4, 4x4 inch) on clamped-clamped quasi-isotropic curved Gr-Ep panels that were 12 inches high and had a 12 inch chord and 12 inch radius. He demonstrated the tendency for mode shapes to switch for large cutouts. Walley used STAGSC-1 and holographic analysis to determine the mode shapes and natural frequencies.

A logical extension to Walley's efforts is to investigate the effects of different cutout orientations on the natural frequencies and mode shapes of curved Gr-Ep panels and to determine if the mode switching phenomena is a property dependent on cutout orientation.

## Approach

A two part parallel effort was needed to complete this testing. First, STAGSC-1 (a finite element analysis program) was used to determine the first five natural frequencies and

mode shapes of curved rectangular Gr-Ep panels with cutouts oriented at 0°, +45°, 90°, -45°. Secondly, holographic interferometry was used to compare the results of STAGSC-1 to the actual panel. The comparison of these results allows an evaluation of the effectiveness and accuracy of STAGSC-1 to predict the experimental results.

# II. THEORY

## Finite Element Method-STAGSC-1

STAGS is a series of computer programs that have been under development for fifteen years. STAGS was developed by B. O. Almroth, F. A. Brogan, and G. M. Stanley of the Lockheed Palo Alto Research Laboratory for the structural analysis of general shells. The latest version, STAGSC-1, has been operational since 1979 and is the version used to conduct the analysis for this thesis.

STAGSC-1 is an energy based finite element code using the Kirchoff-Love hypothesis [1]. The Kirchoff-Love hypothesis for shells can be summarized as follows. If the laminate is thin, a line originally straight and perpendicular to the middle surface of the laminate is assumed to remain straight and perpendicular to the middle surface when the laminate is extended and bent. Requiring the line perpendicular to the midsurface to remain straight and perpendicular under deformation is the equivalent to ignoring the shear strains in planes perpendicular to the midsurface, or $\gamma_{xz}=\gamma_{yz}=0$, where z is the direction normal to the midsurface in Figure 1. In addition, the normals are presumed to have constant length so that the strain

perpendicular to the midsurface is ignored as well, or $e_z=0$. [4]

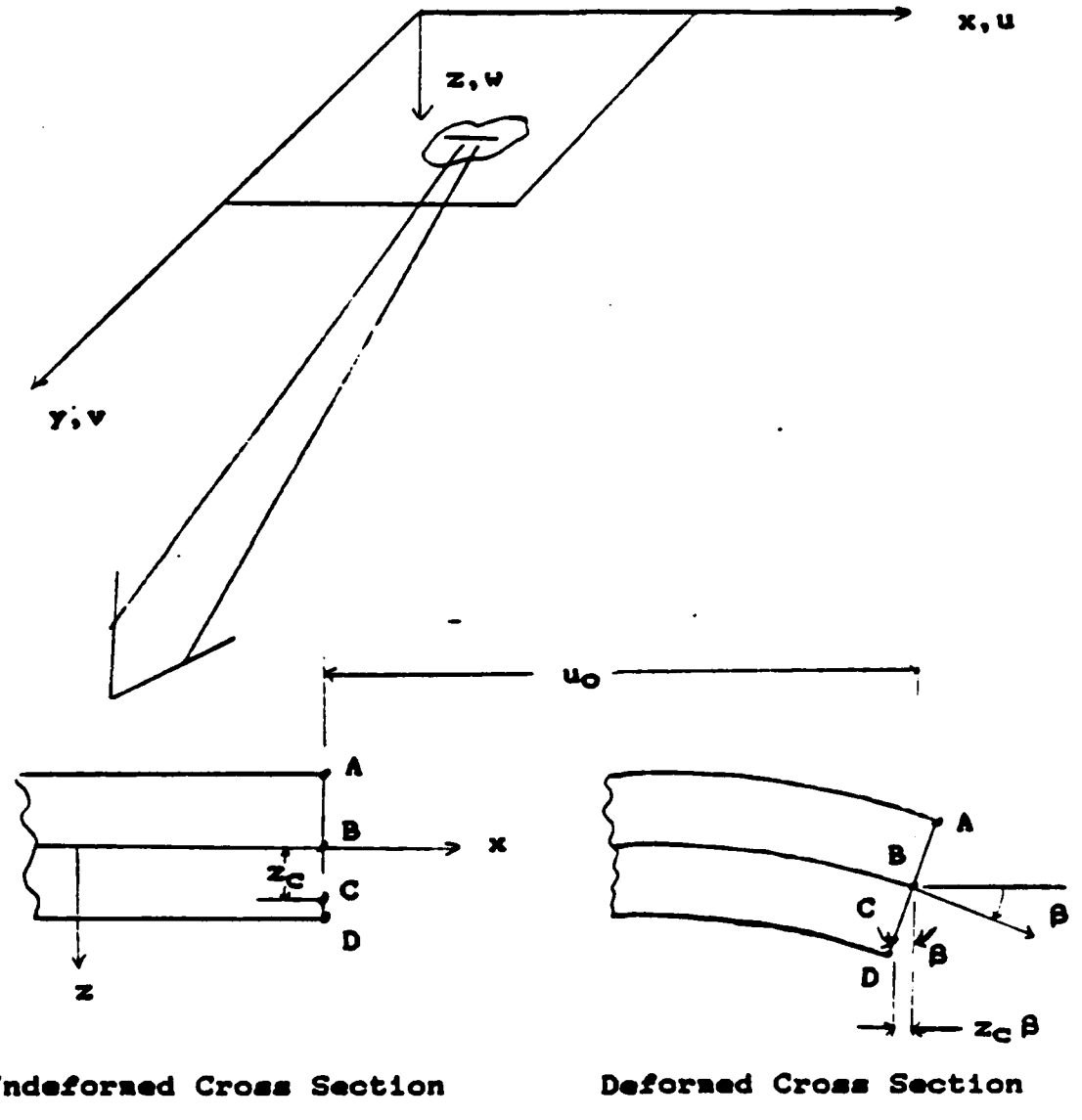


Figure 1 Geometry of Deformation in X-Z Plane.

From Newton's Second Law the governing equation of motion can be derived.

$$\Sigma F = M\ddot{x}(t) \qquad (1)$$

where F is the generalized forces, M is the mass of the system, $\ddot{x}(t)$ is the acceleration. For free vibration, there are no externally applied forces. This leaves the internal damping forces and the internal elastic forces. Since this is a low mass, high stiffness structure, the internal damping forces are neglected. Equation (1) reduces to

$$-Kx(t) = M\ddot{x}(t) \qquad (2)$$

where K is the elastic constant and x(t) is the displacement. Equation (2) becomes the classical differential equation of motion for the undamped free vibration case.

$$M\ddot{x}(t) + Kx(t) = 0 \qquad (3)$$

Satisifying the conditions for a conservative system in equilibrium, the total potential energy must be stationary and the first variation of the potential energy must be zero. The total potential energy of the system is the strain energy of the body minus the work done on the body by externally applied forces.

$$\Pi = U - W \tag{4}$$

where $\Pi$ is the total potential energy, U is the strain energy, and W is the work done on the body. The equation for strain energy is defined as

$$U = 1/2 \int_{Vol} (\sigma_x e_x + \sigma_y e_y + \tau_{xy} \gamma_{xy}) \, dVol \tag{5}$$

As stated before, for the case of free vibration, the work done on the body by externally applied forces is equal to zero. Therefore, equation (4) reduces and the total potential energy becomes:

$$\Pi = U \tag{6}$$

The governing kinematic relations in STAGSC-1, expressing total stain as a linear variation of the extensional and bending strains at the midsurface, are based on Sander's shell equations.[2] The laminate is presumed to consist of a layup of perfectly bonded laminae and to be infinitesmally thin, as well as non-shear deformable. In other words, the displacements are continuous across the lamina boundaries so that no lamina can slip relative to another.[3] Therefore, the midsurface strains are [3]

$$e_x = u,_x + 1/2\phi_x^2 + 1/2\phi^2 \tag{7}$$

$$e_y = v,_y + w/R + 1/2\phi_y^2 - 1/2\phi^2 \tag{8}$$

$$2e_{xy} = v,_x + u,_y + \phi_x\phi_y \tag{9}$$

and the midsurface curvatures are

$$K_x = \phi_x,_x \tag{10}$$

$$K_y = \Phi_{y,y} \tag{11}$$

$$2K_{xy} = 2K_{yx} = \Phi_{y,x} + \Phi_{x,y} + \Phi/R \tag{12}$$

where $\Phi_x$, $\Phi_y$, and $\Phi$ are the components of rotation about the coordinate lines and normal to the surface (Figure 2). R is defined as the radius of curvature and u, v, w, are the displacements in the x, y, z directions, respectively.

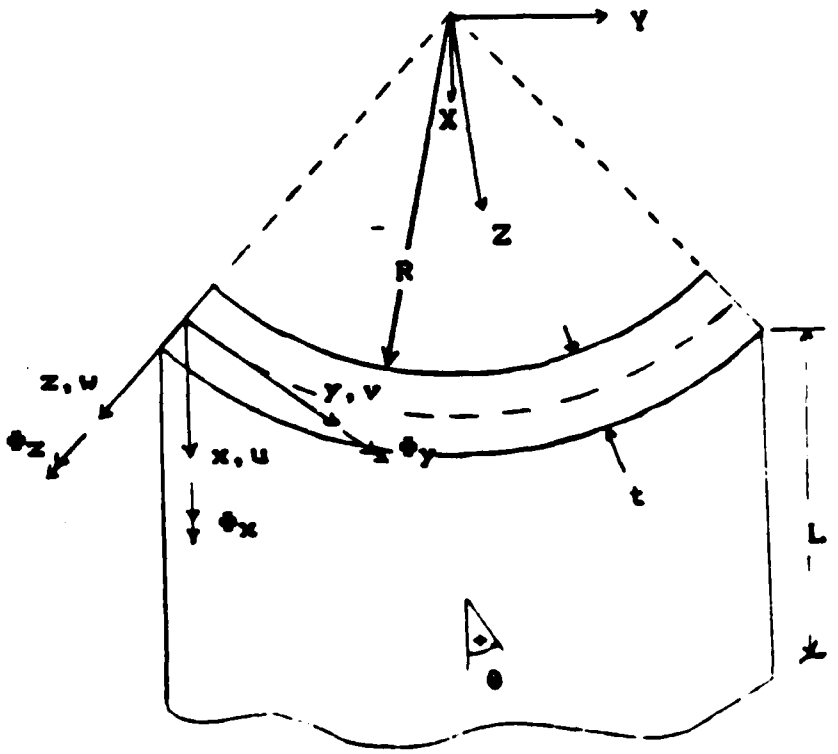


Figure 2 Coordinate System for Panel

The rotations in terms of displacements are:

$$\phi_x = -w_{,x} \tag{13}$$

$$\phi_y = -w_{,y} + v/R \tag{14}$$

$$\phi = 1/2(v_{,x} - u_{,y}) \tag{15}$$

Using the above equations for midsurface strain and curvature while employing the Kirchoff-Love hypothesis, the strain relationship for any layer of the laminate becomes

$$\begin{Bmatrix} \epsilon_x \\ \epsilon_y \\ \gamma_{xy} \end{Bmatrix} = \begin{Bmatrix} \epsilon_x^\circ \\ \epsilon_y^\circ \\ \gamma_{xy}^\circ \end{Bmatrix} + z \begin{Bmatrix} K_x \\ K_y \\ K_{xy} \end{Bmatrix} \tag{16}$$

Applying the orthotropic constituitive equations, the stresses for the $k^{th}$ layer of the laminate become [4]

$$\begin{Bmatrix} \sigma_x \\ \sigma_y \\ \tau_{xy} \end{Bmatrix}_k = [\bar{Q}]_k \begin{Bmatrix} \epsilon_x \\ \epsilon_y \\ \gamma_{xy} \end{Bmatrix}_k \tag{17}$$

Now, substituting Equation (16) into (17) gives

$$\begin{Bmatrix} \sigma_x \\ \sigma_y \\ \tau_{xy} \end{Bmatrix} = [\bar{Q}]_k \begin{Bmatrix} \epsilon_x^\circ \\ \epsilon_y^\circ \\ \gamma_{xy}^\circ \end{Bmatrix} + z \begin{Bmatrix} K_x \\ K_y \\ K_{xy} \end{Bmatrix} \tag{18}$$

where $[Q]_k$ is the transformed stiffness matrix.

$$[\bar{Q}]_k = \begin{bmatrix} \bar{Q}_{11} & \bar{Q}_{12} & \bar{Q}_{16} \\ \bar{Q}_{12} & \bar{Q}_{22} & \bar{Q}_{26} \\ \bar{Q}_{16} & \bar{Q}_{26} & \bar{Q}_{66} \end{bmatrix} \tag{19}$$

where: $\bar{Q}_{11}=Q_{11}m^4+2(Q_{12}+2Q_{66})m^2n^2+Q_{22}n^4$ (20)

$\bar{Q}_{12}=(Q_{11}+Q_{22}-4Q_{66})n^2m^2+Q_{12}(n^4+m^4)$ (21)

$\bar{Q}_{16}=(Q_{11}-Q_{12}-2Q_{66})nm^3+(Q_{12}-Q_{22}+2Q_{66})n^3m$ (22)

$\bar{Q}_{22}=Q_{11}n^4+2(Q_{12}+2Q_{66})n^2m^2+Q_{22}m^4$ (23)

$\bar{Q}_{26}=(Q_{11}-Q_{12}-2Q_{66})mn^3+(Q_{12}-Q_{22}+2Q_{66})nm^3$ (24)

$$\bar{Q}_{66}=(Q_{11}-Q_{22}-2Q_{12}-2Q_{66})n^2m^2+Q_{66}(n^4+m^4) \quad (25)$$

$$m = \cos\theta \quad (26)$$

$$n = \sin\theta \quad (27)$$

$$Q_{11}=E_1/(1-\nu_{21}\nu_{12}) \quad (28)$$

$$Q_{22}=E_2/(1-\nu_{12}\nu_{21}) \quad (29)$$

$$Q_{12}=\nu_{12}E_2/(1-\nu_{12}\nu_{21})=\nu_{21}E_1/(1-\nu_{21}\nu_{12}) \quad (30)$$

$$Q_{66}=G_{12} \quad (31)$$

(Refer to Figure 3 for the definition of θ and fiber orientation.)

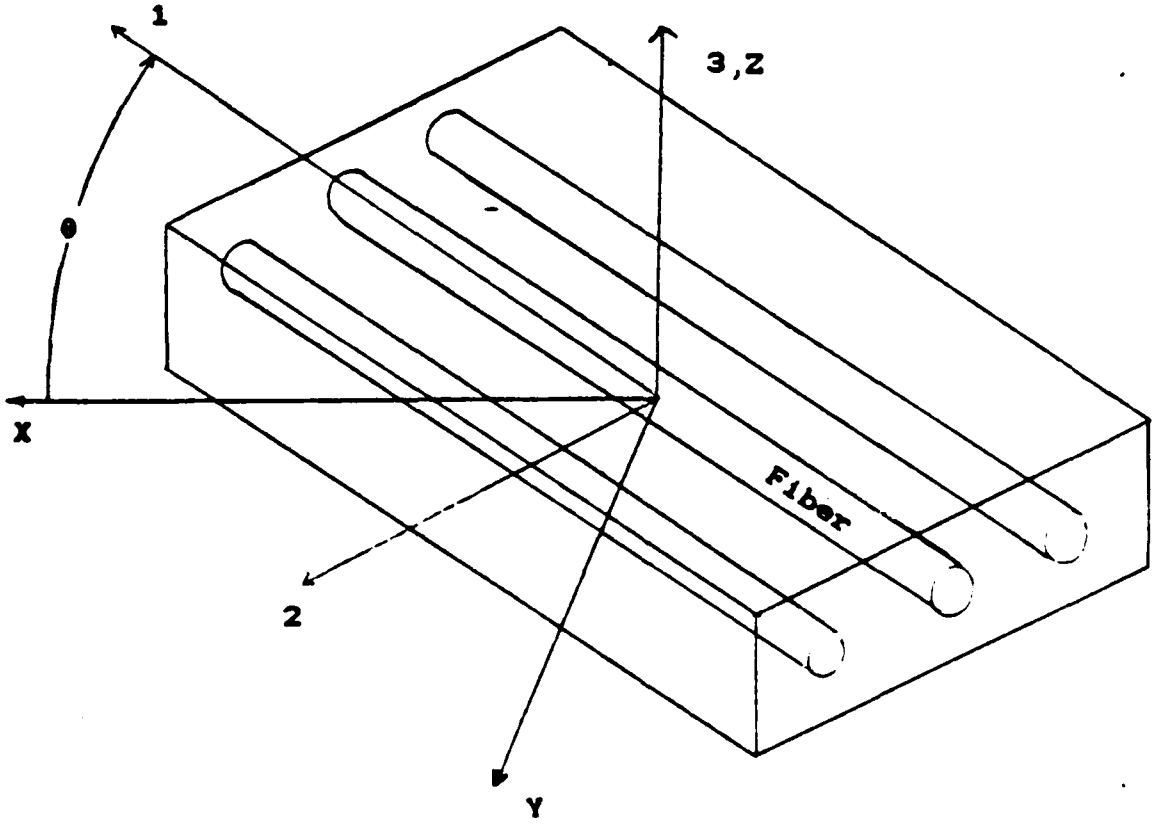


Figure 3. Principal axis and Fiber Direction

The resultant forces and moments acting on a laminate are obtained by integration of the stresses on each layer through the laminate thickness. The resulting forces and moments per unit length are respectively,

$$\begin{Bmatrix} N_x \\ N_y \\ N_{xy} \end{Bmatrix} = \int_{-t/2}^{t/2} \begin{Bmatrix} \sigma_x \\ \sigma_y \\ \tau_{xy} \end{Bmatrix} dz = \sum_{k=1}^{N} \int_{z_{k-1}}^{z_k} \begin{Bmatrix} \sigma_x \\ \sigma_y \\ \tau_{xy} \end{Bmatrix}_k dz \qquad (32)$$

$$\begin{Bmatrix} M_x \\ M_y \\ M_{xy} \end{Bmatrix} = \int_{-t/2}^{t/2} \begin{Bmatrix} \sigma_x \\ \sigma_y \\ \tau_{xy} \end{Bmatrix} z dz = \sum_{k=1}^{N} \int_{z_{k-1}}^{z_k} \begin{Bmatrix} \sigma_x \\ \sigma_y \\ \tau_{xy} \end{Bmatrix}_k z dz \qquad (33)$$

where the in plane forces $N_x$, $N_y$, $N_{xy}$ are shown in Figure 4, the moments $M_x$, $M_y$, $M_{xy}$ are shown in Figure 5 and $z_k$, $z_{k-1}$ are defined in Figure 6. The forces and moments do not depend on z after integration, but are functions of x and y only, the coordinates in the plane of the laminate midsurface [4].

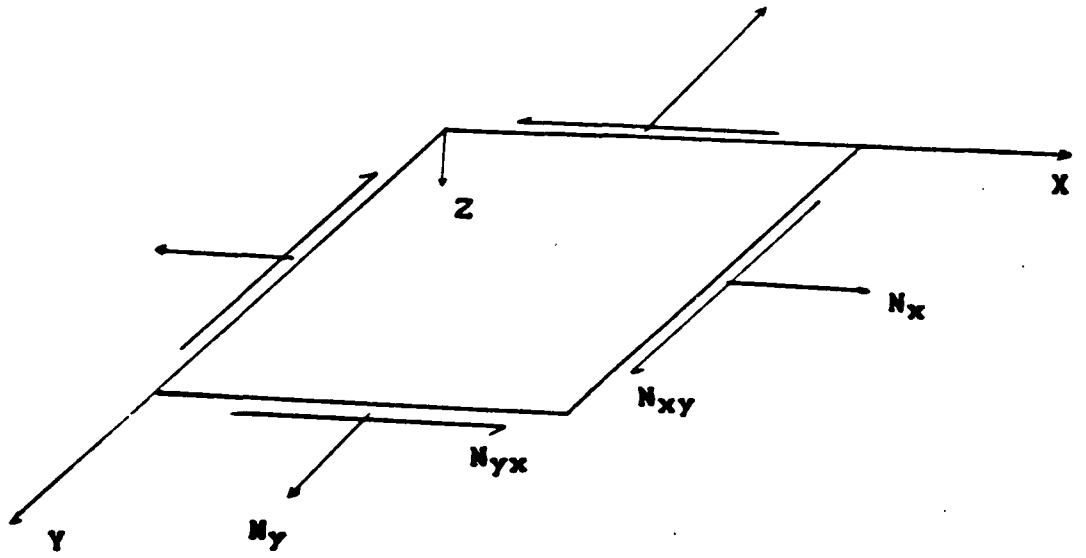


Figure 4. In Plane Forces on the Laminate.

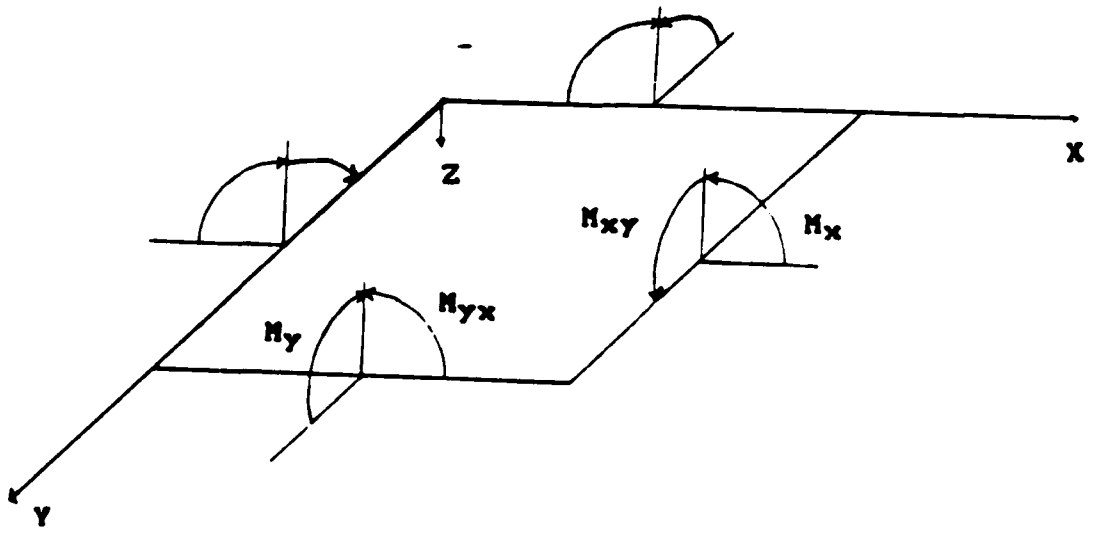


Figure 5. Moments on a Laminate.

Undeformed Cross Section

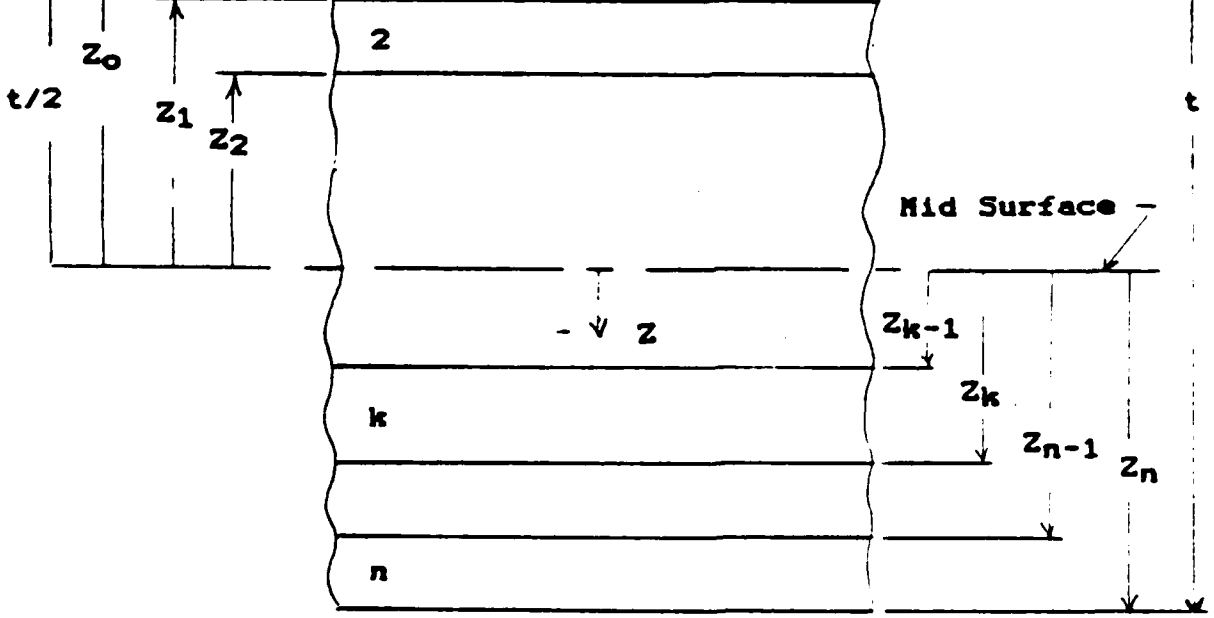


Figure 6. Geometry of an N-Layered Laminate

The integration of Equations (32) and (33) can be rearranged to take advantage of the fact that the stiffness matrix for a lamina is constant within the lamina, unless the lamina

has temperature dependent properties and a temperature gradient across the lamina exists [4]. For our case there are no temperature gradients in the lamina since the panels are at room temperature. Substituting the stress-strain relationships of Equation (18) and realizing that the transformed reduced stiffness matrix moves outside the integration for each layer, Equations (32) and (33) can be reduced to

$$\begin{Bmatrix} N_x \\ N_y \\ N_{xy} \end{Bmatrix} = \sum_{k=1}^{N} \int_{z_{k-1}}^{z_k} \begin{Bmatrix} \epsilon_x^o \\ \epsilon_y^o \\ \gamma_{xy}^o \end{Bmatrix} dz + \int_{z_{k-1}}^{z_k} \begin{Bmatrix} K_x \\ K_y \\ K_{xy} \end{Bmatrix} z \, dz \qquad (34)$$

$$\begin{Bmatrix} M_x \\ M_y \\ M_{xy} \end{Bmatrix} = \sum_{k=1}^{N} \int_{z_{k-1}}^{z_k} \begin{Bmatrix} \epsilon_x^o \\ \epsilon_y^o \\ \gamma_{xy}^o \end{Bmatrix} z dz + \int_{z_{k-1}}^{z_k} \begin{Bmatrix} K_x \\ K_y \\ K_{xy} \end{Bmatrix} z^2 \, dz \qquad (35)$$

Since $\epsilon_x^o$, $\epsilon_y^o$, $\gamma_{xy}^o$, $K_x$, $K_y$, $K_{xy}$ are not functions of z but are mid surface values, they can be removed from the summation signs. Equations (34) and (35) can be written in matrix notation such that

$$\begin{Bmatrix} N_x \\ N_y \\ N_{xy} \end{Bmatrix} = \begin{bmatrix} A_{11} & A_{12} & A_{16} \\ A_{12} & A_{22} & A_{26} \\ A_{16} & A_{26} & A_{66} \end{bmatrix} \begin{Bmatrix} \epsilon^o_x \\ \epsilon^o_y \\ \gamma^o_{xy} \end{Bmatrix} + \begin{bmatrix} B_{11} & B_{12} & B_{16} \\ B_{12} & B_{22} & B_{26} \\ B_{16} & B_{26} & B_{66} \end{bmatrix} \begin{Bmatrix} K_x \\ K_y \\ K_{xy} \end{Bmatrix} \quad (36)$$

$$\begin{Bmatrix} M_x \\ M_y \\ M_{xy} \end{Bmatrix} = \begin{bmatrix} B_{11} & B_{12} & B_{16} \\ B_{12} & B_{22} & B_{26} \\ B_{16} & B_{26} & B_{66} \end{bmatrix} \begin{Bmatrix} \epsilon^o_x \\ \epsilon^o_y \\ \gamma^o_{xy} \end{Bmatrix} + \begin{bmatrix} D_{11} & D_{12} & D_{16} \\ D_{12} & D_{22} & D_{26} \\ D_{16} & D_{26} & D_{66} \end{bmatrix} \begin{Bmatrix} K_x \\ K_y \\ K_{xy} \end{Bmatrix} \quad (37)$$

given that: $$A_{ij} = \sum_{k=1}^{N} (\bar{Q}_{ij})_k (z_k - z_{k-1}) \quad (38)$$

$$B_{ij} = 1/2 \sum_{k=1}^{N} (\bar{Q}_{ij})_k (z^2_k - z^2_{k-1}) \quad (39)$$

$$D_{ij} = 1/3 \sum_{k=1}^{N} (\bar{Q}_{ij})_k (z^3_k - z^3_{k-1}) \quad (40)$$

where $A_{ij}$ is the extensional stiffness matrix, $B_{ij}$ is the coupling stiffness matrix, and $D_{ij}$ is the bending stiffness matrix. Relating the stress in the strain energy equation, (6), to the force and moment equations, (36) and (37), reduces the strain energy equation to

$$U = 1/2 \int_A \{e\}^T \begin{bmatrix} N \\ M \end{bmatrix} dA \qquad (41)$$

expanding to the final form of the energy equation gives:

$$U = 1/2 \int_A \begin{Bmatrix} \epsilon_x^o \\ \epsilon_y^o \\ \gamma_{xy}^o \\ K_x \\ K_y \\ K_{xy} \end{Bmatrix}^T \begin{bmatrix} A_{ij} & B_{ij} \\ B_{ij} & D_{ij} \end{bmatrix} \begin{Bmatrix} \epsilon_x^o \\ \epsilon_y^o \\ \gamma_{xy}^o \\ K_x \\ K_y \\ K_{xy} \end{Bmatrix} dA \qquad (42)$$

In this section the final form of the energy equation for STAGSC-1 was derived. The next section will discuss the element formulation for the elements used in STAGSC-1.

## Element Formulation

In order for compatibility to be enforced at the nodes, the exact and assumed displacements must match at the nodes but may differ elsewhere in the element. This is accomplished by interpolation formulas. The interpolation formulas can be used as assumed displacement fields and finite elements can be generated from them. Interpolation does not imply that nodal values are exact. STAGSC-1 uses a Hermitian interpolation in which the displacements and slopes of the end points of the plate elements are forced to match. Once the shape functions are evaluated and the displacements within the element are defined, the strains in equation (42) can be expressed in terms of nodal displacements using the strain-displacement matrix, B,

$$\begin{Bmatrix} e \\ K \end{Bmatrix} = [\ B\ ]\ \{\ d\ \} \qquad (43)$$

where d is the displacement vector and B is defined as:

$$[\,B\,] = \begin{bmatrix} N,x & 0 \\ 0 & N,y \\ N,y & N,x \end{bmatrix} \tag{44}$$

where N is the shape function. The strain energy, U, can now be defined as:

$$U = 1/2 \int_A \{\,d\,\}^T [\,k_{ij}\,] \{\,d\,\}\ dA \tag{45}$$

where $k_{ij}$ is the elemental stiffness matrix used to form the global stiffness matrix, $K_{ij}$.

$$[\,K_{ij}\,] = \int_A [\,B\,]^T \begin{bmatrix} A_{ij} & B_{ij} \\ B_{ij} & D_{ij} \end{bmatrix} [\,B\,]\ dA \tag{46}$$

Presently only a diagonal mass matrix is available in STAGSC-1.[2] This mass matrix is a lumped diagonal mass matrix with zero rotary inertia. A lumped mass matrix is positive semi-definite if zeros appear on the diagonal. Lumped mass matrices are simpler to form, cheaper to use and usually yield natural frequencies that are less than the

exact values.[13] Based on the above assumptions, the problem reduces to an eigenvalue problem of the form:

$$[[\ K_{ij}\ ]-\lambda[\ M_{ij}\ ]]\{x\}=0 \qquad (47)$$

where $\lambda$ are the eigenvalues and represent the square of the natural frequencies and $\{x\}$ are the eigenvectors. From equation (47) the eigenvector is found and describes the relative displacements of the nodes to give the mode shapes. Since the form of an eigenvector is unique but has arbitrary amplitude, it follows that the mode shape is unique for a natural frequency but not its amplitude. STAGSC-1 utilizes the Inverse Power Method to solve equation (47).[2]

## Holographic Interferometry

With holography, one records not the optically formed image of the object but the object wave itself.[5] To record the object wave, a coherent light source is needed. The HeNe laser provides a coherent monochromatic light source capable of displaying interference effects that are stable in time. The laser beam is split into two beams with a beam splitter. The two beams are called the reference beam and the object beam. As shown in Figure 7, the object beam is directed toward the panel fixture and is diffracted by the panel before the object wave is recorded by the photographic plate. The reference wave remains unaltered as it is recorded by the plate.

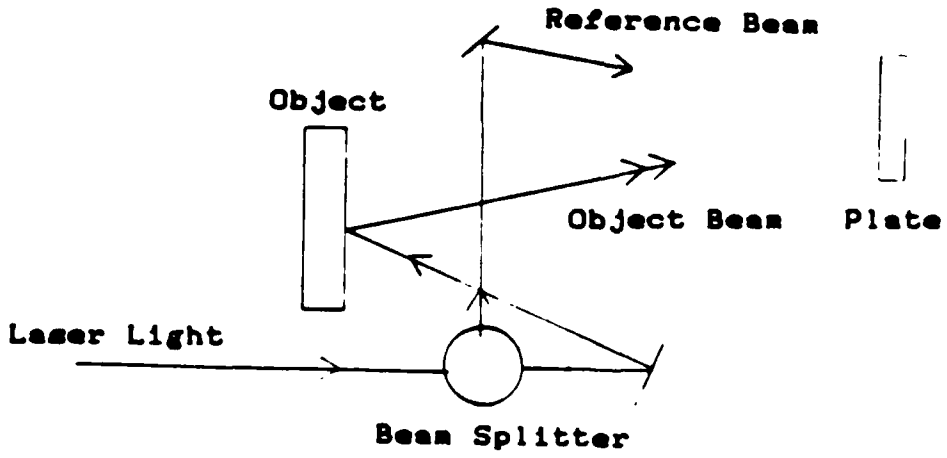


Figure 7. Holographic Test Setup

Since the object and reference waves are mutually coherent, they will form a stable interference pattern or field when they meet at the photographic plate. The interference is of two types, constructive and destructive. In Figure 8, the constructive interference adds to the light intensity while the destructive interference decreases the light intensity.

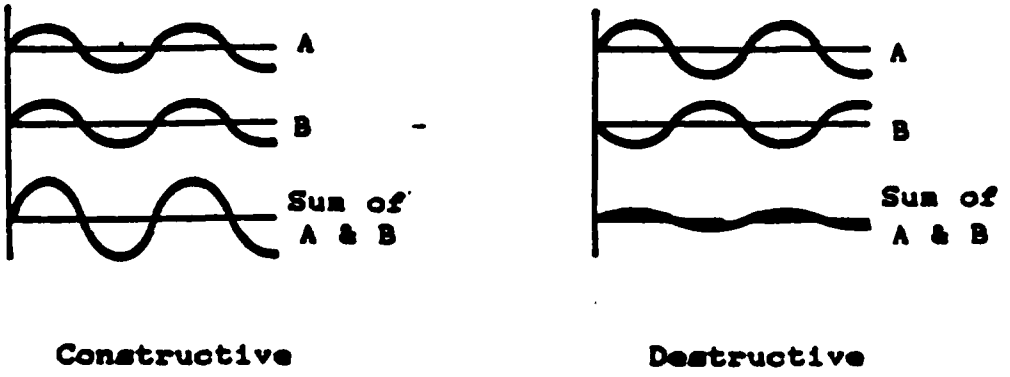


Constructive Destructive

Figure 8. Constructive & Destructive Inteference Effects on Light Intensity.

This interference pattern forms fringes that are recorded on the photographic plate and a hologram is formed. (Figure 9)[8] When the hologram is illuminated with the original or an exact duplicate of the reference wave used to record the hologram, a reconstructed wave front is formed

(Figure 10) and one sees an exact reproduction of the original object. This is possible since the hologram consists of a series of alternating clear and opaque strips on the photographic plate. This phenomena is referred to as defraction grating.[5]

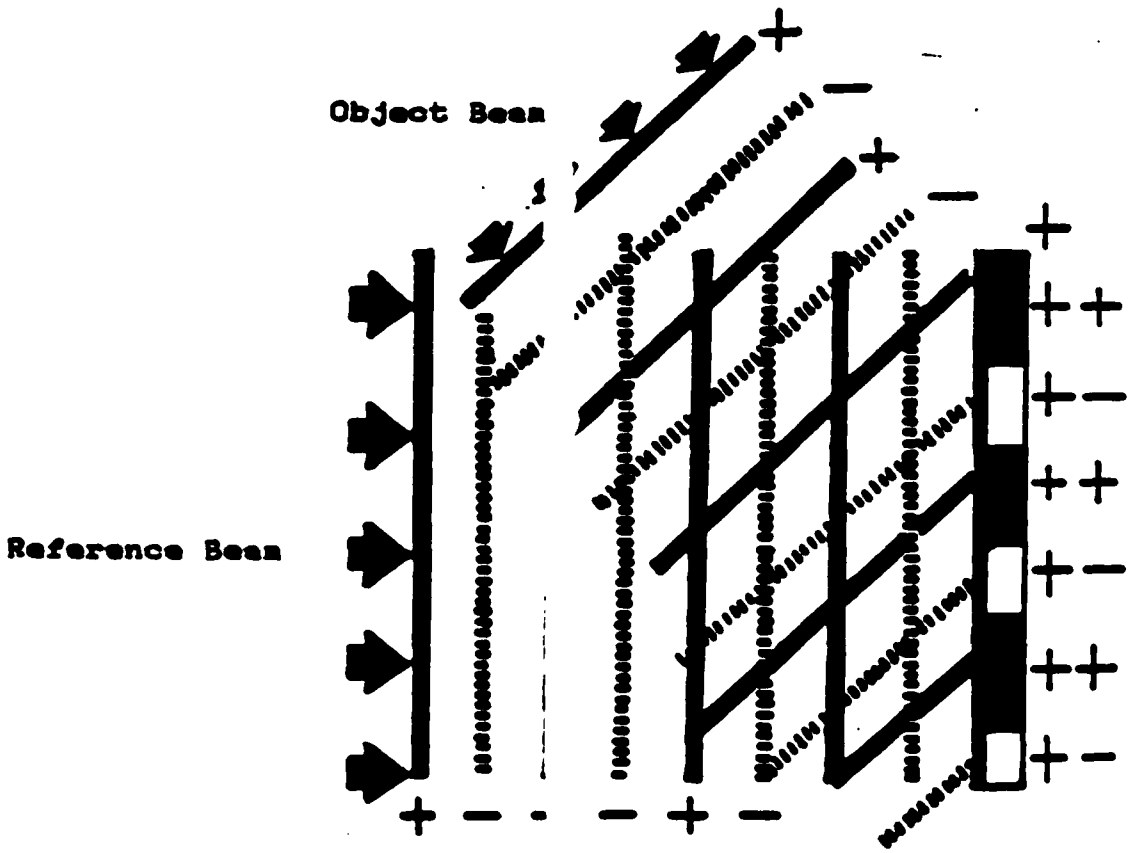


Figure 9. Fringe Pattern Formation on Plate.

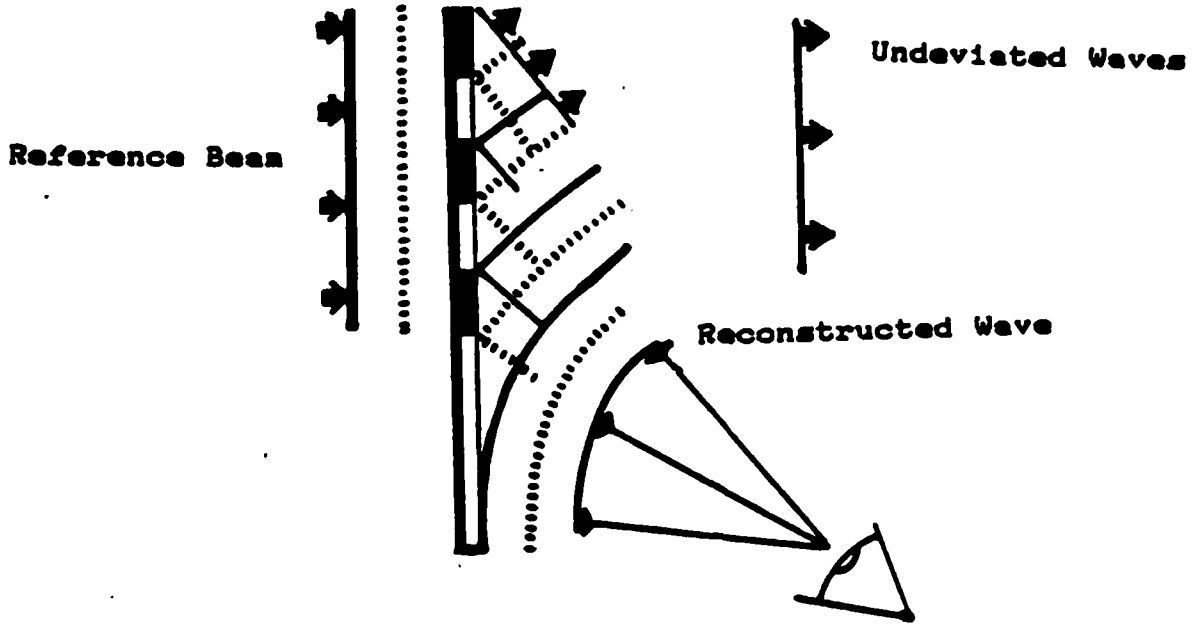


Figure 10. Reconstructed Wave Formation.

A time averaging holographic technique is used when conducting vibration analysis. The panel is acoustically excited at its natural frequency and the photographic plate records the interference pattern that existed for the exposure period. It is important that the phase difference between the two beams remain constant during the exposure. [5] The photographic plate records all fields that existed during the exposure time in proportion to the fraction of time during which the wave front existed, even though the fields are reconstructed simultaneously by the reference

beam.[7] The fringes recorded as a hologram indicate the areas of constant amplitude on the panel for that particular excitation frequency.

The theory for the analytical and experimental portions of this thesis have been discussed. Next the panel characteristics, material properties and how the holes were cutout will be discussed.

## III. PANEL CHARACTERISTICS

Prior to any analysis it is important to establish the physical characteristics of the object of the analysis. Also it is important to establish the geometric characteristics of the panel including a local and global axis system to properly define the forces, moments, displacements, and rotations.

The specific analyses of the fiber and resin used to manufacture the panels are shown in Appendix D. The final panel properties are given below in Table 1. The panels are made of Gr-Ep Hercules AS4/3501-6 and have a quasi-isotropic ply layup of $[\ 0,-45,+45,90\ ]_s$.

Table 1. Panel Material Properties

| | | |
|---|---|---|
| $E_1$ | $= 18.8 \times 10^6$ | psi |
| $E_2$ | $= 1.47 \times 10^6$ | psi |
| $G_{12}$ | $= 0.91 \times 10^6$ | psi |
| $\nu_{12}$ | $= 0.28$ | |
| $\nu_{21}$ | $= 0.022$ | |
| $\rho$ | $= 0.055$ | $lb/in^3$ |

There are eight plies in the layup and the laminate varied in thickness as shown in Figures (11, 12, 13, 14, 15).

| | | |
|---|---|---|
| .040 | .040 | .038 |
| .040 | .039 | .040 |
| .041 | .039 | .040 |

Figure 11. Panel 1

| | | |
|---|---|---|
| .040 | .040 | .041 |
| .042 | .041 | .040 |
| .040 | .040 | .041 |

Figure 12. Panel 2

| | | |
|---|---|---|
| .042 | .041 | .040 |
| .040 | .040 | .040 |
| .040 | .040 | .039 |

Figure 13. Panel 3

| | | |
|---|---|---|
| .041 | .041 | .040 |
| .040 | .041 | .040 |
| .041 | .041 | .040 |

Figure 14. Panel 4

| | | |
|---|---|---|
| .041 | .041 | .040 |
| .040 | .041 | .040 |
| .040 | .041 | .041 |

Figure 15. Panel 5

Panels 1, 2, 3, 4, and 5 corresponded to the solid, 0°, 90°, +45°, and -45° cutouts, respectively. The average thickness used for the analytical results was determined by measuring the thickness of the panel at various stations and then averaging the measurements. The average ply thickness was obtained by dividing the average thickness by eight.

The overall dimensions of the panel are a 16 inch chord, 16 inch height and a 12 inch radius of curvature. The panel was painted with a flat white paint on the photographic side to enhance the holographic images. The addition of the paint to the surface added less than 0.0001 inch to the thickness and increased the density by only 0.002 $lb/in^3$. These two small increases were neglected in the STAGSC-1 analysis.

Cutout Technique

The fabrication of the panels was conducted by personnel at the Air Force Flight Dynamics Laboratory. The panels were cured with the same specifications used by Walley [3]. The cure cycle is shown in Appendix A. The properties shown in Table 1 and the ply orientations are input parameters to STAGSC-1. The orientations of the 2x4 inch cutout are based from the short side (2 inch) of the cutout and defined in Figure 16.

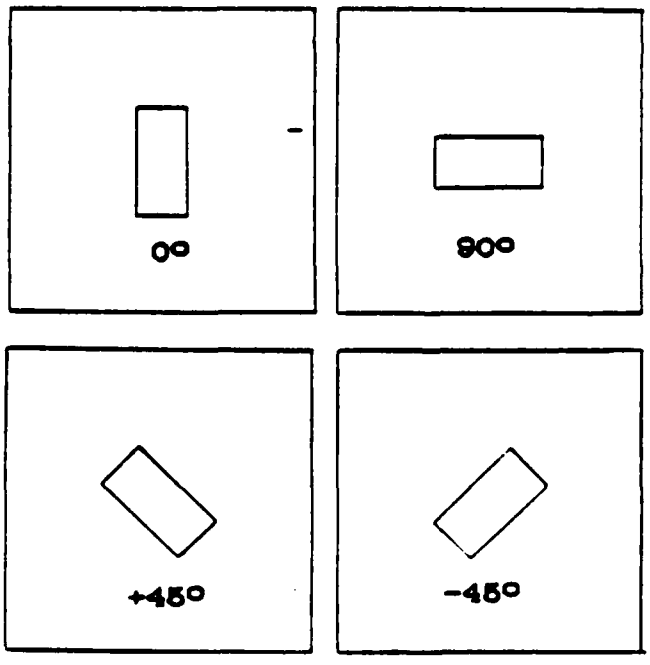


Figure 16. Cutout Orientations

The technique for cutting the rectangular holes in Walley's thesis [15] was to press the panel flat and then clamp it into position for cutting. This process of flattening can potentially cause damage to the matrix and fibers, thereby affecting the overall stiffness of the panel. By flattening the panel prior to cutting, some of the fibers ( 90°, 45°) are placed in tension. When the panel is cut, some local relief in tension at the cut boundary edge will occur. This was documented by Tisler [17]. He showed that the internal stress in the panel is partially relieved when there is a cutout. While the magnitude of this is not paramount for free vibration studies, every effort should be made to minimize damage to the panel.

In order to improve the quality of the hole cut in a curved panel a cutting fixture and jig were designed and used. Certain design constraints were necessary. First, the design must be simple to use and manufacture. Second, the cutting fixture must be reusable for the different cutout orientations. Third, cutting vibrations should be held to a minimum to prevent tool chatter. Fourth, fraying at the cutout edge must be minimized. Fifth, the cutting blade must always be perpendicular to the cutting surface as it traverses the panel. The results of these design constraints are evident in Figure (17). The maple hardwood base permited easy mounting to the bench. The radius of

curvature of the maple base allowed for the layering of the rubber and fiberglass so when the panel was sandwiched between the base and the template, there were no externally induced forces applied to the Gr-Ep panel. The rubber layer was 0.125 inches thick and acted as a very effective damper for the high speed router. The Gr-Ep panel was sandwiched between the 0.04 inch thick fiberglass sheets and helped to reduce the fraying at the cut edge. The steel template is the heart of the fixture since it provides the cutting tool guide for the bit and the smooth surface for the router to slide on.

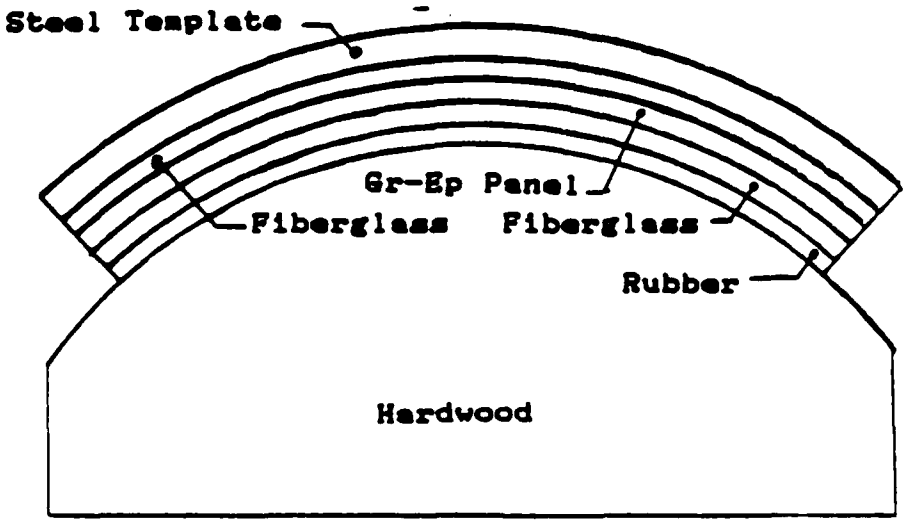


Figure 17. Cutting Fixture.

Once these layers are carefully centered on the base, they are strapped down radially across the mount to prevent movement. The cutting is achieved with 2 hp router and a 0.250 inch diameter carbide bit. Attached to the base plate of the router was a plastic mount with a radius of curvature equal to the outer radius of the steel template. Figure (18) The plastic base plate had a two-fold purpose. The first, to keep the bit perpendicular to the surface at all times. Second, it provided a self-lubricating contact surface on the steel template for ease of operation.

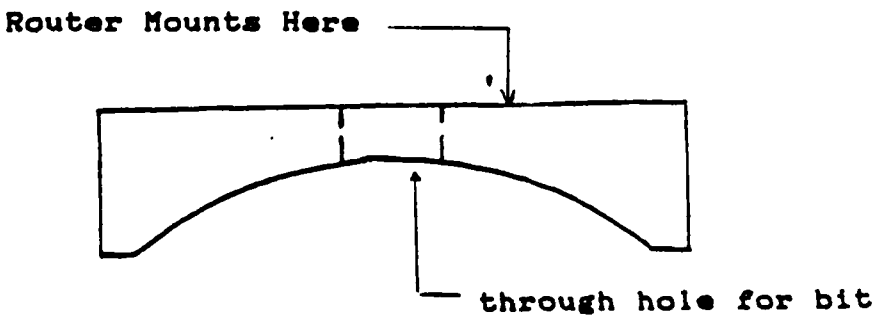


Figure 18. Router Baseplate

The depth of the cutout was set so that the shaft of the bit rested against the steel template and the cutting blade was plunged from the top layer of fiberglass into the rubber. Note: the area immediately below the cutout on the maple base had been routed out for bit clearance. Once this was completed the next step was to trim the outer edges of the Gr-Ep panel. To do this, the holding straps had to be removed. To hold the fixture in place and hold the panels securely, a center bolt and hold down plate were inserted into the fixture. With the hold down plate in position the straps are removed and the outer edge of the steel template was used as a guide for the outer edge trimming.

This setup produced an excellent edge and would be quite adaptable to any other internal and external geometries. This was evident by the precision of the cut made in the panels. The tolerance was held to ±0.005 inch. This was possible only through the use of the steel template.

The panel characteristics have been totally quantified. The next section will discuss the finite element analysis and how the panels were modelled using STAGSC-1.

# IV. FINITE ELEMENT ANALYSIS

## Element Selection

Several families of elements are incorporated into STAGSC-1. The families currently consist of triangular (300 series) and quadrilateral (400 series) flat plate elements. The elements used in this analysis were the 320, 322, 410, 420, and 422 elements. See Figures 20, 21, 22, 23, and 24 respectively. Since each of the elements in STAGSC-1 are flat plate elements, modelling curved shells can result in rotational and displacement incompatibilities between adjoining elements. Figure 19 shows two flat elements modelling part of a cylindrical surface.

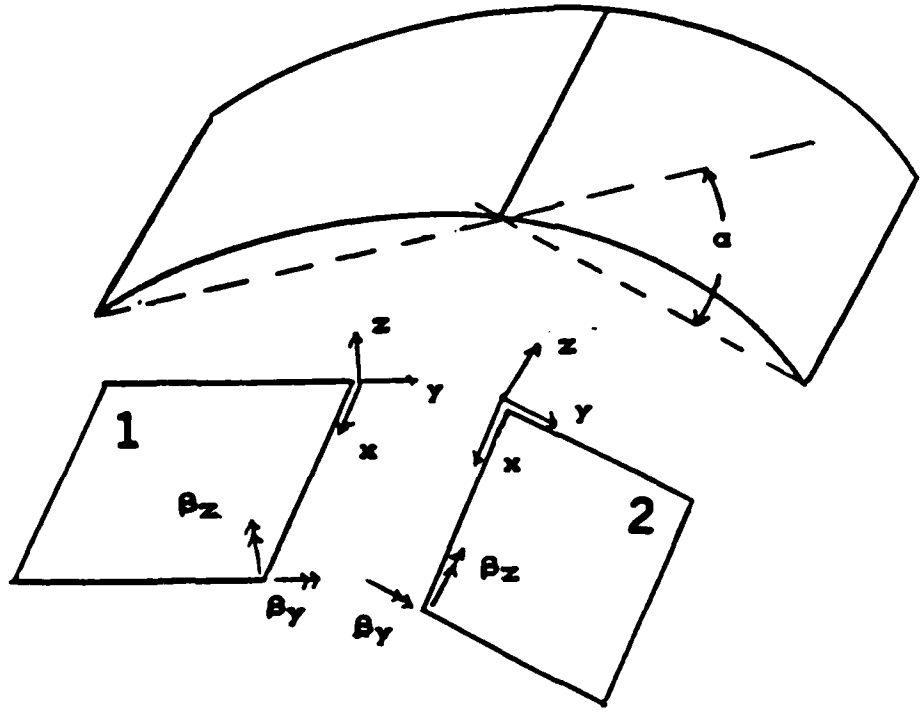


Figure 19 Flat Elements for Curved Shell Analysis [16]

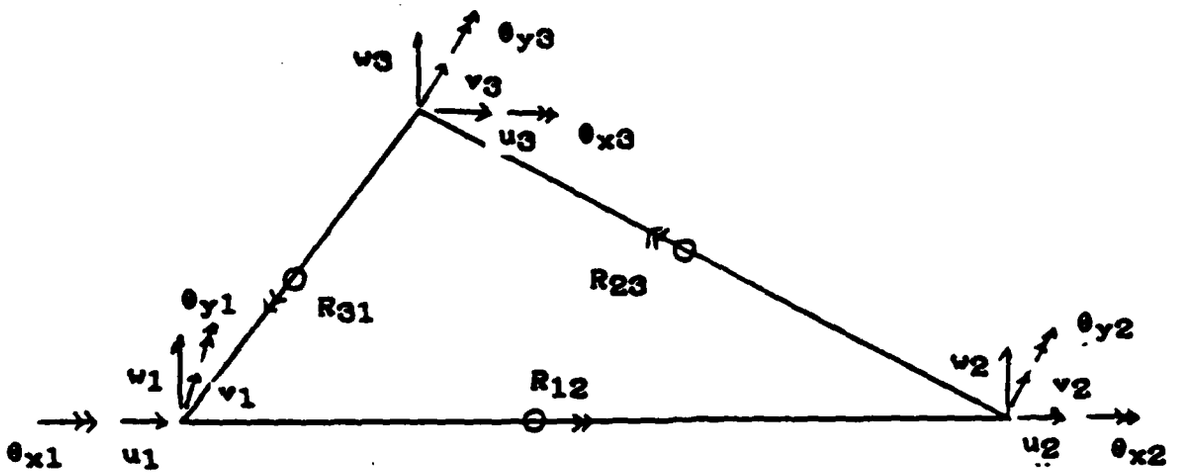


Figure 20 320 Triangular Plate Element

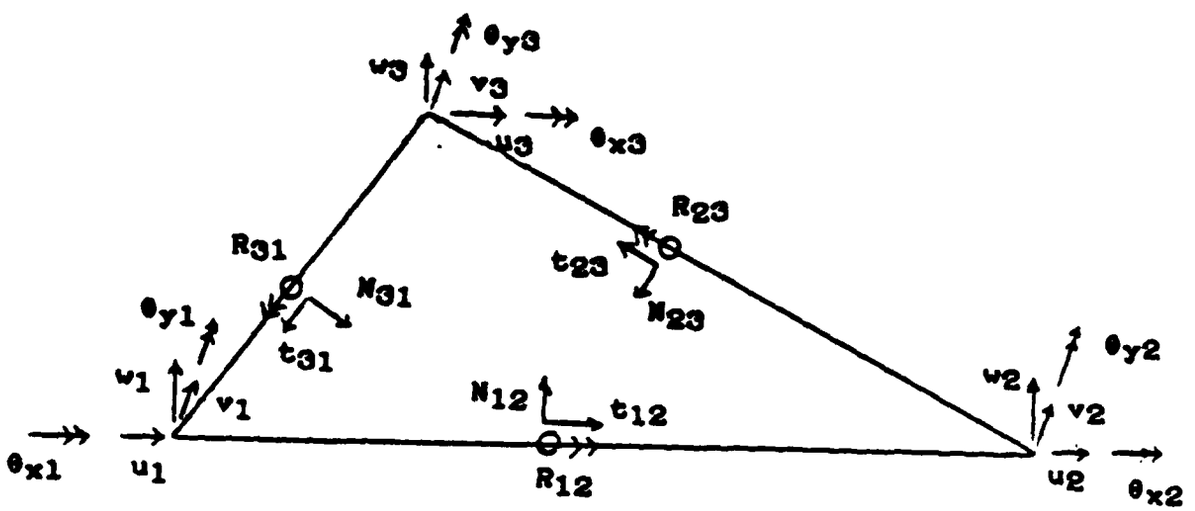


Figure 21 322 Triangular Plate Element

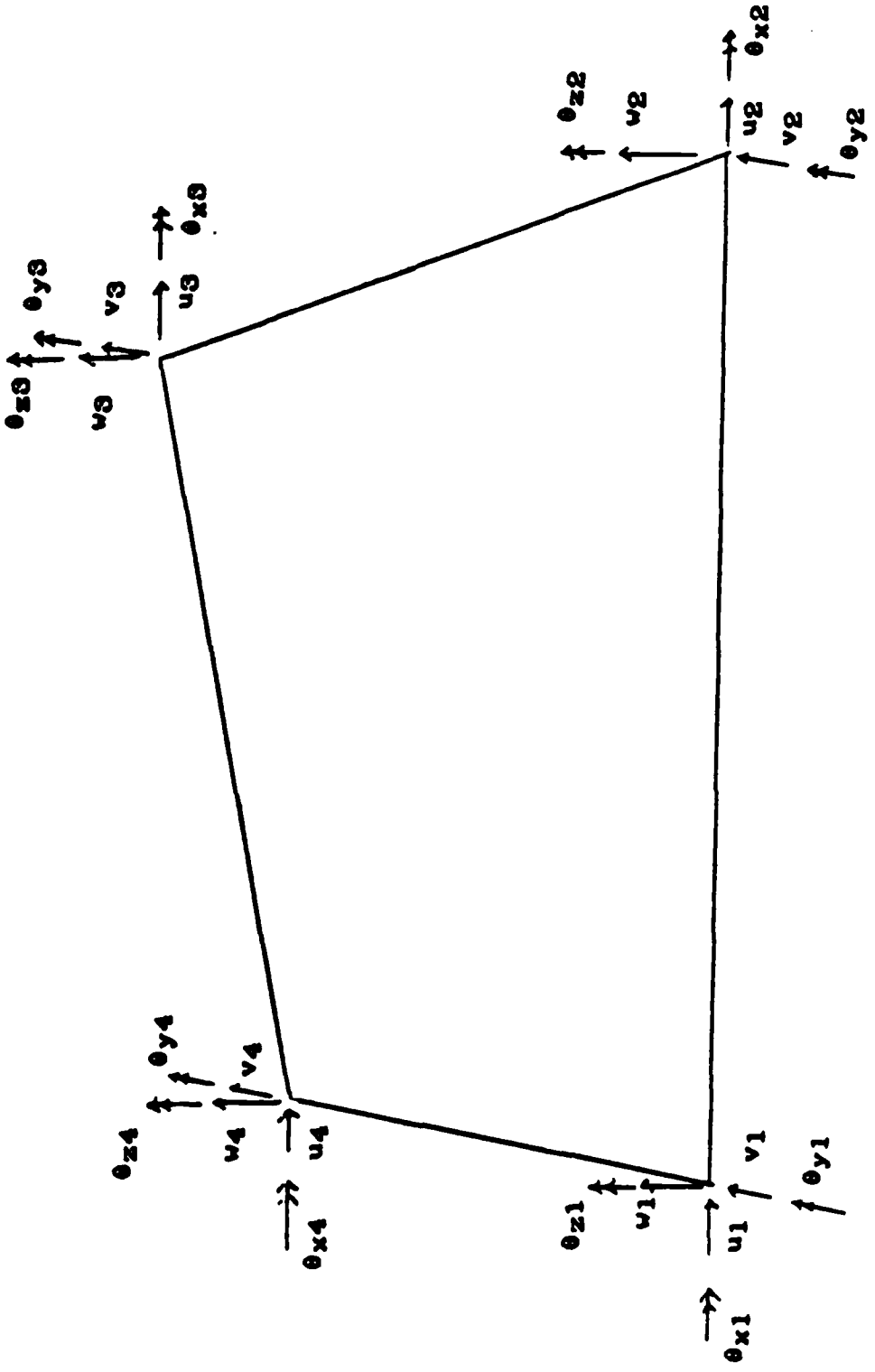


Figure 22 410 Quadrilateral Plate Element

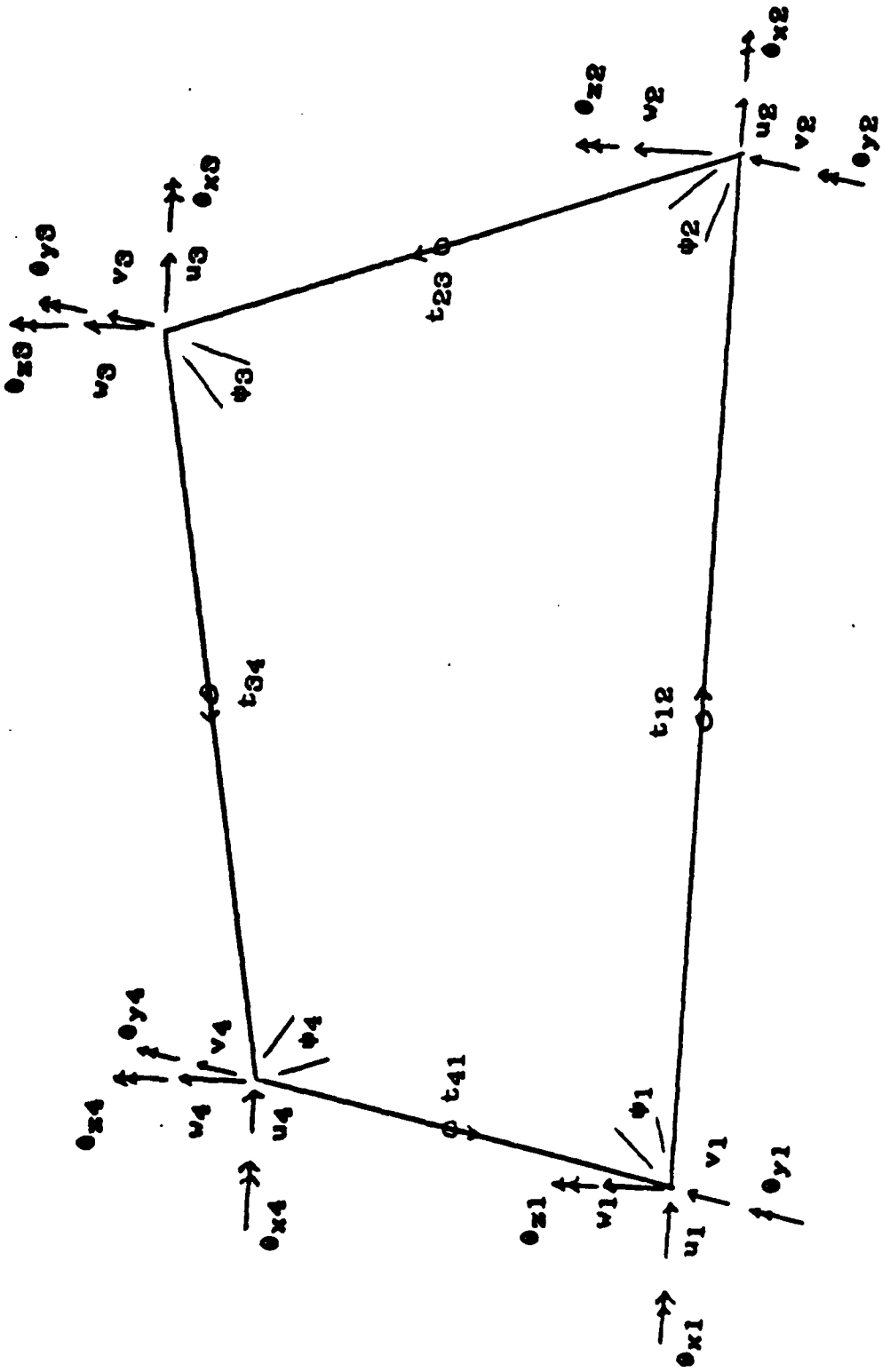


Figure 22A 411 Quadrilateral Plate Element

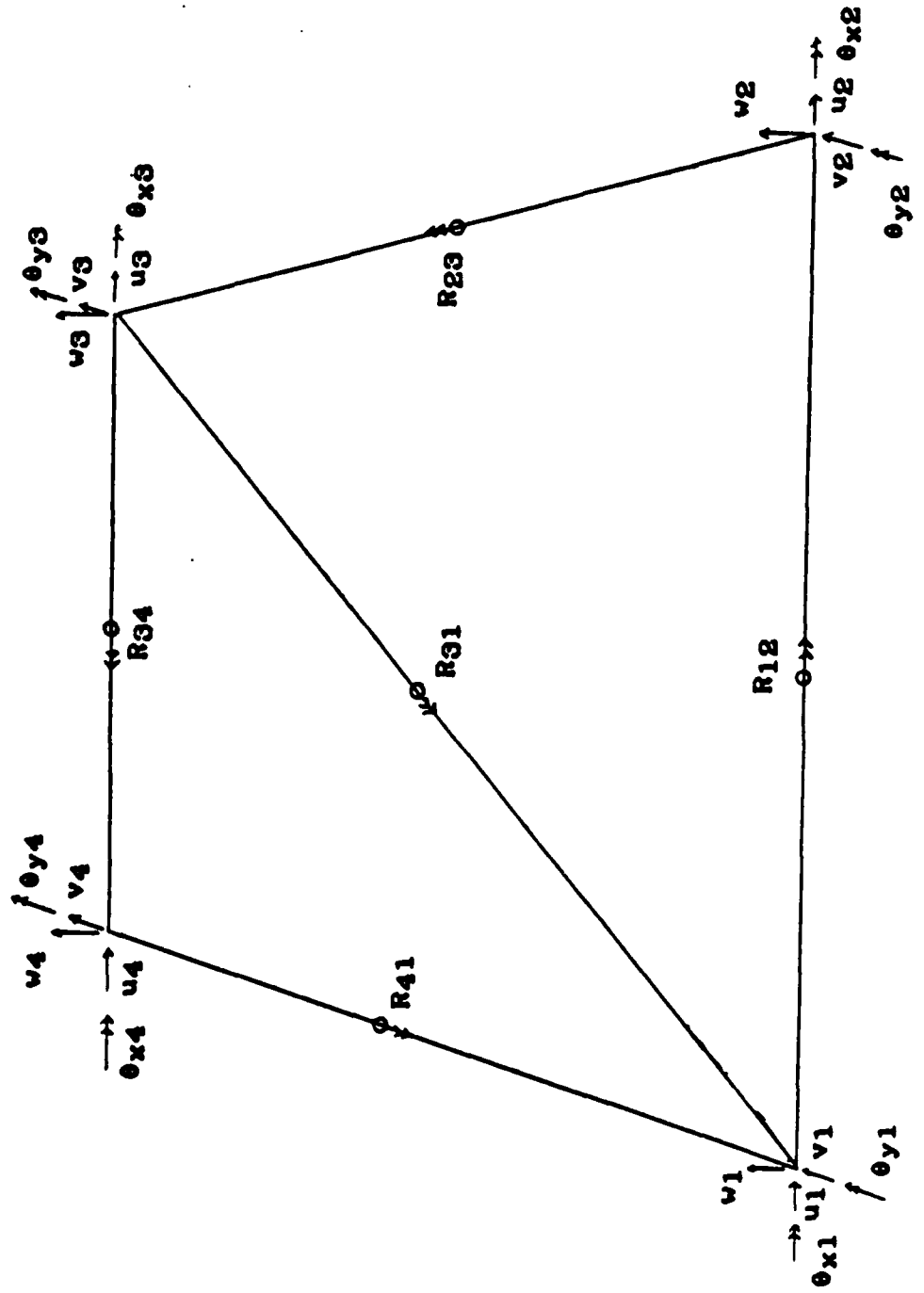


Figure 23 420 Quadrilateral Plate Element

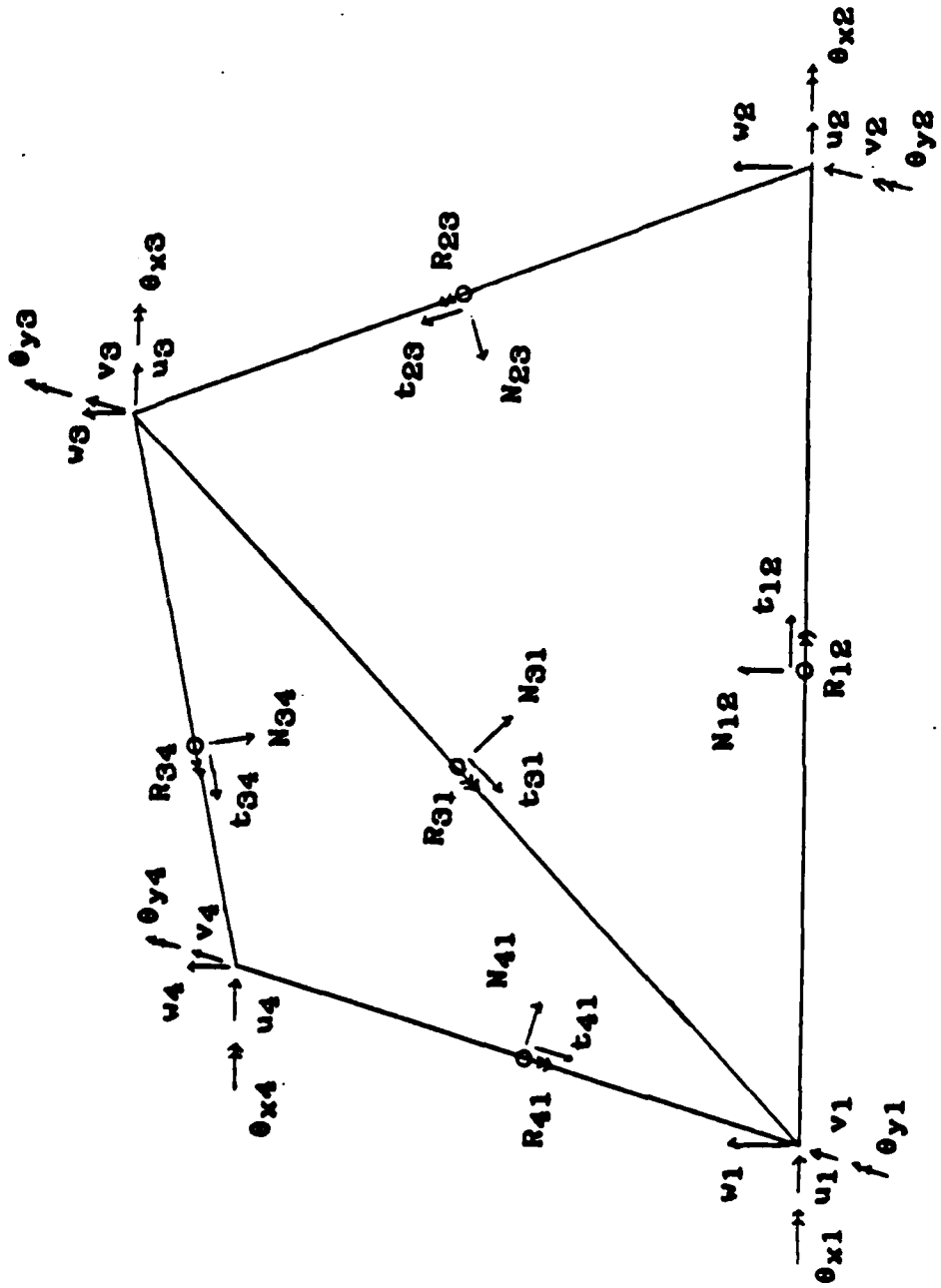


Figure 24 422 Quadrilateral Plate Element

For the total rotation between the two elements to be zero the rotations must be refered to a common coordinate system. Now the components of the y and z rotations can be added to enforce rotational compatibility. From Figure 19 this implies:

$$(\beta_{y1}-\beta_{y2})\cos(\alpha/2) - (\beta_{z1}+\beta_{z2})\sin(\alpha/2) = 0 \qquad (49)$$

$$(\beta_{z1}-\beta_{z2})\cos(\alpha/2) + (\beta_{y1}+\beta_{y2})\sin(\alpha/2) = 0 \qquad (50)$$

where $\beta_{z1}$ and $\beta_{z2}$ are respectively the rotations of element 1 and element 2 about the z axis, $\beta_{y1}$ and $\beta_{y2}$ are respectively the rotations of element 1 and element 2 about the y axis, and $\alpha$ is the angle between the adjacent elements. When flat elements meet at an angle it is necessary to introduce the normal rotation, $\beta_z$, as a freedom of the system. Since the normal rotations do not appear in the strain energy expression, the system of equations becomes increasingly ill-conditioned as the angle between the planes of adjacent elements becomes smaller. STAGSC-1 defines a small limit $\alpha_o$ and if $\alpha<\alpha_o$ the normal rotation $\beta_z$ is ignored and as an approximation the conformity constraint becomes [18]

$$\beta_{y2}=\beta_{y1} \tag{51}$$

Another problem with flat elements when they are used to model curved surfaces is interelement displacement compatibility. The in-plane displacements u and v are first order and the bending strains have second order derivatives. Consequently, w is represented by higher order than u and v. In STAGSC-1, w is cubic with u and v being linear or quadratic within the element.[16] Along the entire boundary of two adjacent elements, displacement compatibility requires:

$$(v_1-v_2)\cos(\alpha/2) - (w_1+w_2)\sin(\alpha/2) = 0 \tag{52}$$

$$(w_1-w_2)\cos(\alpha/2) + (v_1+v_2)\sin(\alpha/2) = 0 \tag{53}$$

where $w_1$ and $w_2$ are the displacements in the z direction and $v_1$ and $v_2$ are the displacements in the y direction for element 1 and element 2 respectively. It is obvious that for equations (52) and (53) to hold, v and w must be of the same order. Displacement compatibility is enforced in STAGSC-1 with a cubic representing w and third order

polynomials representing u and v. This is achieved by including the displacement derivatives as degrees of freedom (DOF). An in-plane displacement field is obtained in which displacements normal to the element boundaries are cubic in the coordinate direction along the boundary.

The 320 and 322 triangular elements are based on the Felippa version of the Clough-Tocher triangle [1]. In Figure 20, the 320 element has 5 DOF at each node (3 translation and 2 rotation), and a parallel edge rotation, for a total of 18 DOF. The 322 triangular element in Figure 21 has 24 DOF by adding an in-plane displacement and a rotation normal to the side along each edge. The results of using these elements are discussed in Panel Modelling and in Section VI. All versions of the triangular elements have a piecewise cubic representation of the normal displacement, w. The 320 element has a linear representation of in-plane displacements and the 322 element has a quadratic representation [1]. When the triangular elements are used to represent a curved surface, a displacement incompatibility is allowed.

In Figure 22, the 410 quadrilateral element has 6 DOF (3 translations and 3 rotations) at each node for a total of 24 DOF. The 410 element does not have the side nodes that are present on the 320, 322, 420, 422 elements and uses only an average normal rotation at the corner nodes. This makes the element have constant strain compatibility tangential to

the boundaries and suppresses shear strain at the corner nodes. This element was used exclusively for the solid, 0 degree and 90 degree panels. These panels are discussed further in Panel Modelling and Section VI.

The 420 quadrilateral element, Figure 23, is formed using two 320 elements and has 25 DOF. The 422 quadrilateral element, Figure 24, is formed using two 322 elements and has 35 DOF. The results using this element are discussed in later sections.

## Panel Modeling

The panels were modelled on STAGSC-1 using two techniques. The first, with a STAGSC-1 generated grid; second, a user generated grid.

### The Solid, 0° & 90° Panels

The solid panel was modelled using the 410 element (Figure 22). The reason for selecting this element was based on the extensive convergence study conducted by Walley[3]. His convergence study for the different elements was conducted using a 25 x 25 grid (see Figure 25) on the VAX 11-785. The 411 element (see Figure 22A) yielded a fundamental frequency of 504 Hz in 5844 cpu seconds while the 410 element gave a fundamental frequency of 506 Hz in

3019 cpu seconds [3]. The 410 element converged nearly twice as fast as the 411 element suggesting that in this case the higher order displacement fields yield a marginal increase in accuracy for a substantial increase in computer time [3]. Since this vibration problem has primarily out of plane displacements because of the clamped-clamped boundary conditions, the addition of in-plane corner node rotations of the 411 element adds little to the solution.

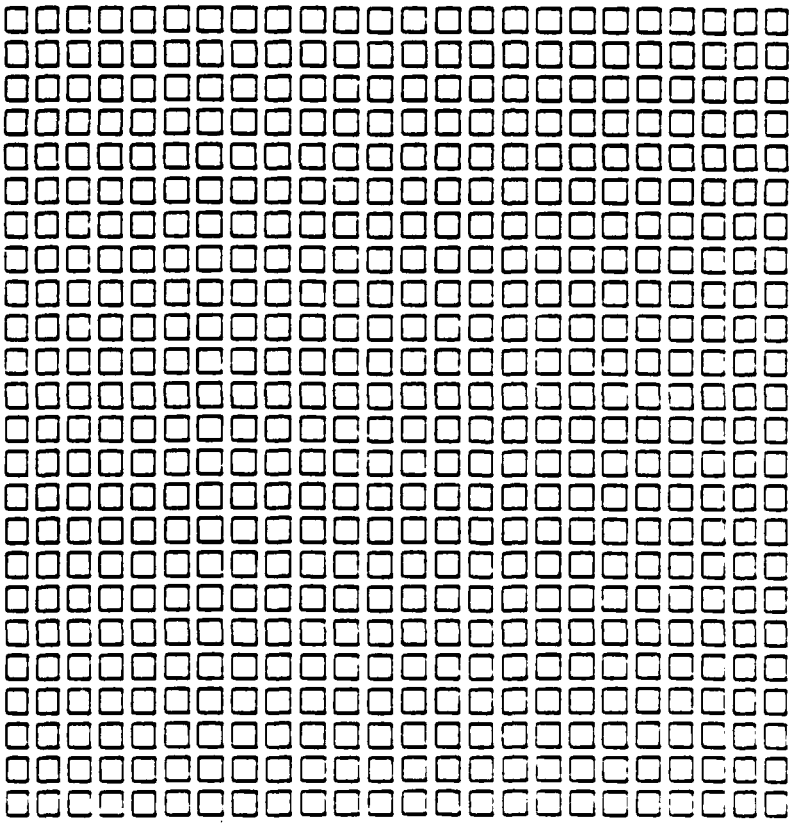

Figure 25 Solid Panel 25 x 25 Mesh

STAGSC-1 has the capability to automatically generate a mesh once the geometric constraints are identified. The automatic grid generator was used to generate the meshes for the solid, 0° and 90° panels. As shown in Appendix B, the input deck is fairly straight forward to create a model of a curved composite panel with and without a cutout.

As with the solid panel, the 410 element and the 25 x 25 grid was used to model the 0° and 90° panels. The grid, with cutouts, was automatically generated by STAGSC-1. (See Appendix B) For a square cutout, the corner nodes are identified by row and column and then input to STAGSC-1.

The +45° & -45° Panels

The 45° panels presented a unique problem in modelling on STAGSC-1. There was no apparent capability in STAGSC-1 to automatically generate a grid with this cutout orientation. (If there was a capability to do this in STAGSC-1 it was not readily apparent in the User's guide.) Therefore, a FORTRAN program was required that calculated the node points in global coordinates, determined connectivity, and output the results in STAGSC-1 input format. While this was at times, time consuming, the programs to do this were not difficult to write. Several different meshes were generated using this method and are

discussed in Section VI. When creating a user generated grid, it is important to input the proper orientaion of the element in local coordinates so the orientation can be referred back to global coordinates. Failure to do so can result in an incorrect material model.

# V. HOLOGRAPHIC ANALYSIS

## Test Fixture

The test fixture used for this experiment was the same fixture used by Walley [3]. This permitted verification of the results Walley obtained on his solid panel and 0 degree cutout panel. It also provided a cost effective method of continuing this study without having to machine a new fixture. The test fixture is capable of simultaneously clamping all four edges of the curved panels. Since the holography technique is capable of detecting rigid body motion of the fixture due to thermal effects or ground vibrations, the fixture had to remain stable over the desired frequency range and not respond quickly to temperature changes in the test room.

To satisify these requirements, the fixture was made from steel and was designed to provide a two inch clamping surface on each edge. The vertical clamps were constructed (Figure 28) from 12 inch sections of 4x4 inch bar stock. A 2 1/8 x 1 1/2 inch slot was milled from one face of each bar to form a U shaped structure. Two alternating rows of 1/4 inch holes were drilled and tapped along each side for Allen head bolts.

Figure 26A Test Fixture

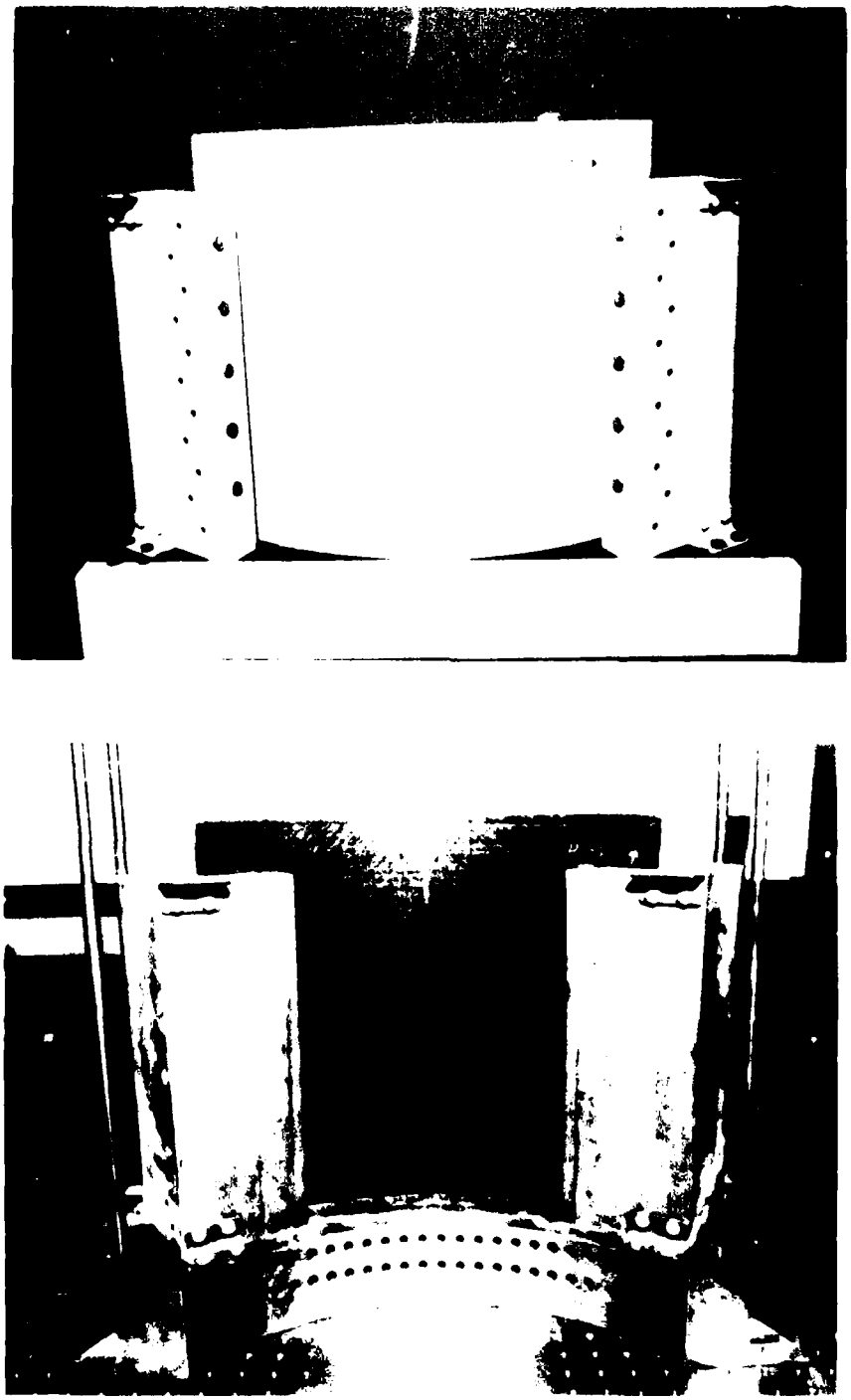

Figure 28B Test Fixture

These bolts were tightened against 1/2 x 2 x 12 inch flat rods placed on each side of the Gr-Ep panel, thus providing a secure clamp. To prevent lateral motion, smaller U shaped clamps were installed on the open face of the vertical clamps. A curved 1 1/4 inch wide by 2 1/8 inch deep path with an outer radius of 12 inches was milled from a 22 x 10 x 3 inch steel bar. The 12 inch outer radius matched that of the panels. A set of 9 curved blocks, 1 inch thick by 2 inches high by 1 3/4 inches chord were milled to match the inner radius of the panels. In order to take up any inaccuracies in the machining of the blocks and to evenly distribute the clamping force, a 40 mil aluminum bushing was added. Holes were drilled and tapped radially on the inner radius of the horizontal sections of the fixture for the clamping bolts. Four 1/2 inch rods were added to provide structural integrity and act as assembly aids when changing the panels. When assembling the fixture, the two vertical clamps and bottom section were joined and the panel inserted between the clamping surfaces. The top clamp was then installed and the radial clamping blocks were inserted from the concave side. Each clamping bolt was tightened to 3 ft-lb. At this clamping pressure the holograms showed that the panels were fully clamped since no nodal lines went to the boundaries.

## Holographic Technique

Off-the-shelf equipment was used in this experiment. (An equipment list is provided in Appendix E). The laser was mounted to an isolation table which had the optical setup shown in Figure 28. To expand the laser beam so that the entire panel was illuminated, 20 x microscope objectives were used. In order to eliminate the possibility of dust causing refractive fringes, pinhole spatial filters were placed in series with the microscope objectives.

Real time holographic interferometry was used to determine the natural frequencies and mode shapes of all the panels tested. For complete details of the step-by-step procedures for taking a hologram see Appendix C. For the majority of the testing, two horns were used to excite the panels. When two horns were used, they were either placed in-phase or 180 degrees out of phase depending on whether the mode shape was symmetric or anti-symmetric respectively. On panels 4 and 5 (+/- 45 degree cutout) one horn was used to excite the fourth mode. Except for the relative amplitude of the mode shape, the positioning of the horns at various locations around the concave side had little effect.

While the panels were being excited by the horns, subharmonics were checked for by an optical displacement meter positioned near the surface of the concave side of the panel. (See Figure 27 for the equipment configuration to

measure for subharmonics). The output signal of the optical displacement meter and the output of the signal generator were simultaneously displayed on an oscilliscope as a Lissajous figure. If an elipse appeared there were no subharmonics present.

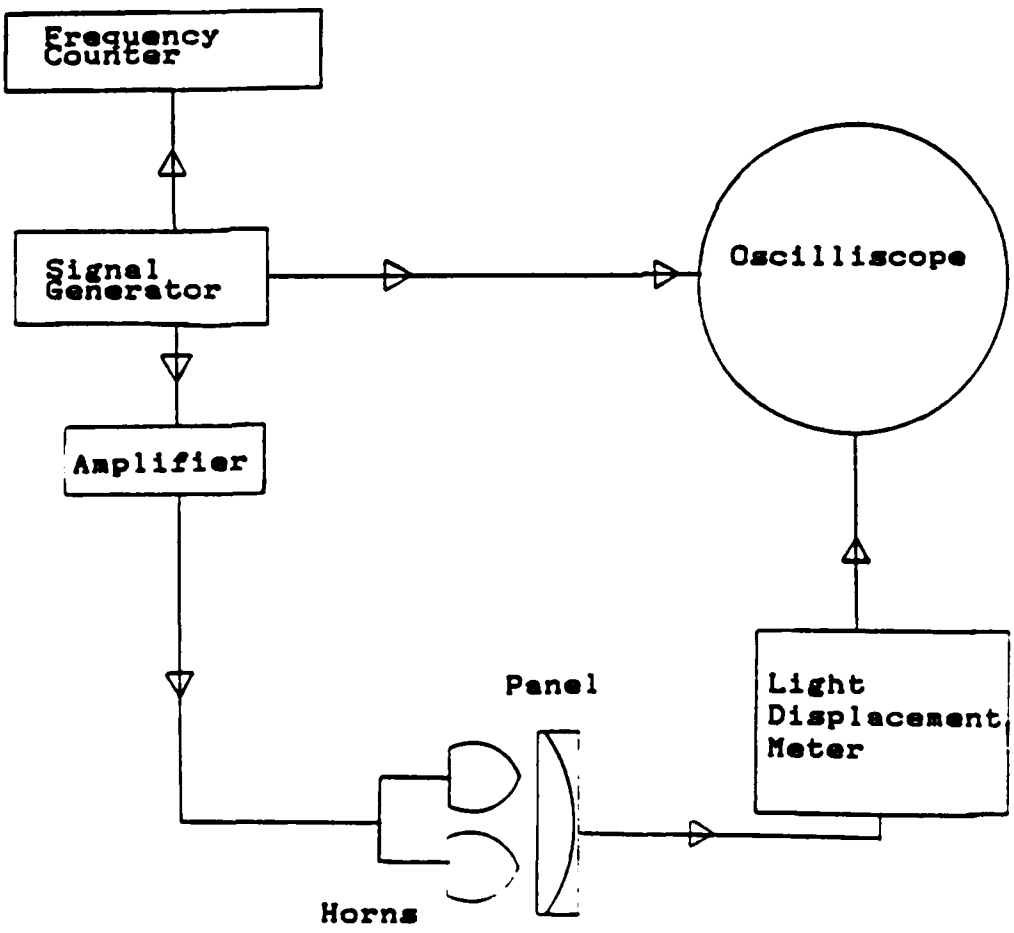


Figure 27 Block Diagram of Equipment Configuration

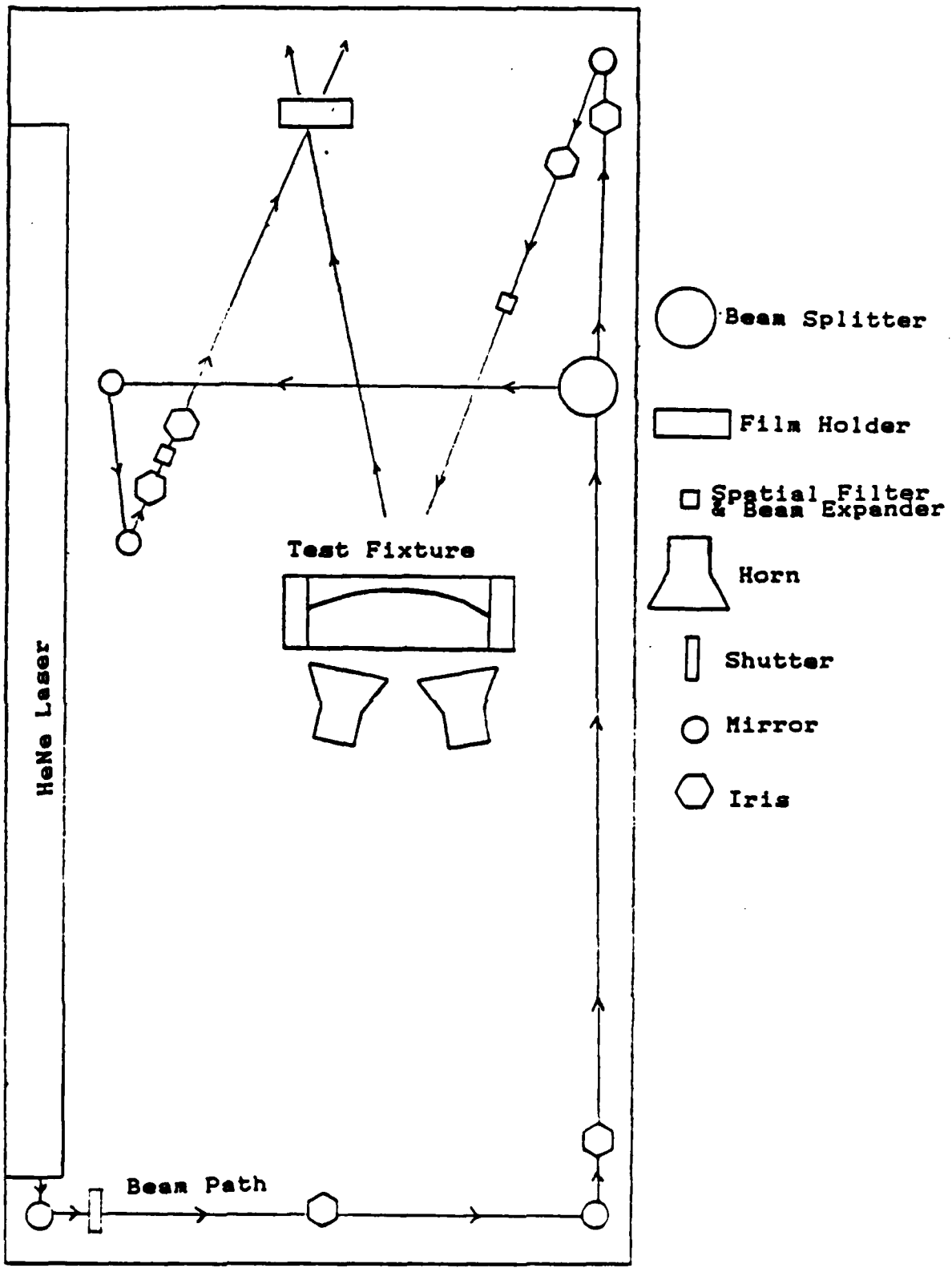


Figure 28 Optical Setup

# VI. RESULTS AND DISCUSSION

This chapter is divided into six sections, the results for the solid, 0°, 90°, +45° and -45° panels and a discussion on the effects of the cutouts. Since no closed form solution is available and a numerical approximation was used to solve for the natural frequencies and mode shapes, the errors in the experimental results can vary both positively and negatively from the numerical approximations.

The experimental technique used in finding the natural frequencies for all of the panels involved scanning the frequency spectrum from zero Hertz to the fifth natural frequency while observing the fringe patterns on the holographic still. Whenever a natural frequency was encountered during the scanning, a well defined mode shape appeared on the holographic still of the panel. The frequency was noted and upward scanning continued until all five natural frequencies were found. Then the procedure was reversed and the natural frequencies were found by downward scanning. Rarely would the natural frequencies be exactly the same for the upward and downward scans, but the difference was never more than 4.5 Hz. When real time holograms were taken the frequency was assumed to split these bounds.

Excitation was provided by a dual horn arrangement in nearly every case. (See Figure 28) The phase of one horn would be changed by 180°, so that the horns were out of phase, in order to intensify the antisymmetric excitation of the panels. The antisymmetric mode (2 & 4) of the +/-45° panels was best accomplished by the use of a single horn centered on the lower edge of the cutout. The reason for using the single horn arrangement can be explained by comparing the orientation of the cutout and the horn locations relative to the cutout. With the -45° panel, the two horns were located almost exactly at each end of the cutout along the two inch edge. Switching the horns so they were aligned along the four inch edge did not strengthen the clarity of the antisymmetric modes.

When comparing the mode shapes from STAGSC-1 and the holograms, the white areas of both represent regions of constant amplitude while the dark lines represent constant displacement fringes.

## The Solid Panel

The experimental and analytical results of the solid panel are shown in Table 2, along with a comparison of the results by Walley.

Table 2. Solid Panel Results

| | Natural Frequencies, Hz | | | |
|---|---|---|---|---|
| Mode | STAGSC-1 | Experiment | Experiment* | % Error# |
| 1 | 508 | 516 | 525 | -1.9 |
| 2 | 524 | 527 | 534 | -0.6 |
| 3 | 693 | 716 | 724 | -3.2 |
| 4 | 703 | 731 | 736 | -3.8 |
| 5 | 770 | 840 | 862 | -8.3 |

* Results from Walley[3]

\# % error between STAGSC-1 and this experiment

Any difference between the experimental results of Walley and the results presented here could be explained by any variations in the lot to lot manufacture of the composite panels. The STAGSC-1 analysis was accomplished with a 25 x 25 mesh using the automatic grid generator, as shown in Figure 25. The holograms and STAGSC-1 mode shapes are compared in Figures 29-33.

Comparing Figures 31 and 32 it is evident that there is biasing toward the -45° ply of approximately five degrees. The -45° ply represents the outermost ply of the 45 degree plies. This conflicts with the results from Walley. In his report, he documented a bias toward the +45°

ply. This immediately indicates that there is a difference between the ply layups used for his panels and the ones tested here. Converstions with Walley [15] indicated that he had no written documentation of the exact ply orientation from the manufacturer of his panels, but was verbally given the ply orientations. The ply layup for this experiment is regarded as known with total certainty. Since both experiments indicate a bias along one or the other 45° ply, a computer run using STAGSC-1 with the ply layup changed to $[0/45/-45/90]_s$ should clarify any differences between the two results. Figure 34 and Figure 35, which correspond to mode 3 and mode 4 of the $[0/45/-45/90]_s$ analysis, agree exactly with Walley's results and indicate that a different ply layup than originally documented.

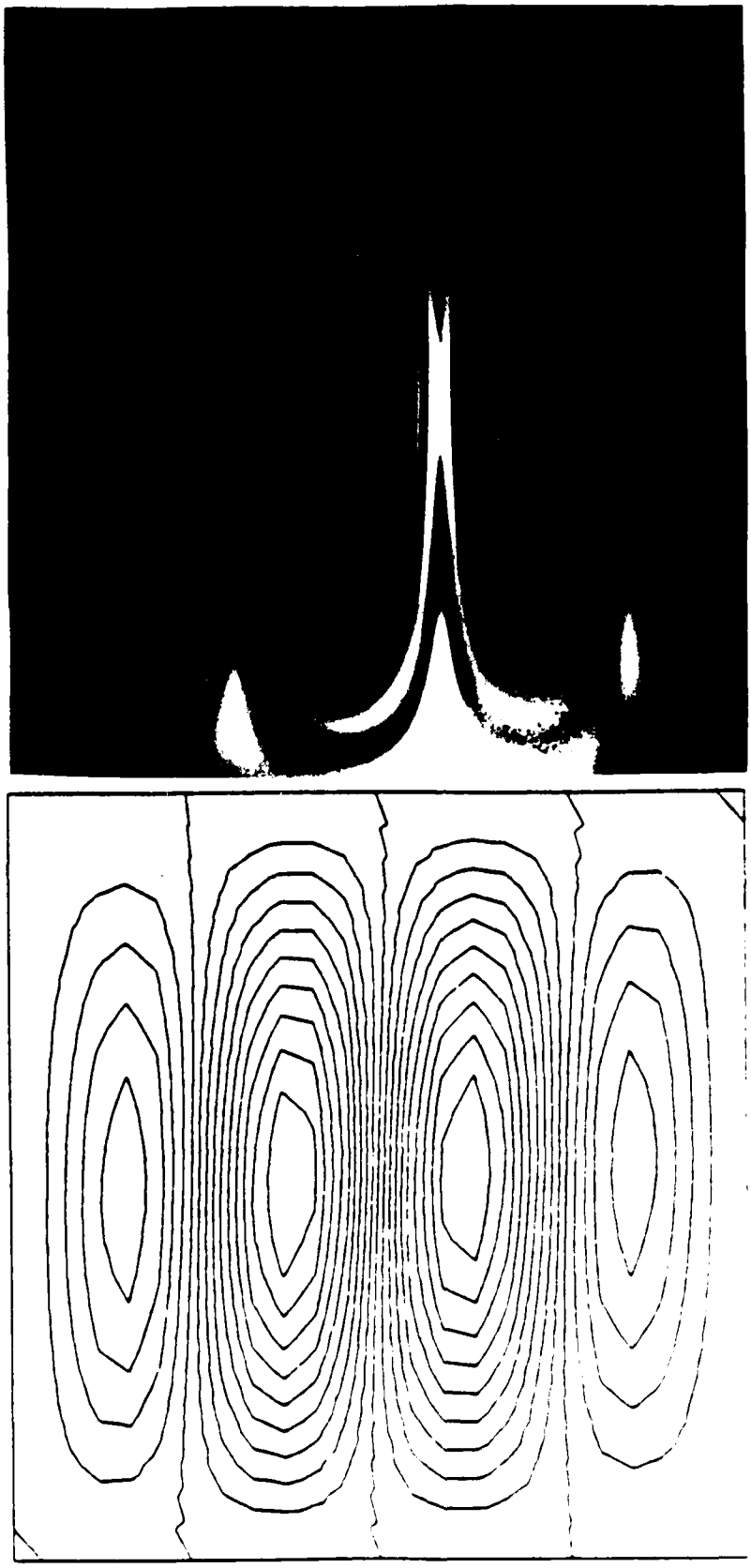

Figure 29 Solid Panel--Mode 1

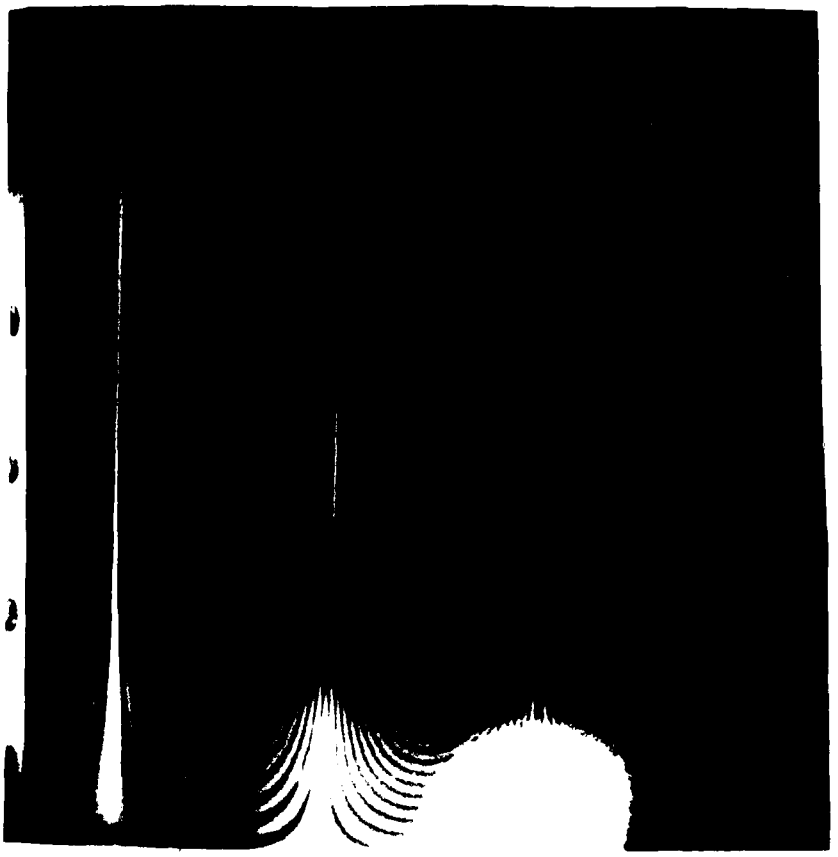

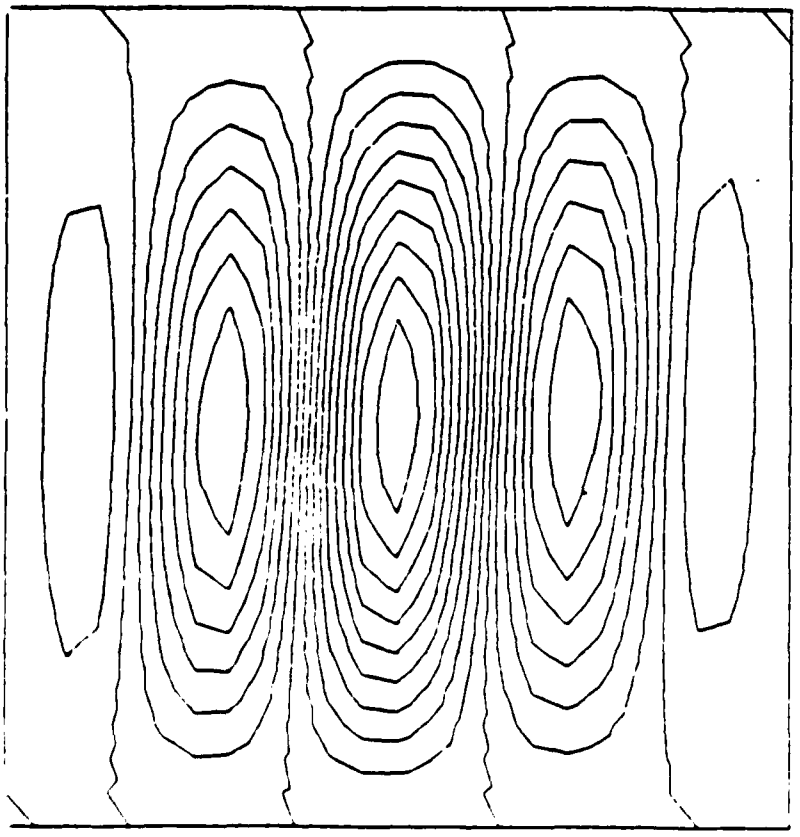

Figure 30 Solid Panel--Mode 2

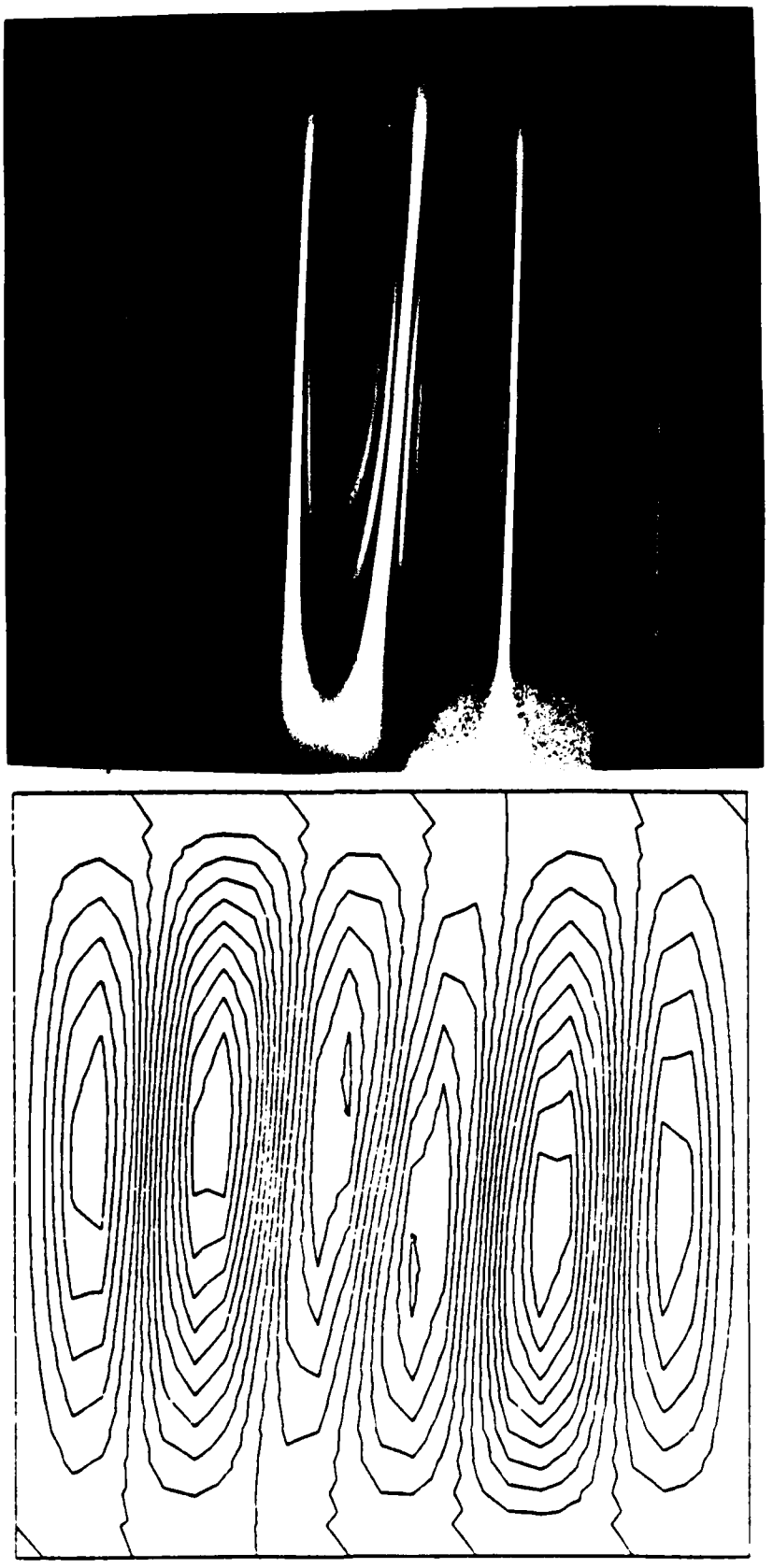

Figure 31 Solid Panel--Mode 3

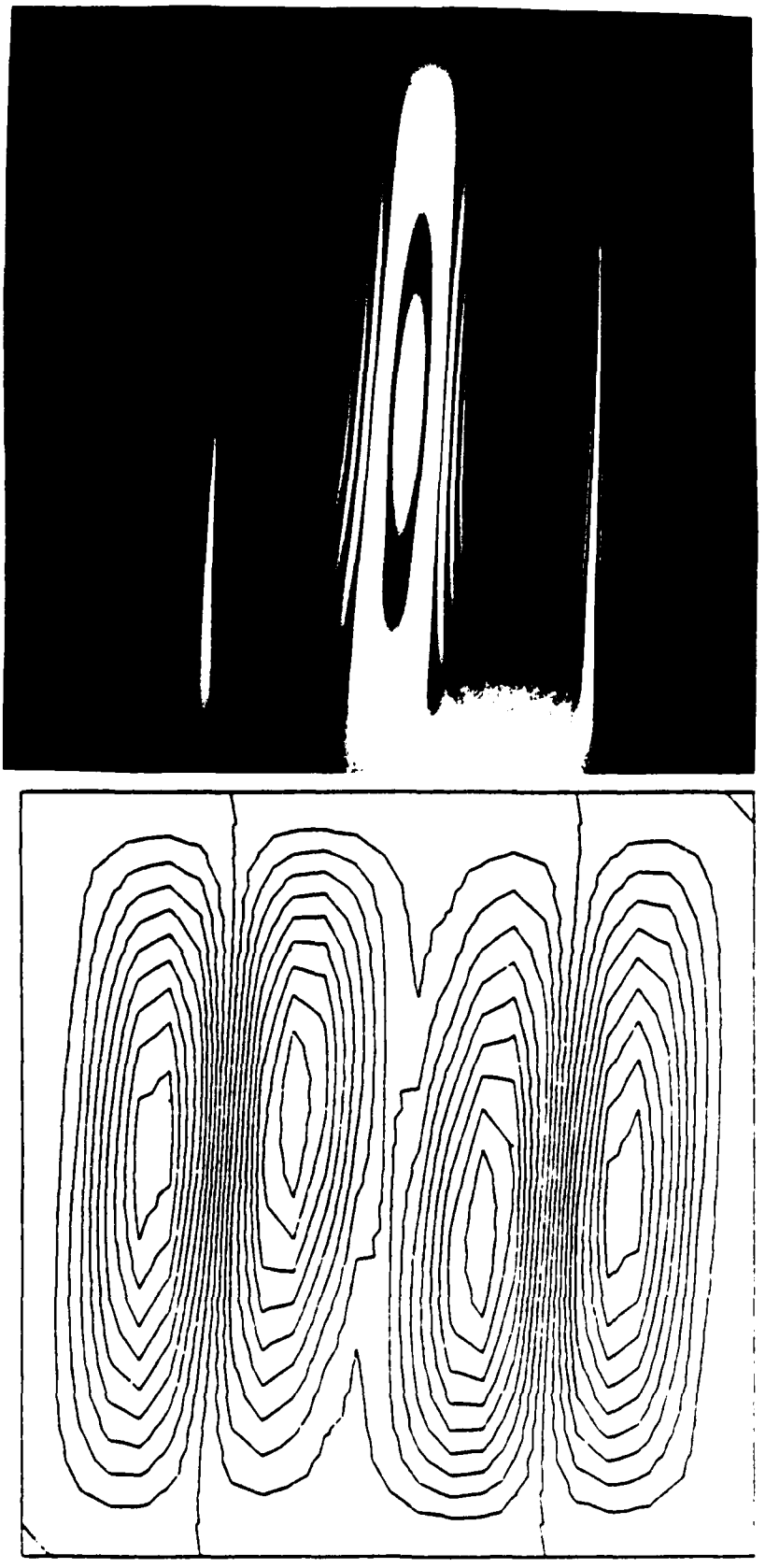

Figure 32 Solid Panel--Mode 4

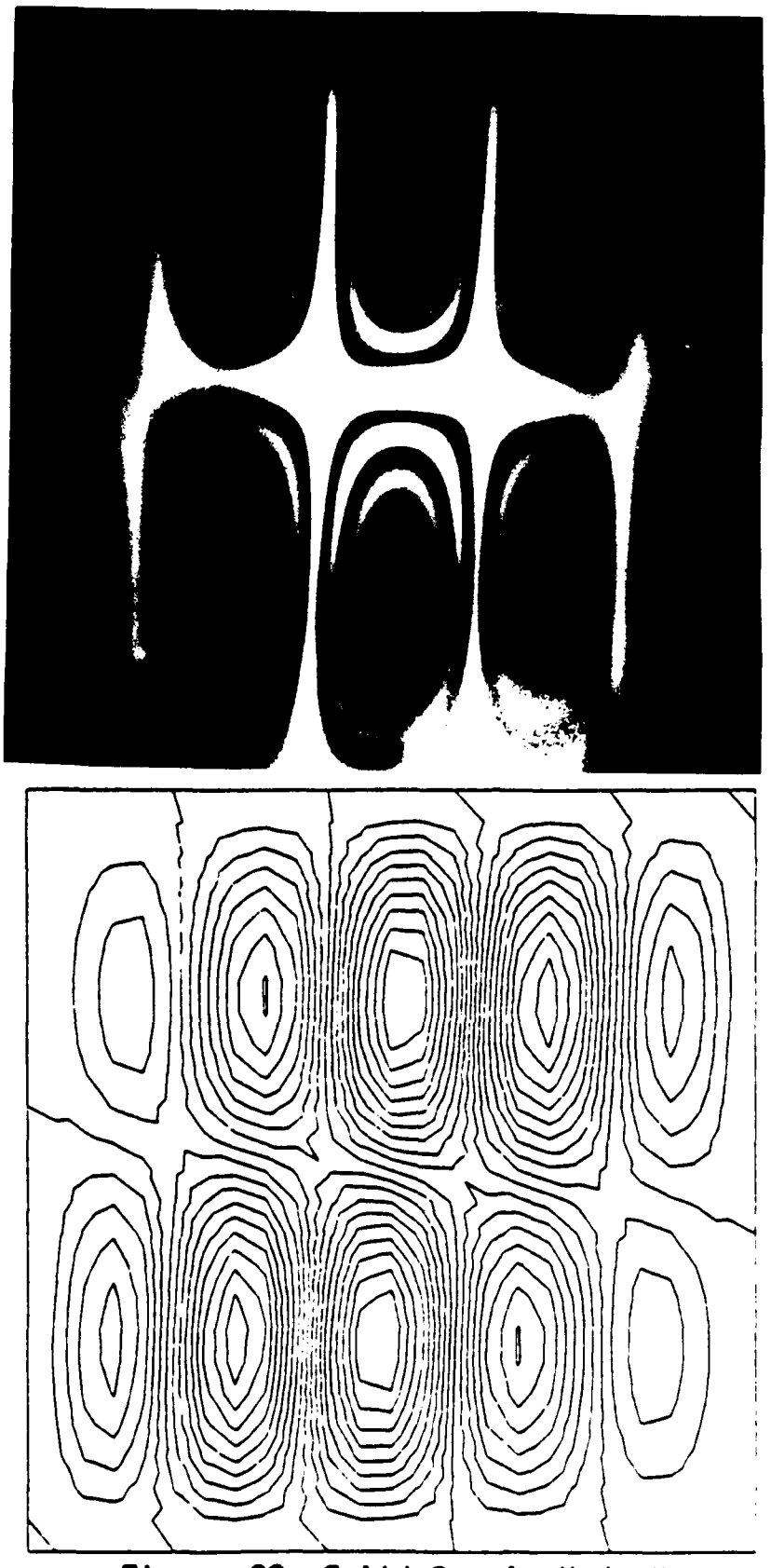

Figure 33 Solid Panel--Mode 5

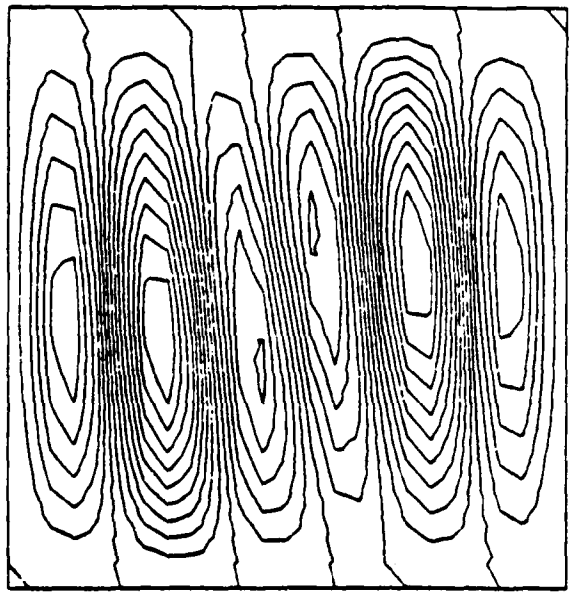

Figure 34 Mode 3 $[0/45/-45/90]_s$

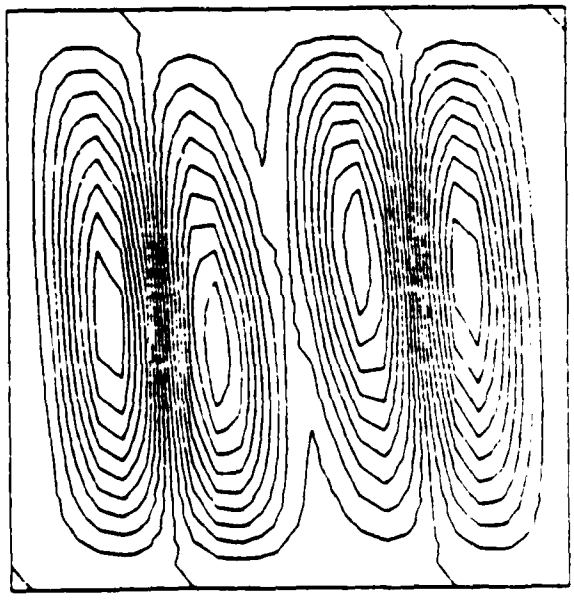

Figure 35 Mode 4 $[0/45/-45/90]_s$

## The 0° Panel

The experimental and analytical results of the 0° panel are shown in Table 3, along with a comparison of the results by Walley.

Table 3. 0° Panel Results

| | Natural Frequencies, Hz | | | |
|---|---|---|---|---|
| Mode | STAGSC-1 | Experiment | Experiment* | % Error# |
| 1 | 454 | 440 | 419 | +3.2 |
| 2 | 536 | 485 | 483 | +10.5 |
| 3 | 562 | 577 | 579 | -2.6 |
| 4 | 631 | 655 | 670 | -3.7 |
| 5 | 703 | 766 | 714 | -8.2 |

* Results from Walley[3]

\# % error between STAGSC-1 and this experiment

The grid used in the analytical analysis was a 25 x 25 mesh with a cutout that was generated by the automatic grid generator, as shown in Figure 36.

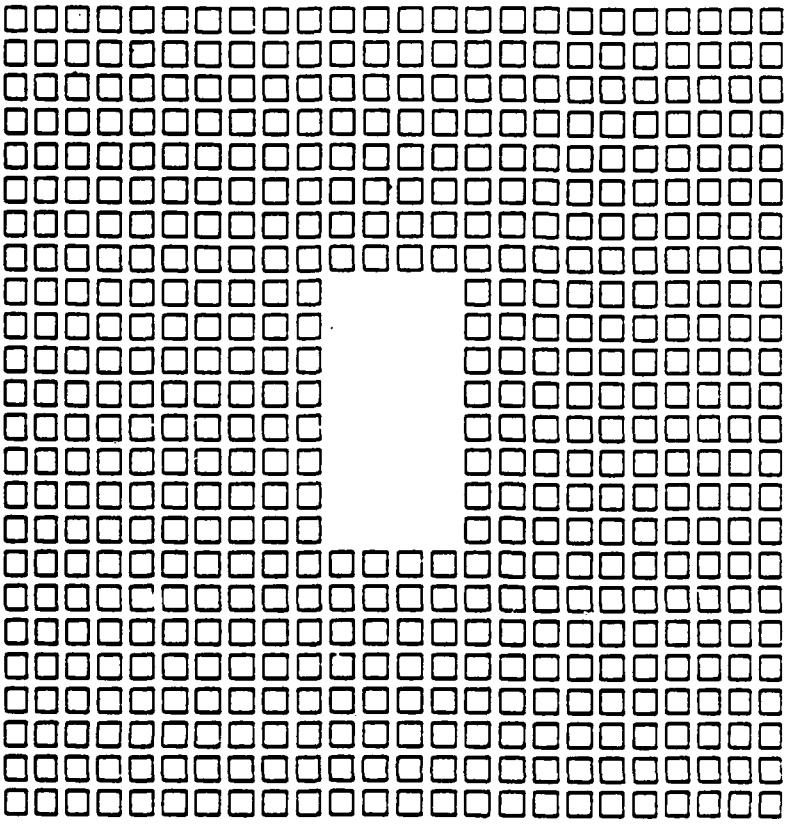

Figure 36 0° Panel 25 x 25 Mesh With Cutout

The holograms and STAGSC-1 mode shapes are compared in Figures 37-41. The tilting of the antinode regions is only descernable for mode 4 in Figure 40. There is an 11.3% reduction in the fundamental frequency from the solid panel. This shows that the cutout at this orientation significantly reduces the stiffness of the panel.

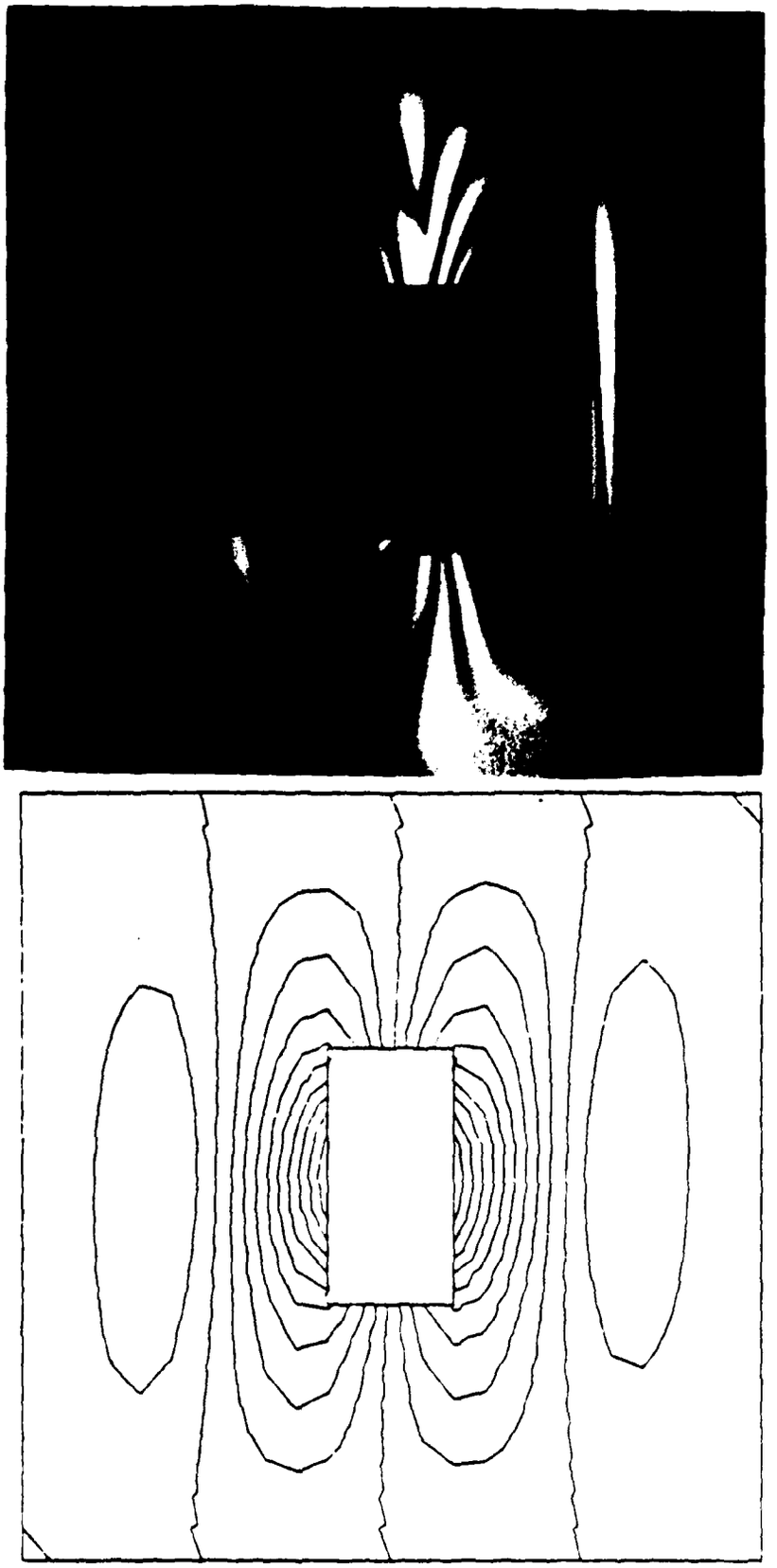

Figure 37 0° Panel--Mode 1

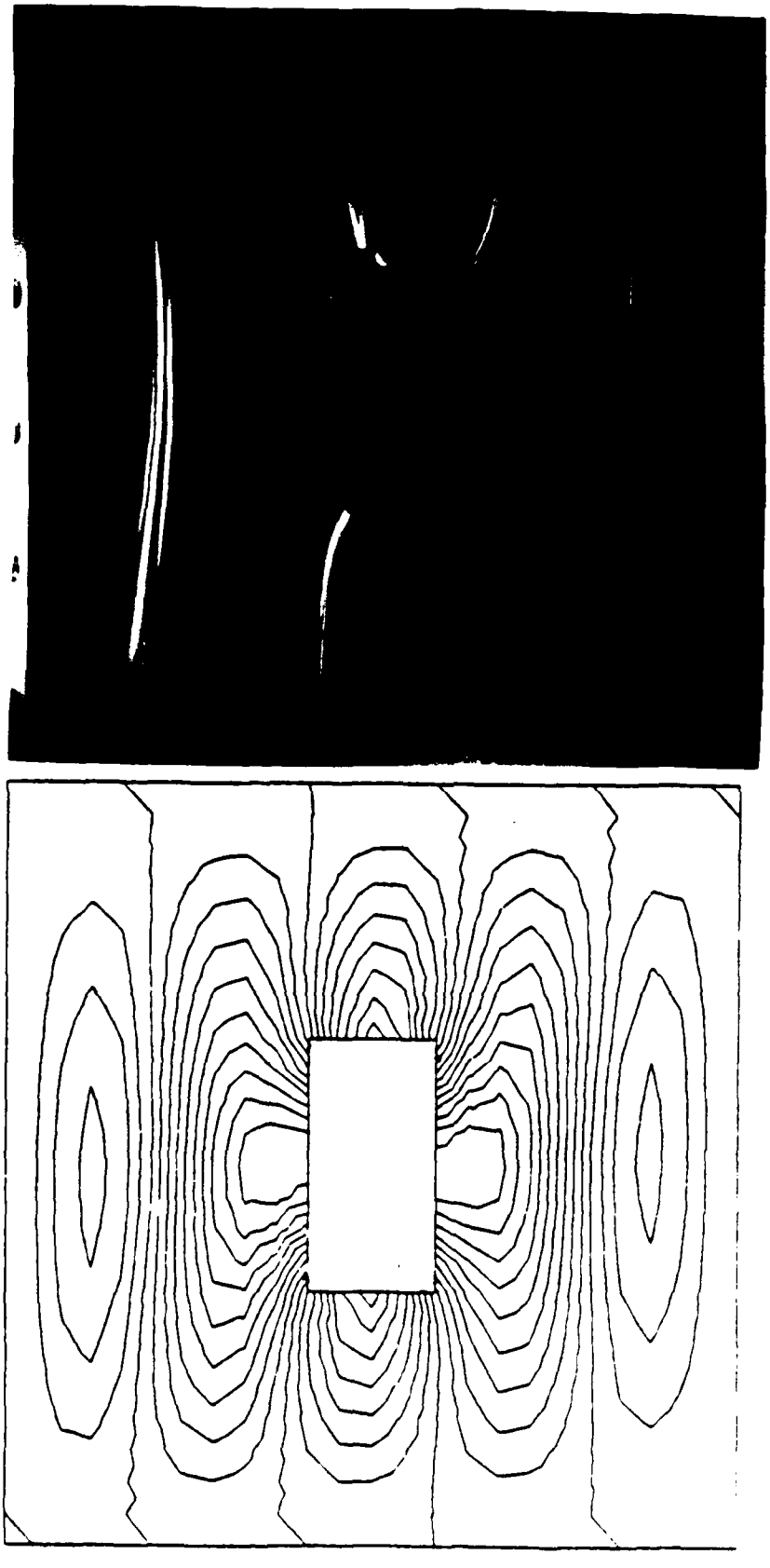

Figure 38 0° Panel--Mode 2

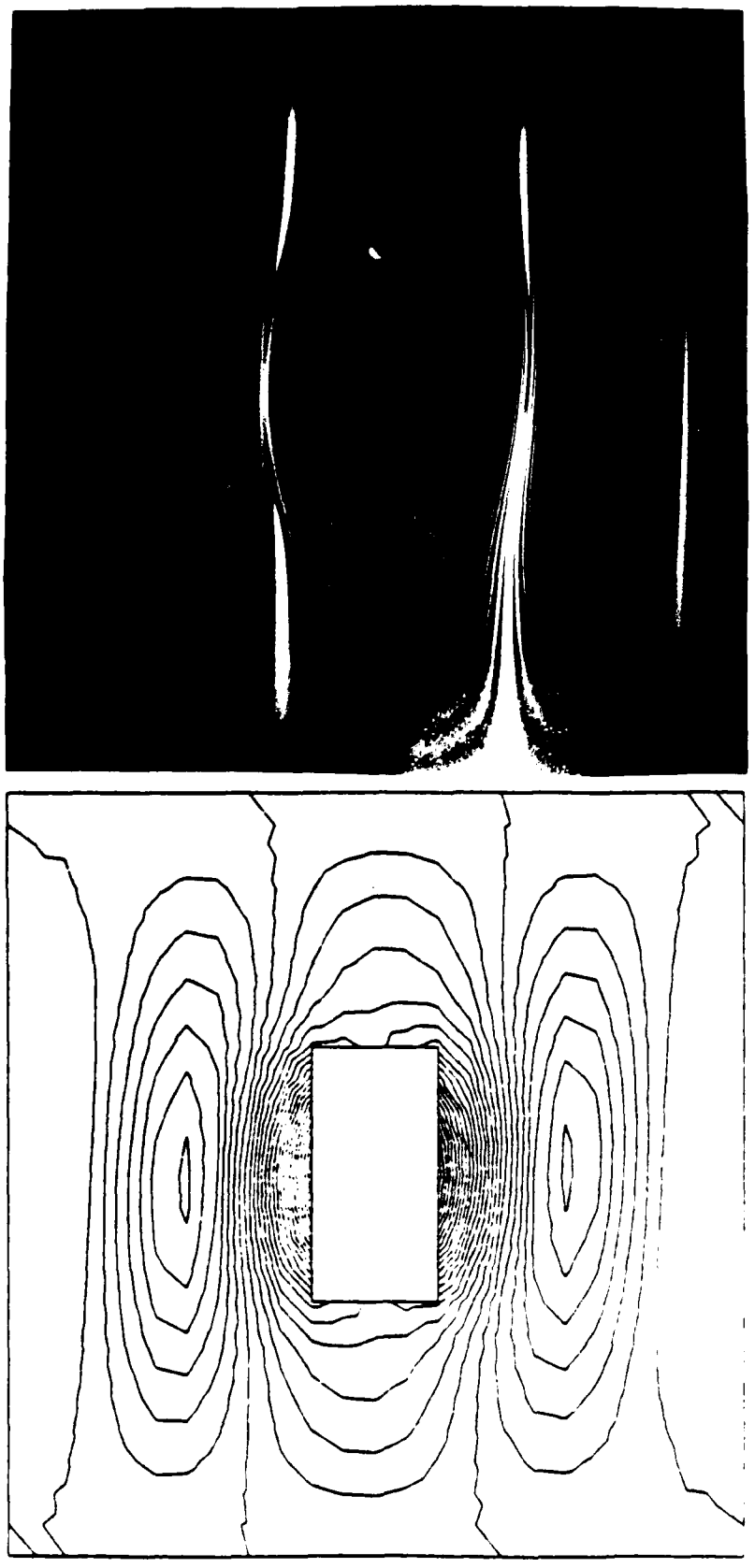

Figure 38 0° Panel--Mode 3

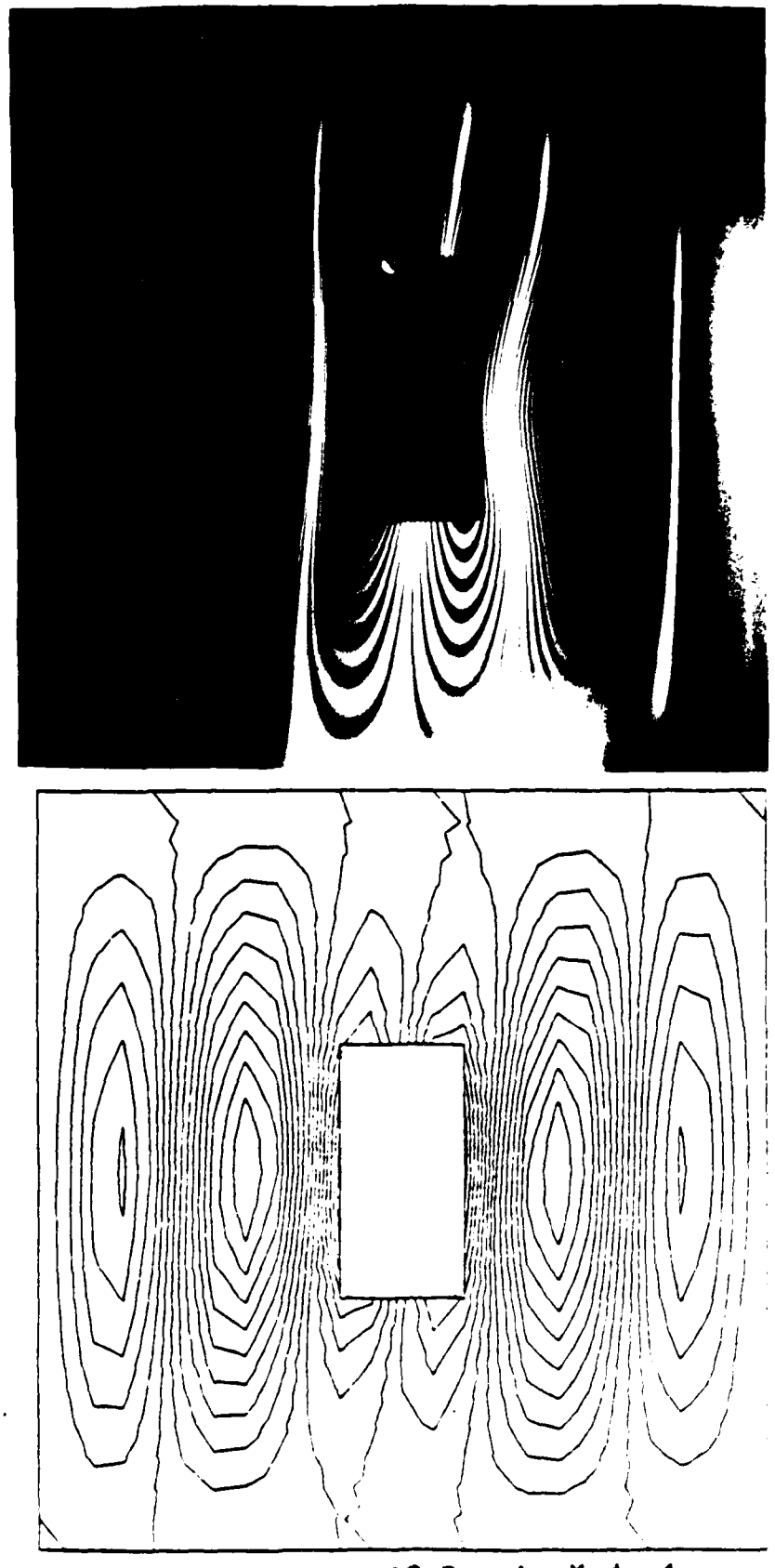

Figure 40 0° Panel--Mode 4

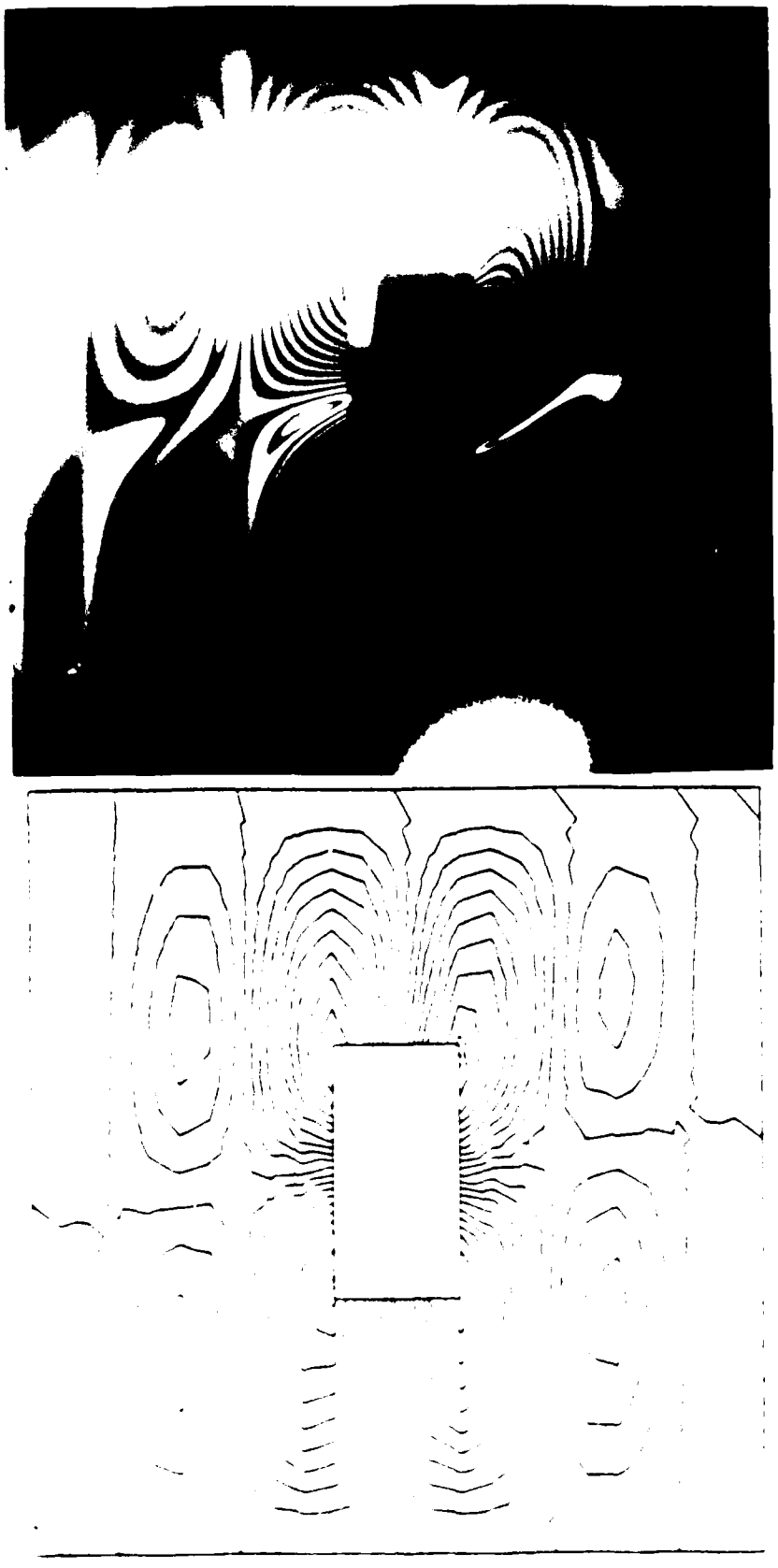

Figure 41 0° Panel--Mode 5

## The 90° Panel

The experimental and analytical results of the 90° panel are shown in Table 4.

Table 4. 90° Panel Results

| Mode | Natural Frequencies, Hz STAGSC-1 | Experiment | % Error |
|---|---|---|---|
| 1 | 514 | 527* | -2.5 |
| 2 | 525 | 496* | +5.8 |
| 3 | 632 | 608 | +3.9 |
| 4 | 675 | 705 | -4.3 |
| 5 | 686 | 731 | -6.2 |

* Mode Switch

The 90° panel was modelled analytically using a 25 x 25 mesh with a cutout from the automatic grid generator, as shown in Figure 42. Overall there is very good correlation between the experimental and analytical data for this panel. There was no evidence of any bias in the antinode regions. It seems that STAGSC-1 consistently overestimates the fundamental frequency and tends to under estimate the higher

natural frequencies for those panels with a cutout. The holographic results are compared to the analytical results in Figures 43-47.

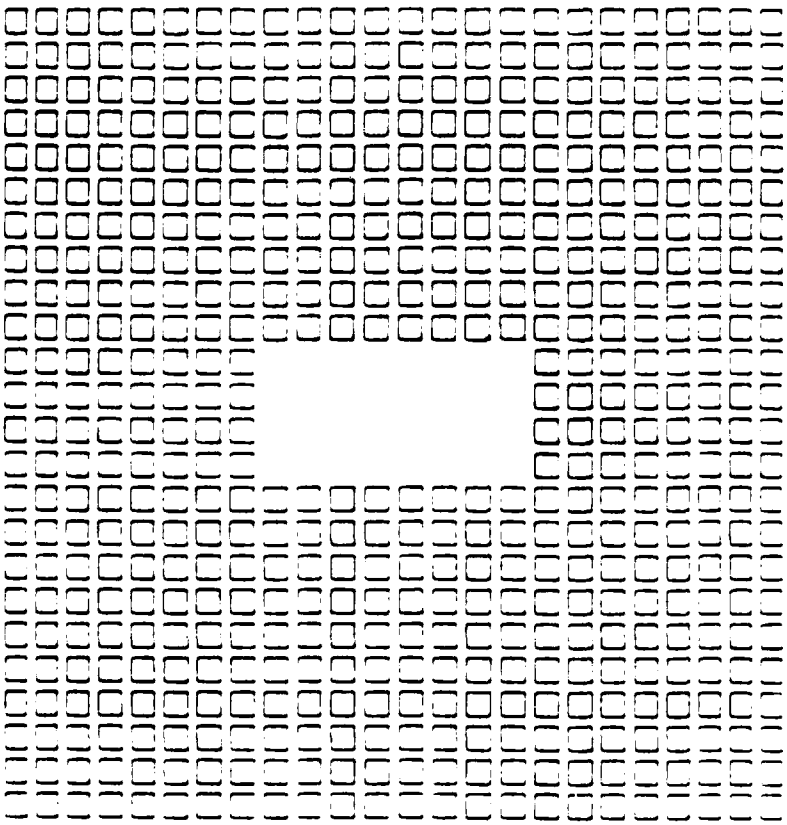

Figure 42 90° Panel -- 25 x 25 Mesh

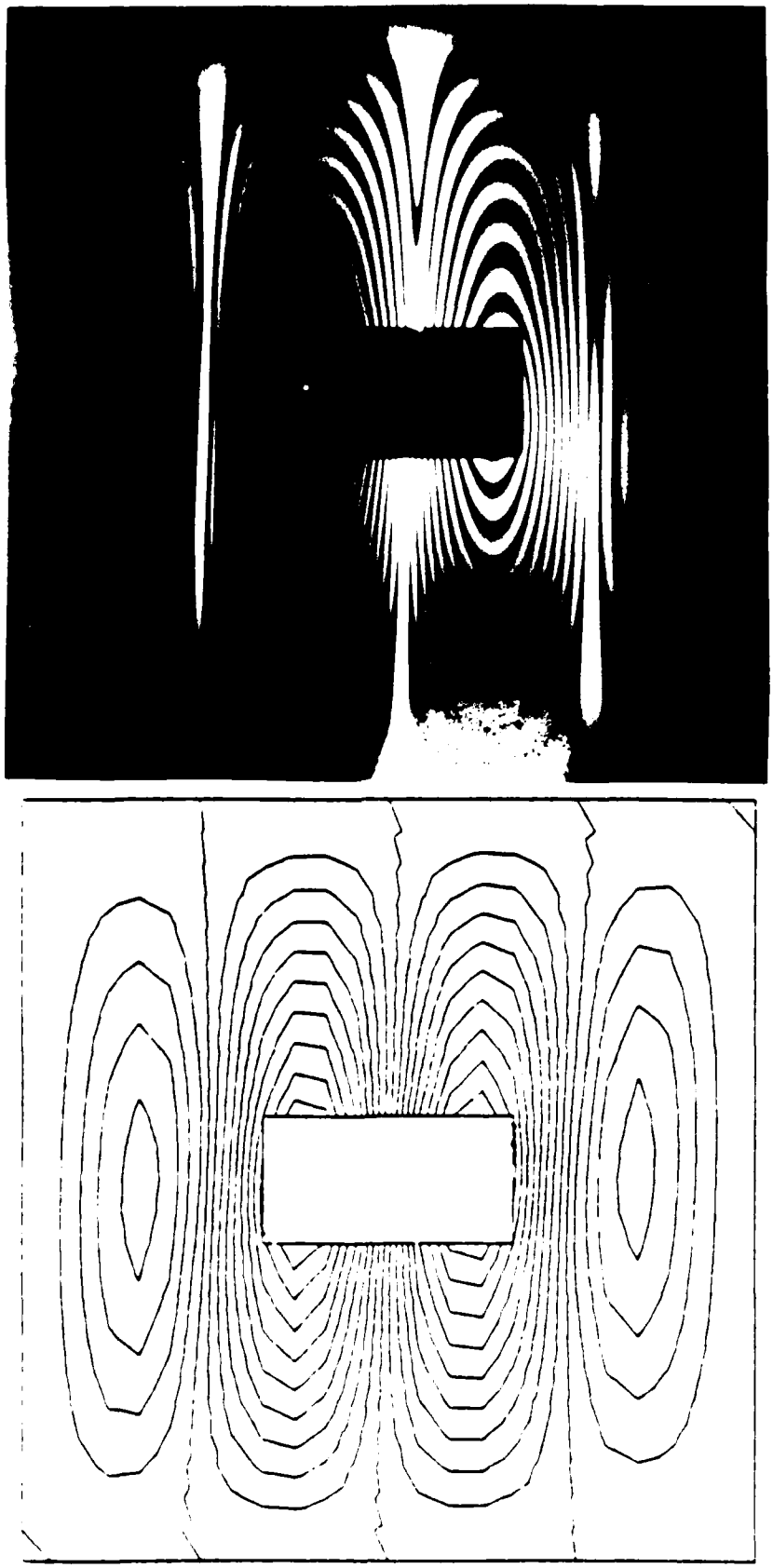

Figure 43 90° Panel--Mode 1

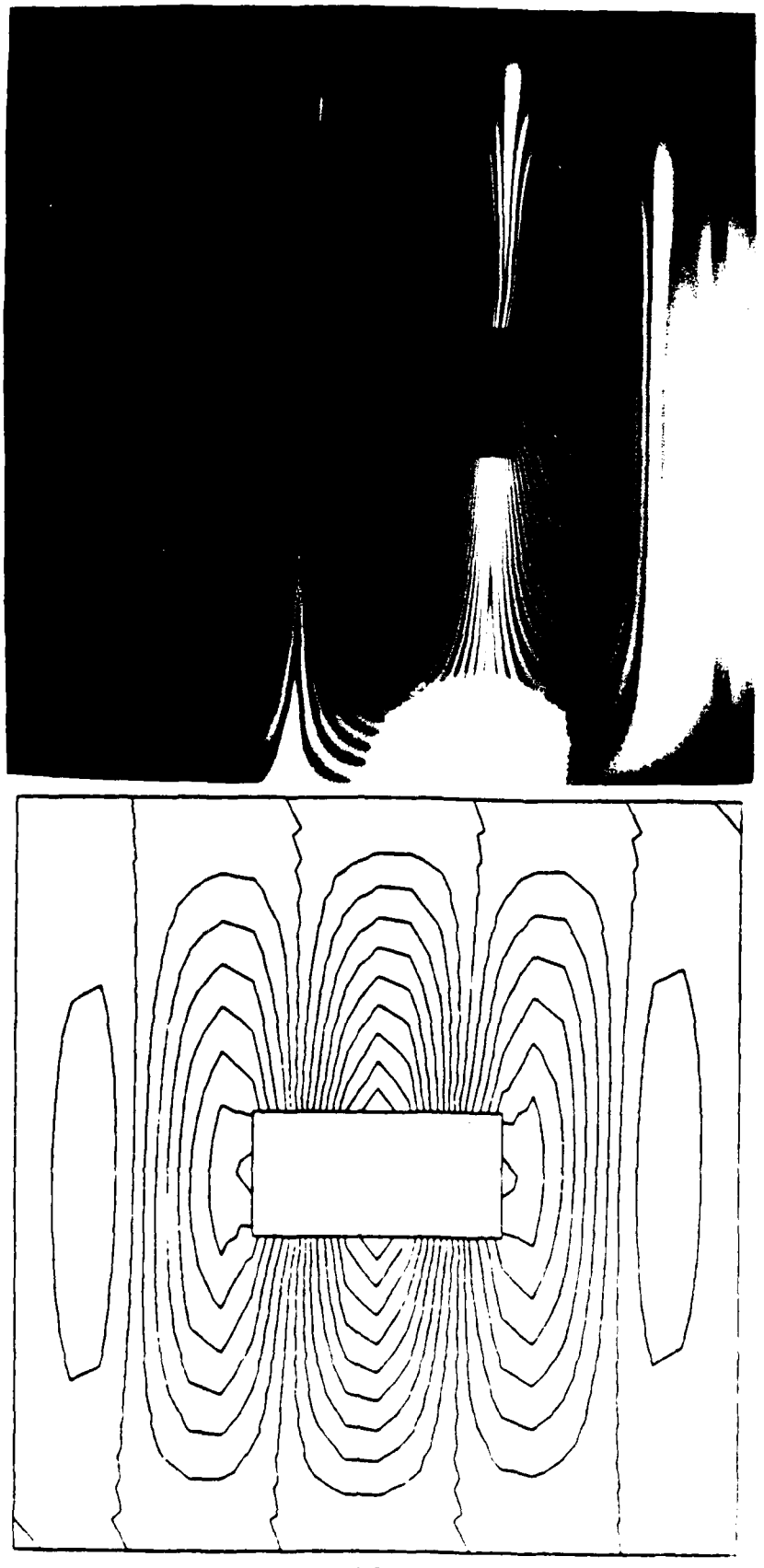

Figure 44 90° Panel--Mode 2

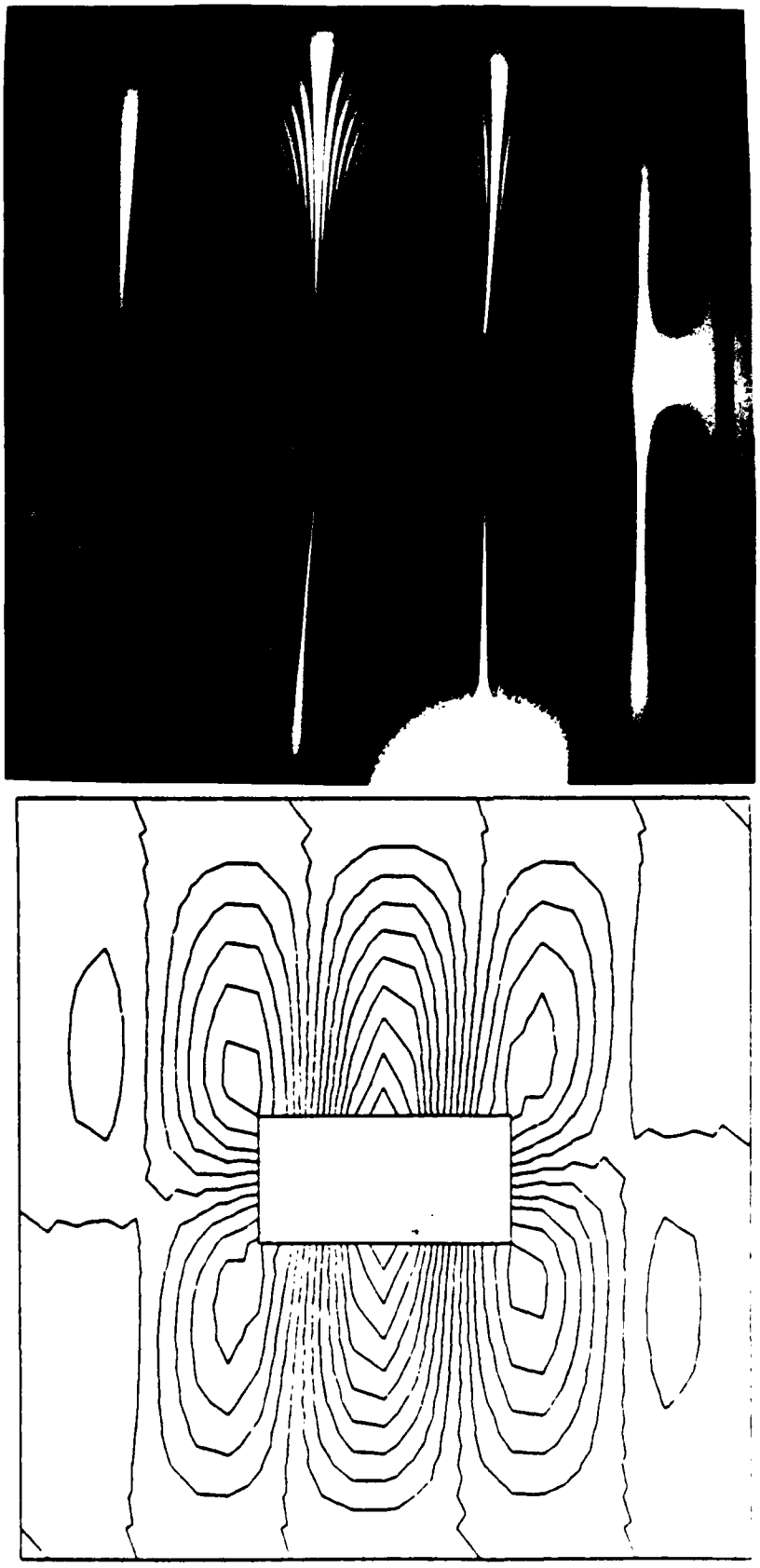

Figure 45 90° Panel--Mode 3

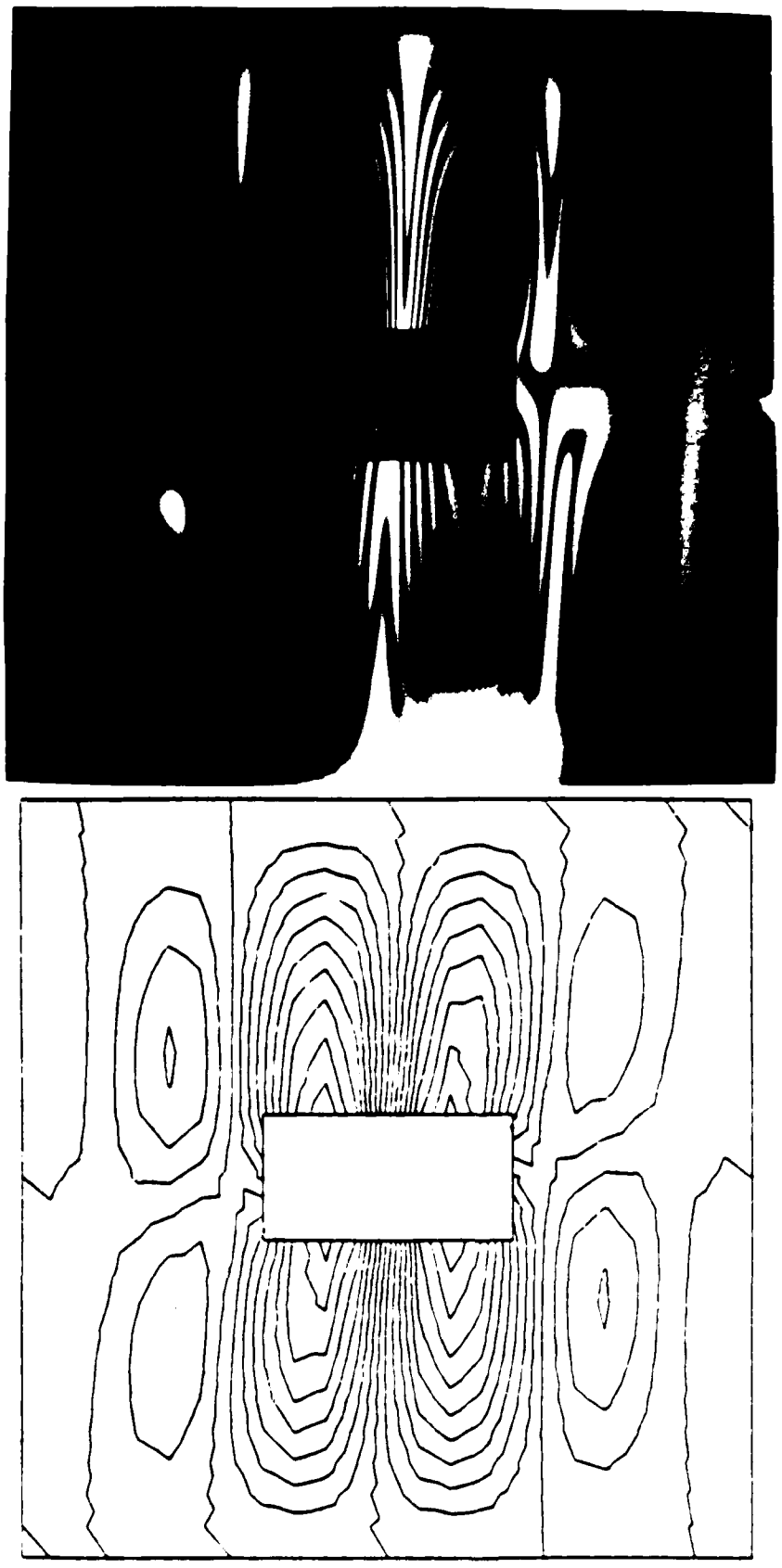

Figure 46 90° Panel--Mode 4

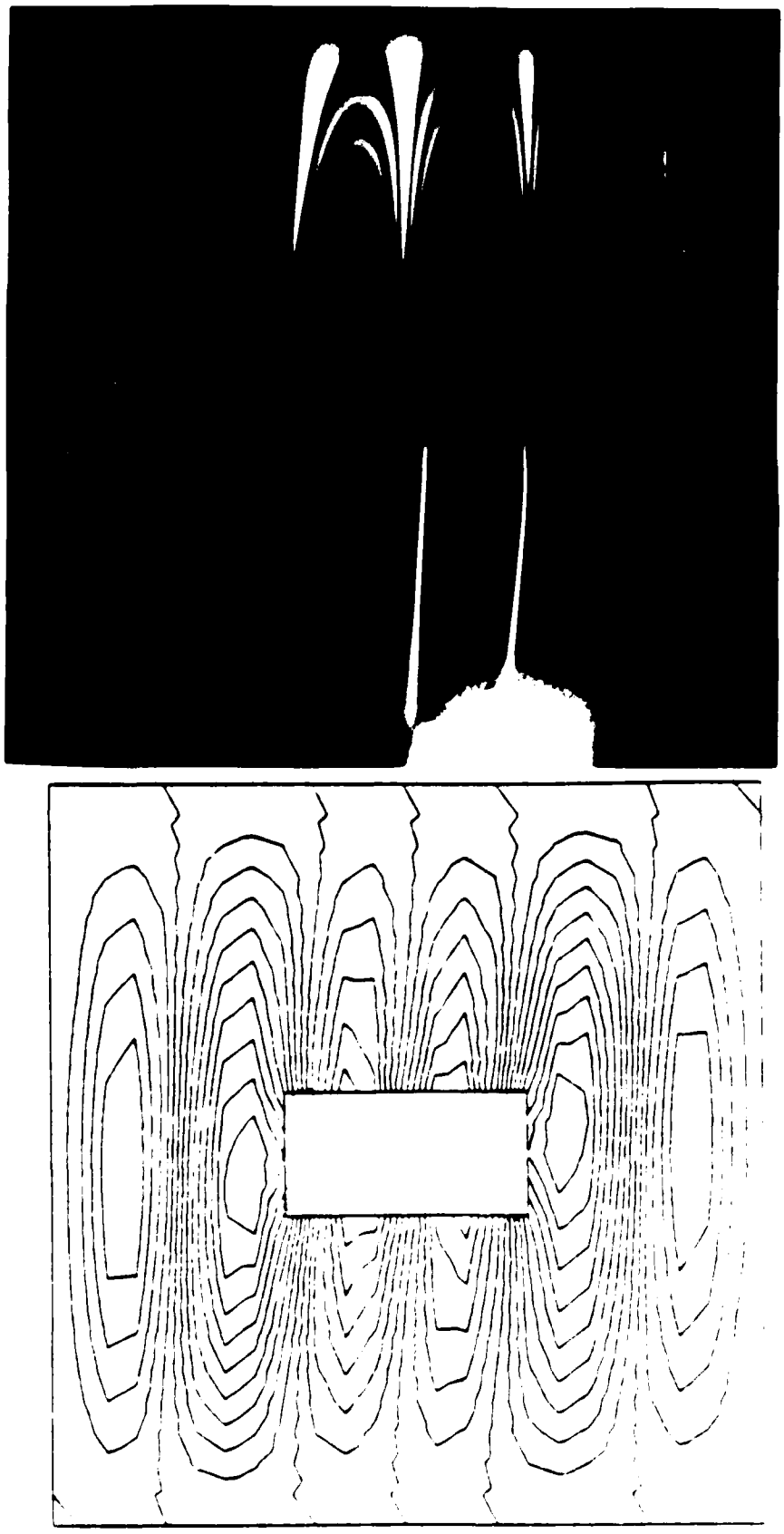

Figure 47 90° Panel--Mode 5

Comparing the results shown in figures 43 and 44 there is a mode switch that took place during the experimental analysis. When this was encountered, the boundary conditions immediately became suspect since STAGSC-1 has "perfect" boundary conditions while the test fixture does a best approximation of clamped-clamped boundary conditions. Therefore, all clamping screws were checked for proper tightness and only two were found to be under the 3 ft-lb requirement. The experiment was repeated with no change in results. The panel was then removed from the test fixture and remounted. The holographic testing was repeated with only a very slight change in the values for the natural frequencies but the mode switch was still present. I do not know why STAGSC-1 failed to predict the proper mode shape in this case. The peculiarities of the results should not preclude this data from being used since mode switching has been documented for flat plates [9] and for curved panels with large cutouts [3]. This phenomenon is discussed in greater detail in the cutout effects section.

## The +45° Panel

The modelling of the +/- 45° panels was quite interesting, especially when determining the mesh layout. The approach that was taken was to create a mesh that would facilitate the removal of both the +45° and -45° cutouts, yet when allowed to model a solid panel, would compare favorably with the results obtained for the automatic grid generated solid panel discussed previously. As a result of this philosophy, the mesh that was generated was a 45° mesh, as shown in Figure 48. The mesh generated for the solid panel by STAGSC-1 in the previous sections will be referred to as the 0° mesh. The 45° mesh created in Figure 48 had 68 triangular elements and 544 quadrilateral elements with 613 nodes. The first run with this configuration had 3342 active DOF using the STAGSC-1 320 and 410 elements. The results of the 45° mesh are compared to the 0° mesh in Table 5. Comparing the results for the two meshes, it was felt that the difference between them was much too large. The first step taken to resolve this was to increase the DOF by choosing a higher order element such as the 420 quadrilateral element shown in Figure 23. This change was easily made in the STAGSC-1 input deck.

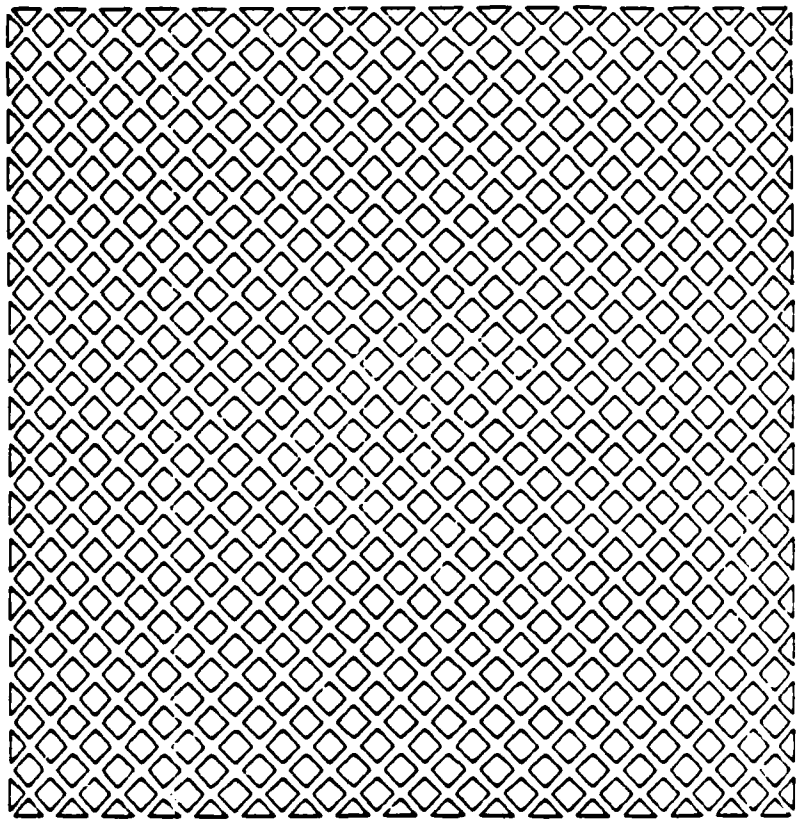

Figure 48 45° Mesh

Table 5 45° Mesh 320-410 Elements

| | Natural Frequency, Hz | | |
|---|---|---|---|
| Mode | 0° Mesh | 45° Mesh | % Difference |
| 1 | 506 | 587 | 13.8 |
| 2 | 524 | 611 | 14.2 |
| 3 | 693 | 769 | 9.9 |
| 4 | 703 | 785 | 10.5 |
| 5 | 770 | 844 | 8.8 |

The 420 element is made of two 320 elements as shown in Figure 20. As a result, the mesh is made entirely of triangular elements as shown in Figure 49. This increased the number of active DOF to 5038. The results of these changes are shown in Table 6. Comparing the 0° and 45° mesh in Table 6, the fundamental and second natural frequencies show slightly better agreement than the 320-410 mesh. It is interesting to note that the natural frequencies of the 320-420 mesh are diverging from the results of the 0° mesh.

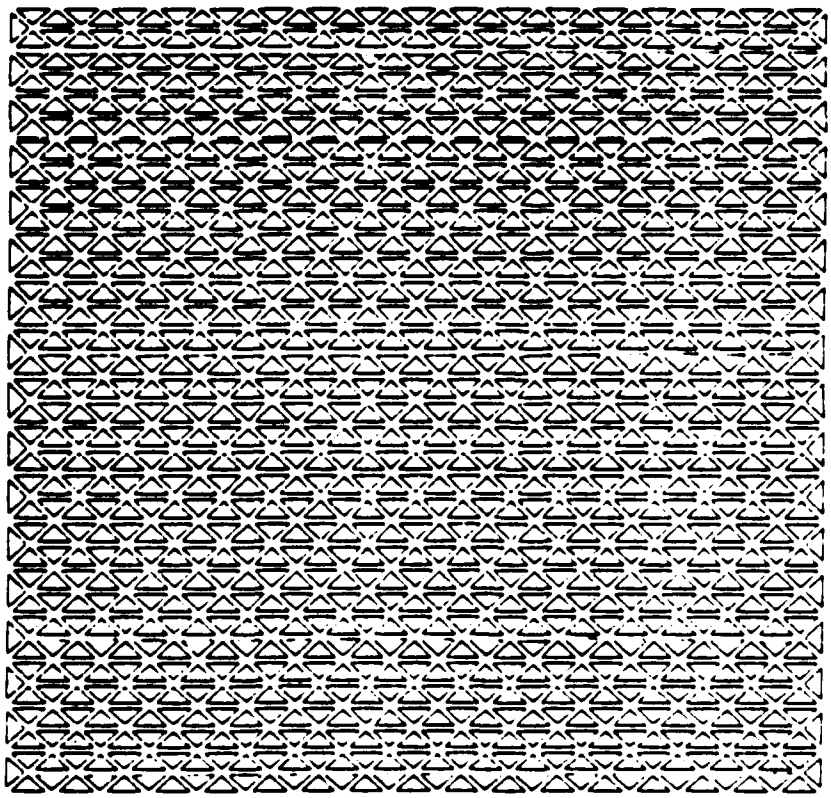

Figure 49 45° Mesh 320-420 Elements

Table 6 45° Mesh 320-420 Elements

| | Natural Frequency, Hz | | |
|---|---|---|---|
| Mode | 0° Mesh | 45° Mesh | % Difference |
| 1 | 506 | 573 | 11.7 |
| 2 | 524 | 602 | 13.0 |
| 3 | 693 | 812 | 14.7 |
| 4 | 703 | 860 | 18.3 |
| 5 | 770 | 950 | 19.0 |

One reason for the divergence can probably be attributed to the 320 element. As shown in Figure 20, the 320 element does not have an out of plane rotation as a degree of freedom and since this vibration problem is primarily an out of plane problem, this could introduce error. Although the model was too stiff with the 320 and 420 elements the mode shapes compared nicely with the mode shapes of the 0° mesh. A mesh was generated consisting entirely of 322-422 elements at this point. The results of this run are not available since the run exceeded memory availability on the VAX 11-785. At the point of termination, the program had been executing in excess of 5000 cpu seconds and convergence was still not reached. At this point a new approach and analysis had to be taken.

There appeared to be an artificial stiffness being incorporated into the mesh due to its elemental

configuration. Cook [13] states that the inexperienced person may generate a grid that artificially increases the stiffness of a mesh due to element selection and boundary conditions. In order to determine if this problem was present in the 45° mesh and if it was due to the triangles along the boundary, the triangles were removed as shown in Figure 50.

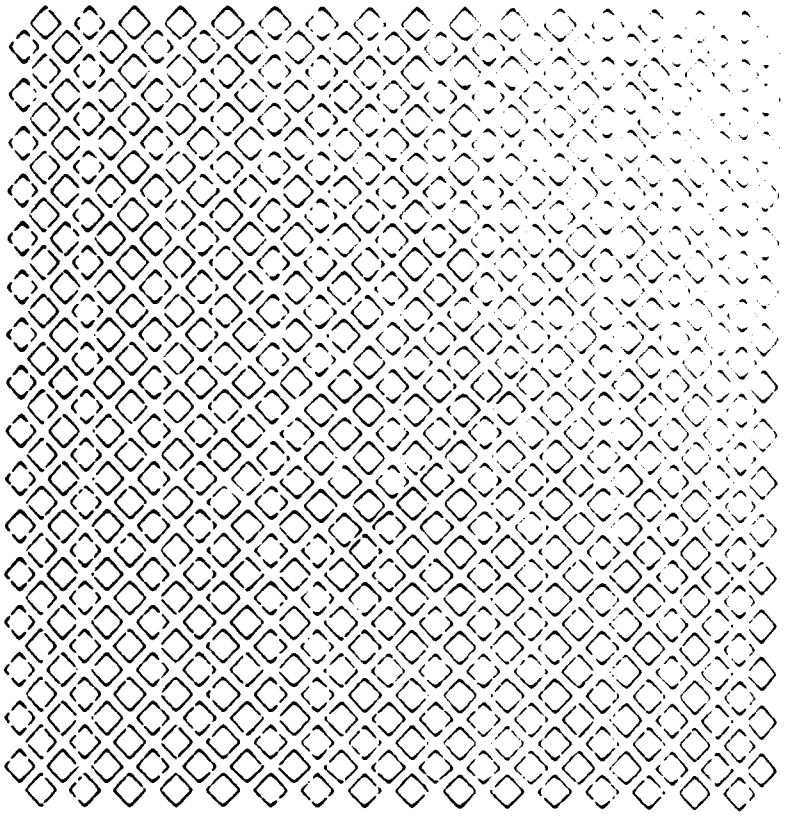

Figure 50 45° Mesh Triangles Removed

As one would expect, the results showed insignificant changes in the natural frequencies from the 320-420 mesh. Since there was little effect due to the removal of the triangular elements, it was apparent that an analysis of the mesh was needed.

The first step was to determine if the STAGSC-1 code was operating properly when the user was defining a grid in the input deck. To do this, a 0° mesh, as in Figure 25, was created and entered in STAGSC-1. The results of this run gave exact agreement to the STAGSC-1 generated mesh. Therefore, now there were only two differences in the 45° mesh from the 0° mesh. The first was the triangular elements along the boundary, the second was the quadrilateral elements that were rotated 45°. To see if either of these differences influenced the panel model an isotropic case was run on STAGSC-1 comparing the 45° and 0° mesh. Surprisingly, there was a difference between the two runs that amounted to a 10% difference in the natural frequencies.

Based on these results, a different grid design was developed that incorporated only the 410 quadrilateral elements and minimized orientation changes around the boundary. This grid design is shown in Figure [illegible] the 45° mesh was maintained in the center part [illegible] mesh in Figure 51, again to facilitate the [illegible] cutouts.

AD-A170 630 EFFECTS OF CUTOUT ORIENTATIONS ON NATURAL FREQUENCIES 2/2
AND MODE SHAPES OF..(U) AIR FORCE INST OF TECH
WRIGHT-PATTERSON AFB OH SCHOOL OF ENGI.. G J CYR
UNCLASSIFIED DEC 86 AFIT/GAE/AA/86D-3 F/G 11/4 NL

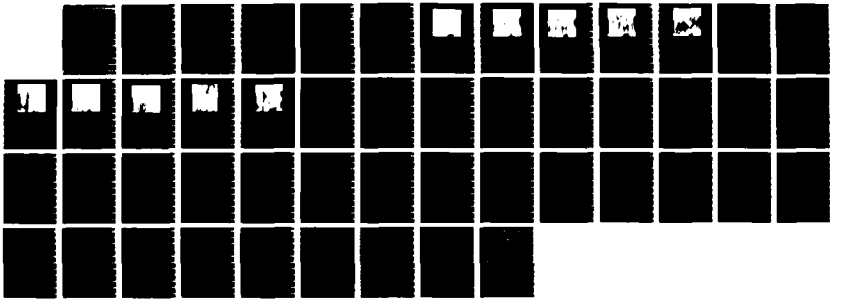

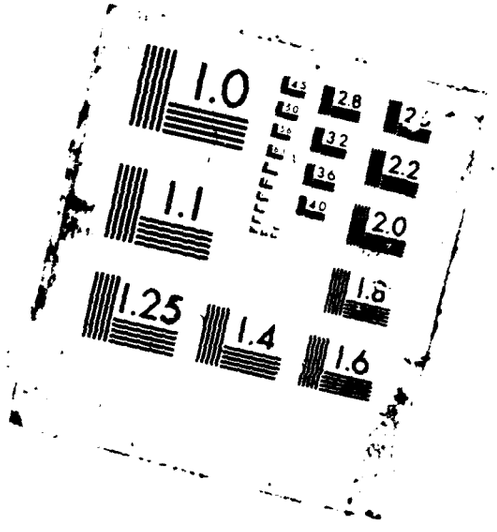
1.0
1.1
1.25
1.4
1.6
2.8
3.2
3.6
4.0
2.2
2.0
1.8

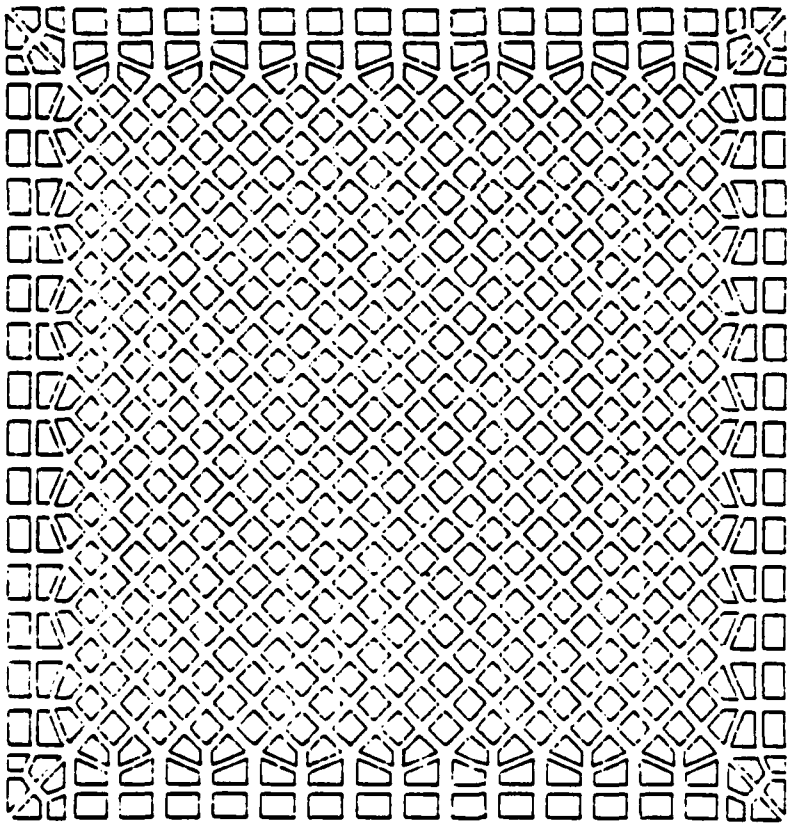

Figure 51 Complex 45° Mesh

The results for the mesh generated in Figure 51 are shown in Table 7.

Table 7 Complex 45° Mesh

| | Natural Frequency, Hz | | |
|---|---|---|---|
| Mode | 0° Mesh | 45° Mesh | % Difference |
| 1 | 506 | 585 | 13.5 |
| 2 | 524 | 610 | 14.1 |
| 3 | 693 | 762 | 9.1 |
| 4 | 703 | 784 | 10.3 |
| 5 | 770 | 842 | 8.6 |

These errors were still felt to be too high to have a high confidence level for the runs with the cutouts. It still appeared that the orientation of the mesh itself was a contributing factor to the lack of agreement to the 0° mesh results.

As a result, the mesh was designed so as to minimize the changes in element orientation throughout the grid. The new mesh is shown in Figure 52. The only orientation change occurs in the immediate vicinity of the cutout. The results of this mesh are shown in Table 8.

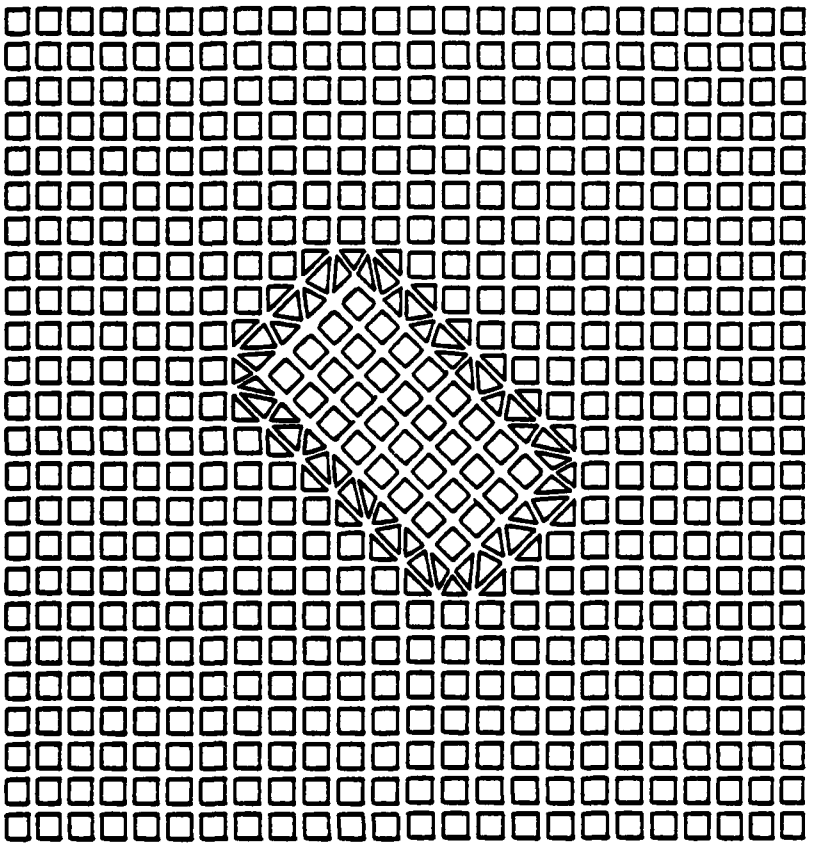

Figure 52 Final Mesh 410-320 Elements

Table 8 Final Mesh 410-320 Elements

| | Natural Frequency, Hz | | |
|---|---|---|---|
| Mode | 0° Mesh | 45° Mesh | % Difference |
| 1 | 506 | 527 | 4.0 |
| 2 | 524 | 557 | 5.9 |
| 3 | 693 | 731 | 5.2 |
| 4 | 703 | 764 | 8.0 |
| 5 | 770 | 803 | 4.1 |

With this mesh design, the cutout at +45° was removed. The mesh with a +45° cutout is shown in Figure 53. The results of the numerical and experimental analysis are shown in Table 9.

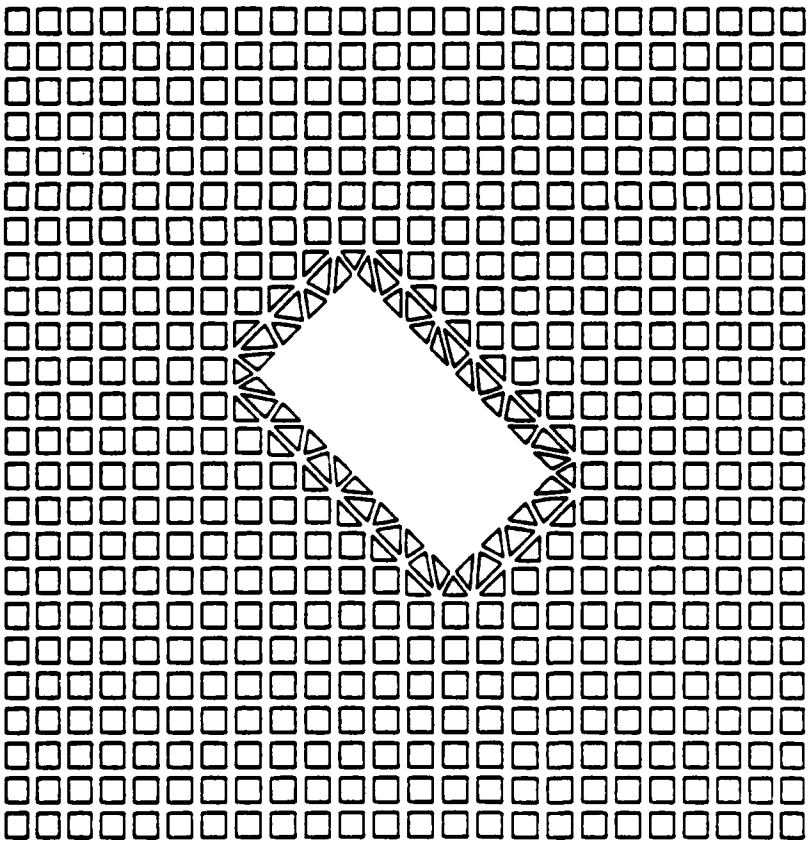

Figure 53 +45° Cutout 320-410 Elements

Table 9 +45° Mesh 320-410 Elements

| | Natural Frequency, Hz | | |
|---|---|---|---|
| Mode | STAGSC-1 | Experiment | % Error |
| 1 | 519 | 513 | +1.2 |
| 2 | 545 | 533 | +2.3 |
| 3 | 651 | 663 | -1.8 |
| 4 | 673 | 700 | -3.9 |
| 5 | 723 | 764 | -5.4 |

Once the mesh was properly designed, the correlation between the analytical and experimental results are very good for this cutout. A comparison between STAGSC-1 and the holograms are shown in figures 54-58. As stated earlier, mode 2 and 4 were the most difficult to excite. The task was best accomplished with one horn. No biasing or mode switching occurred for this panel.

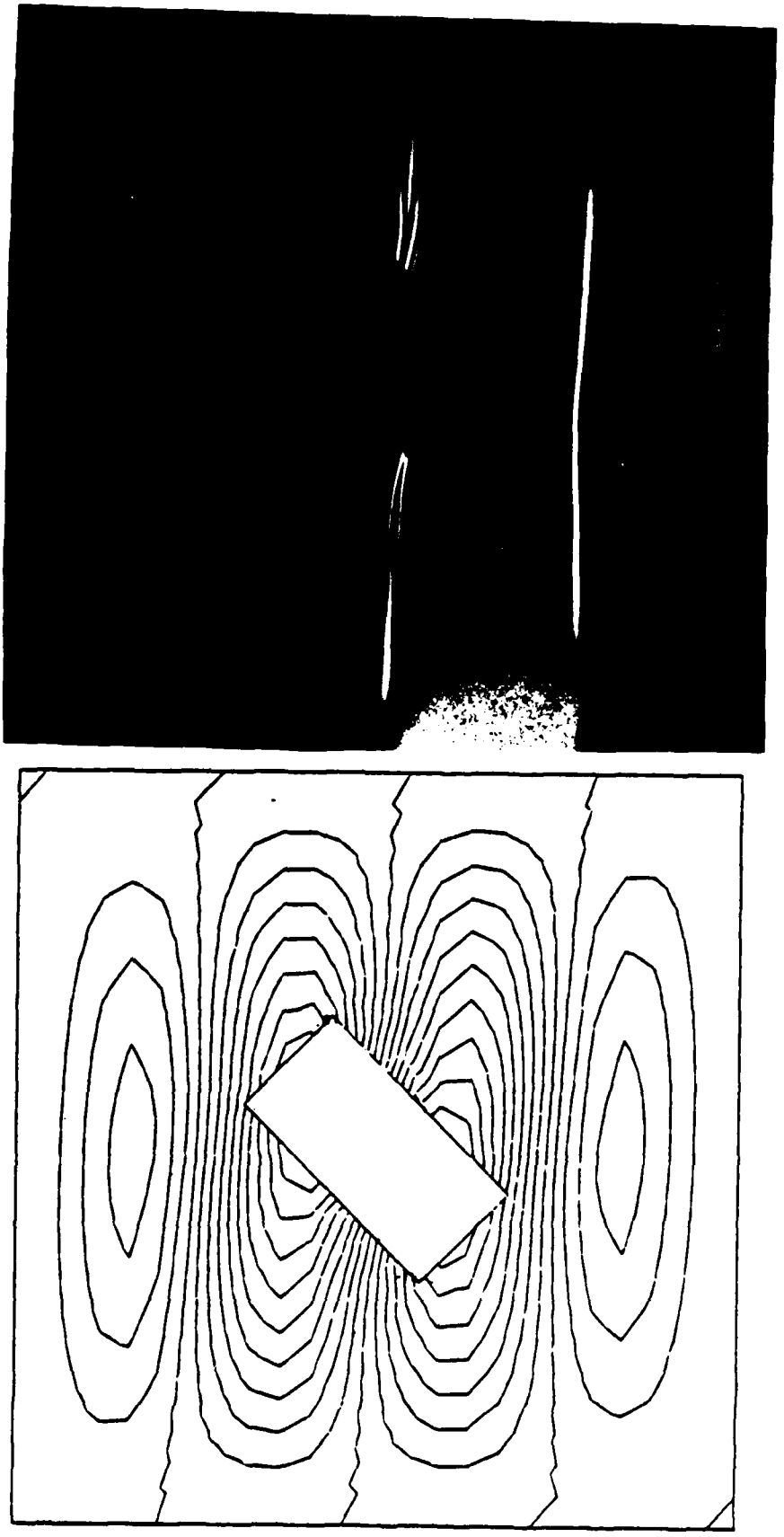

Figure 54 +45° Panel Mode 1

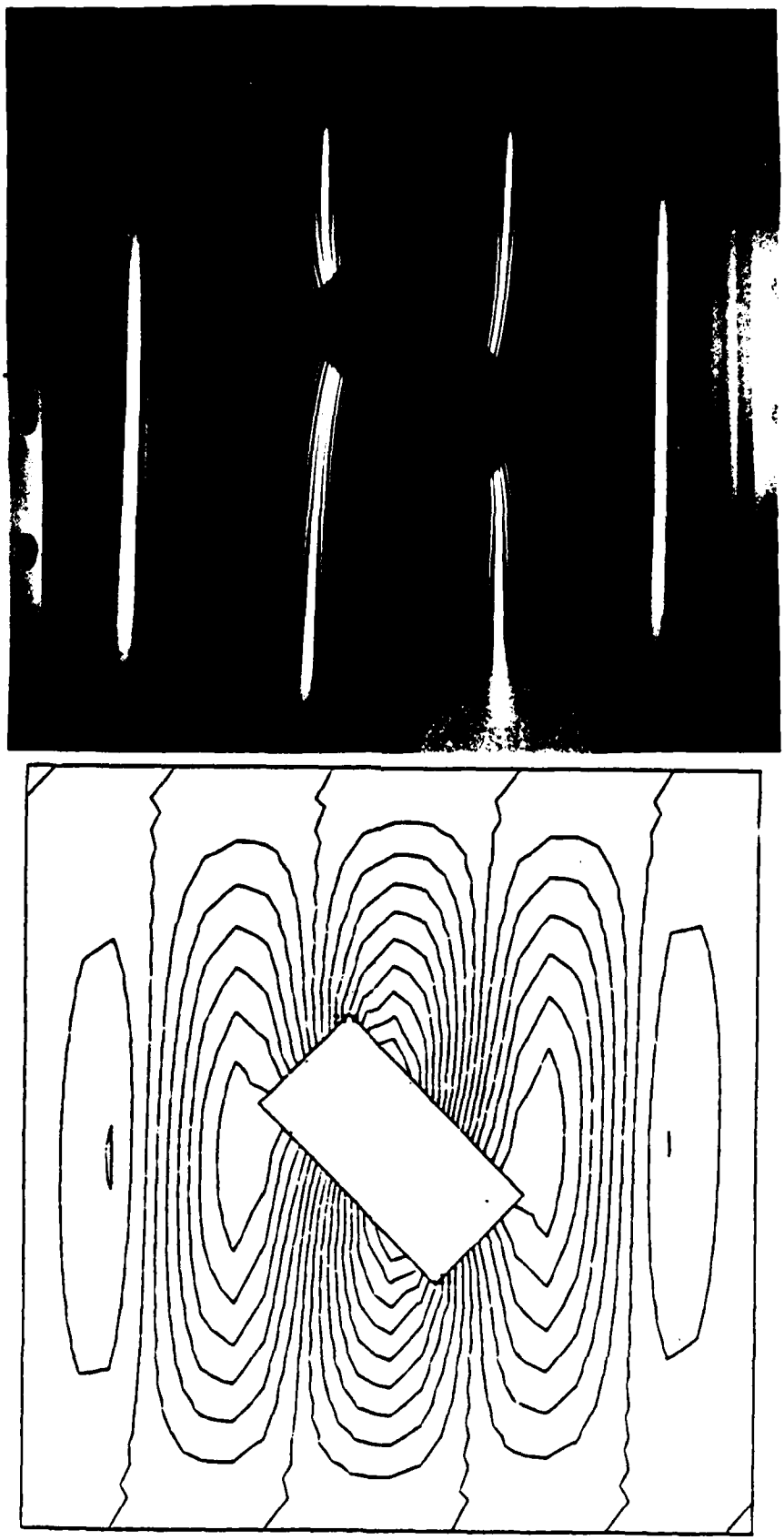

Figure 55 +45° Panel Mode 2

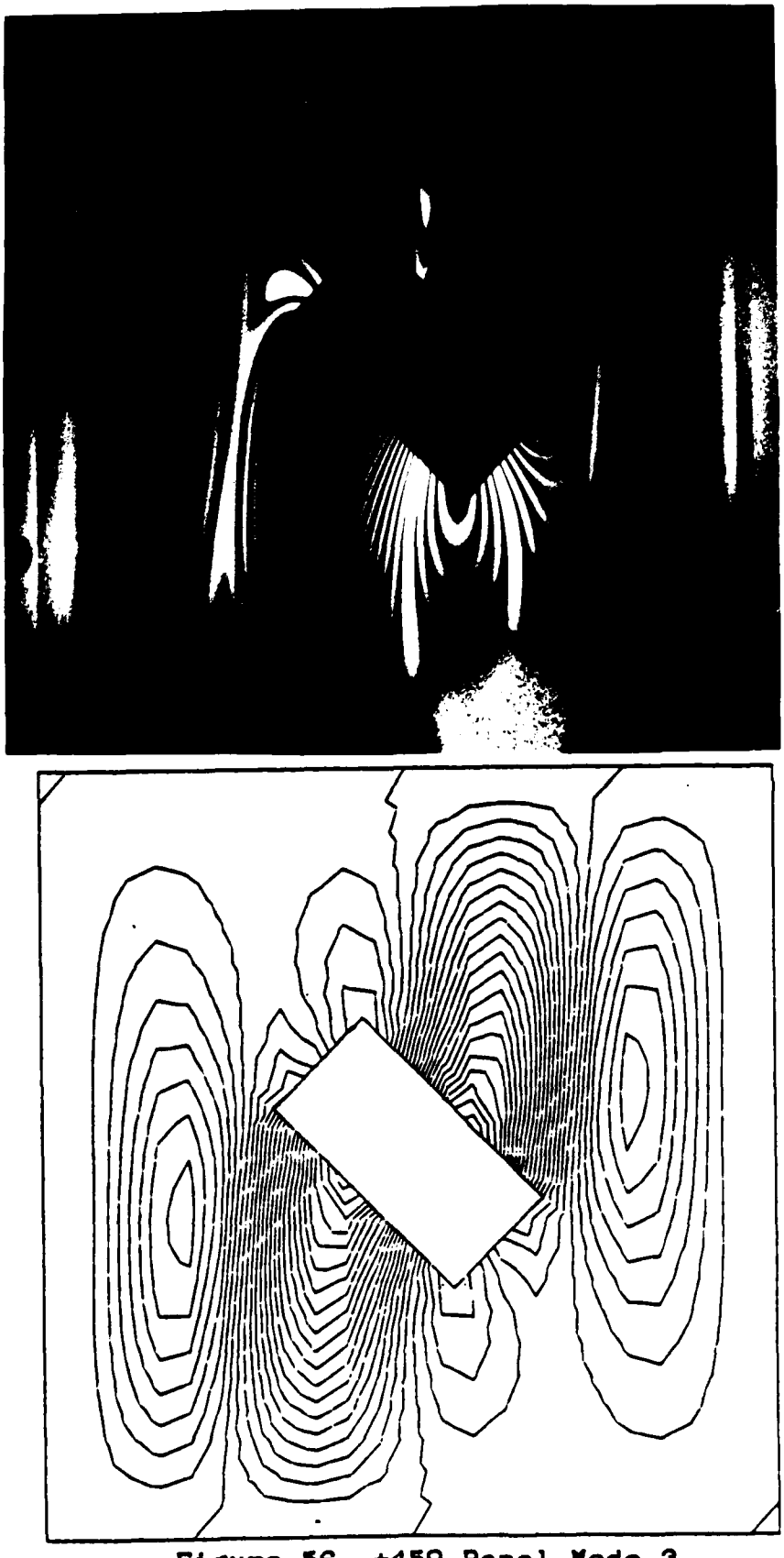

Figure 56 +45° Panel Mode 3

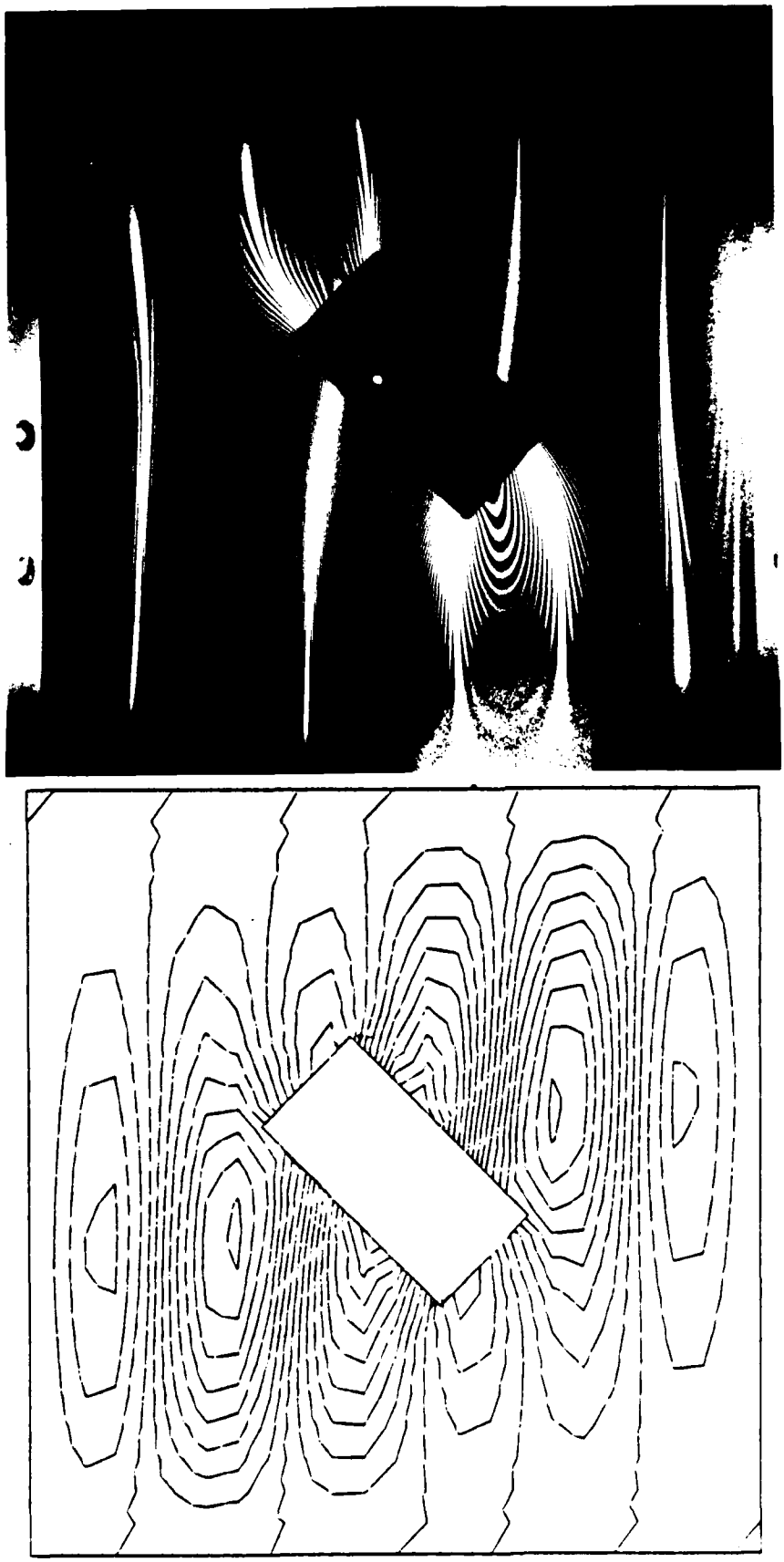

Figure 57 +45° Panel Mode 4

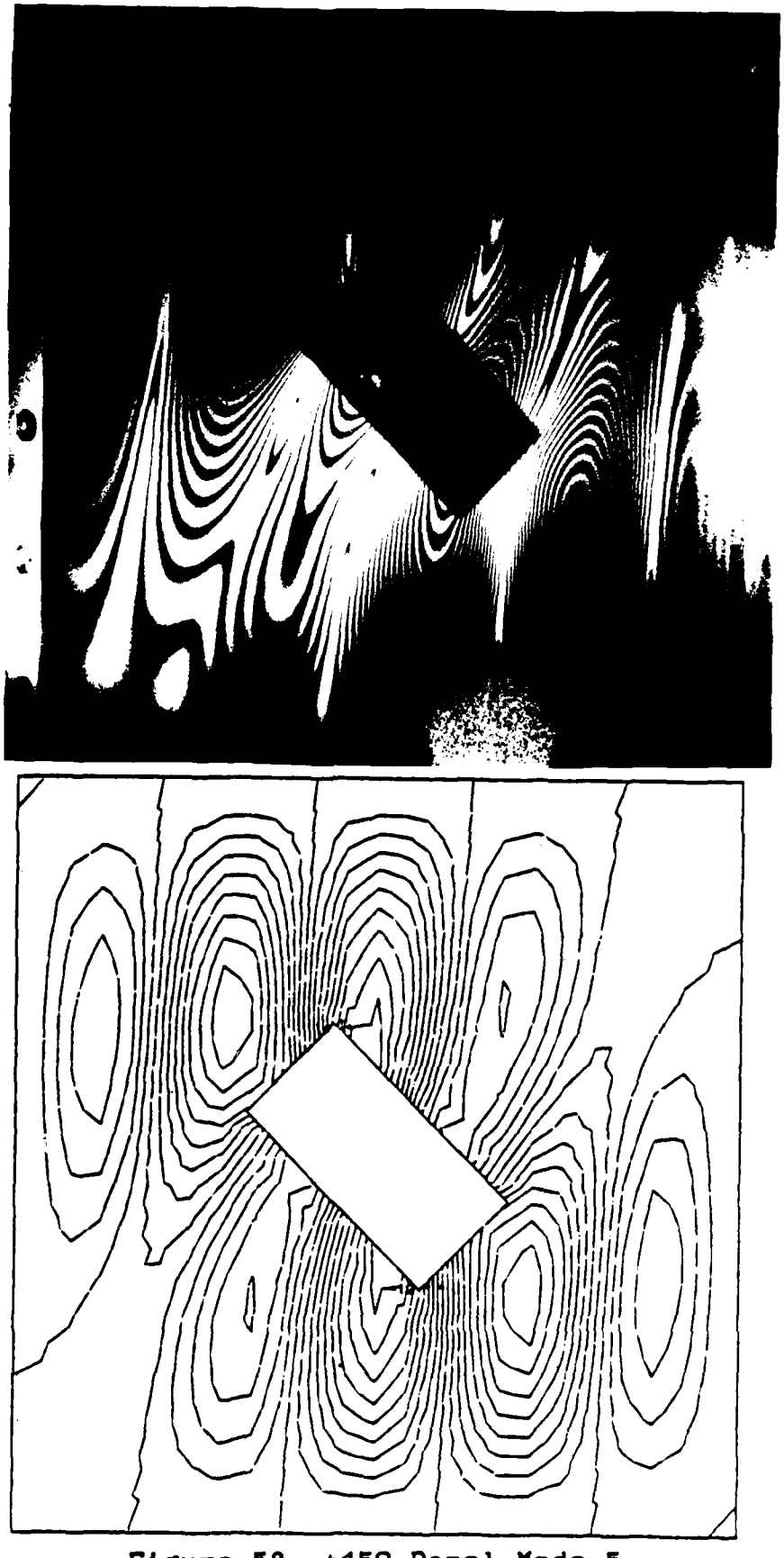

Figure 58 +45° Panel Mode 5

## The -45° Panel

Once the problems in modeling the panels were solved, the -45° panel analysis was not difficult to accomplish. The mesh used in the -45° panel is shown in Figure 59. Table 10 shows the comparison of the natural frequencies between the STAGSC-1 analysis and experimental results. Figures 60-64 compare the mode shapes from the holographic results and the STAGSC-1 analysis.

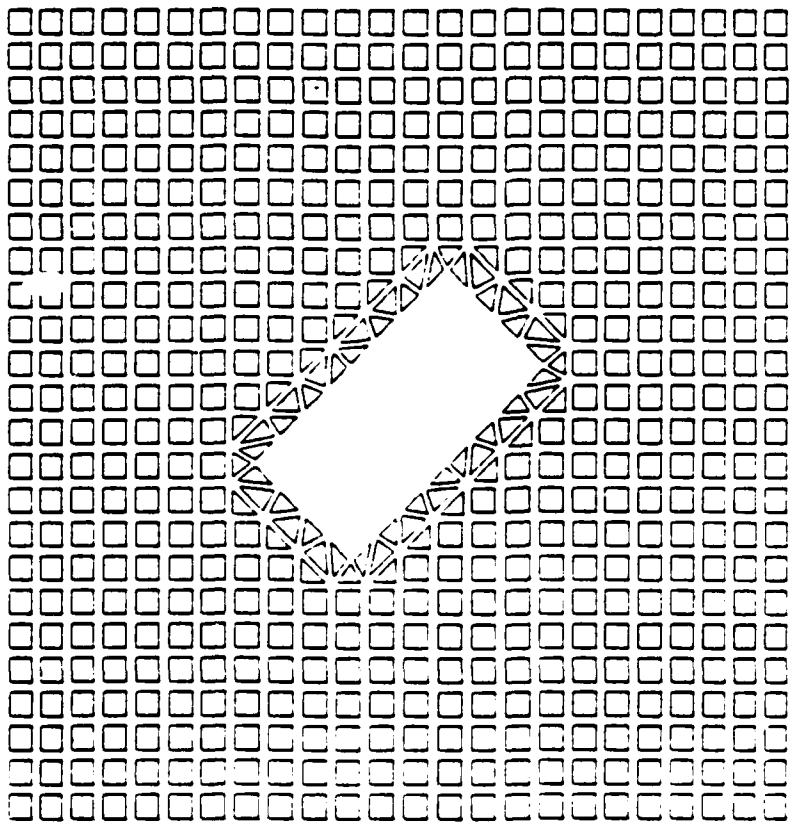

Figure 59 -45° Cutout 320-410 Elements

Table 10 -45° Cutout Results

| Mode | Natural Frequency, Hz STAGSC-1 | Experiment | % Error |
|---|---|---|---|
| 1 | 524 | 494 | +6.1 |
| 2 | 551 | 519 | +6.2 |
| 3 | 664 | 608 | +9.2 |
| 4 | 674 | 625 | +7.8 |
| 5 | 744 | 794 | -6.3 |

This panel overall had only fair correlation with the STAGSC-1 analysis. The magnitude of the errors seem to indicate that there was a systematic error introduced. This error could have been introduced either through the STAGSC-1 analysis by an improper nodal coordinate (this is possible since the nodal coordinates along the cutout were generated by hand and doubled checked by hand) that could stiffen the panel locally, or the test fixture allen head bolts could have loosened slightly during testing. Comparing mode 5, the points of maximum amplitude of the STAGSC-1 analysis do not correspond with the experimental results. This could be due to the error mentioned above. As with the +45° cutout, there was no evidence of biasing or mode switching.

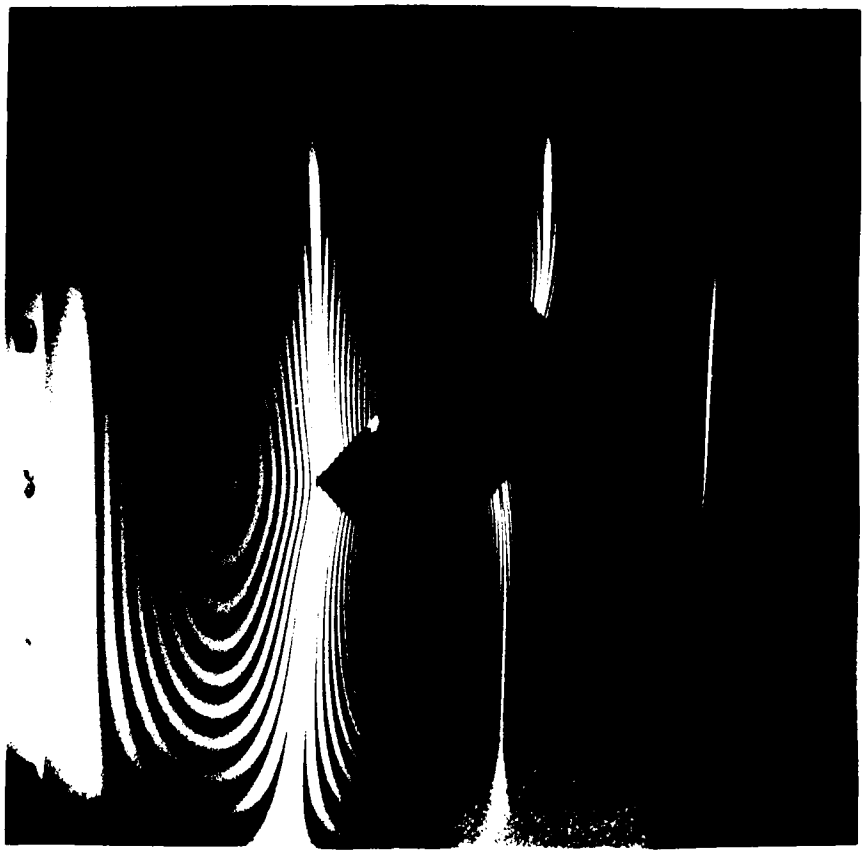

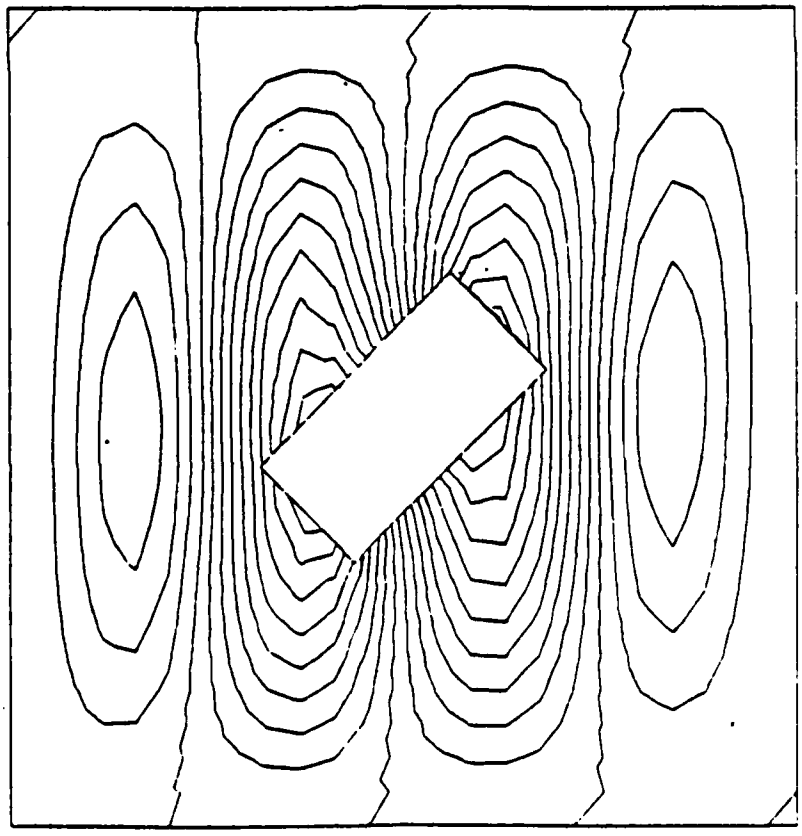

Figure 60 -45° Panel Mode 1

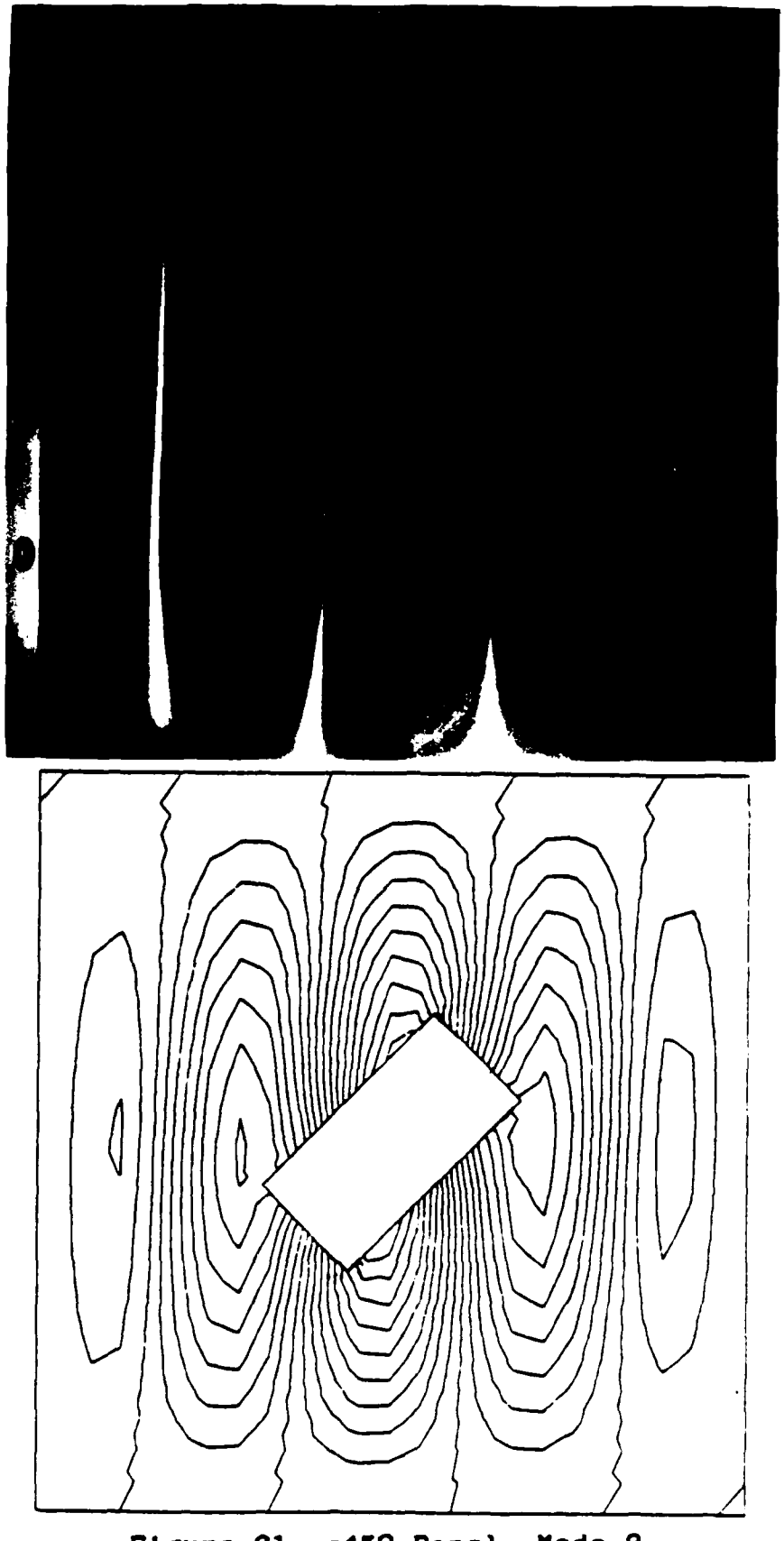

Figure 61 -45° Panel Mode 2

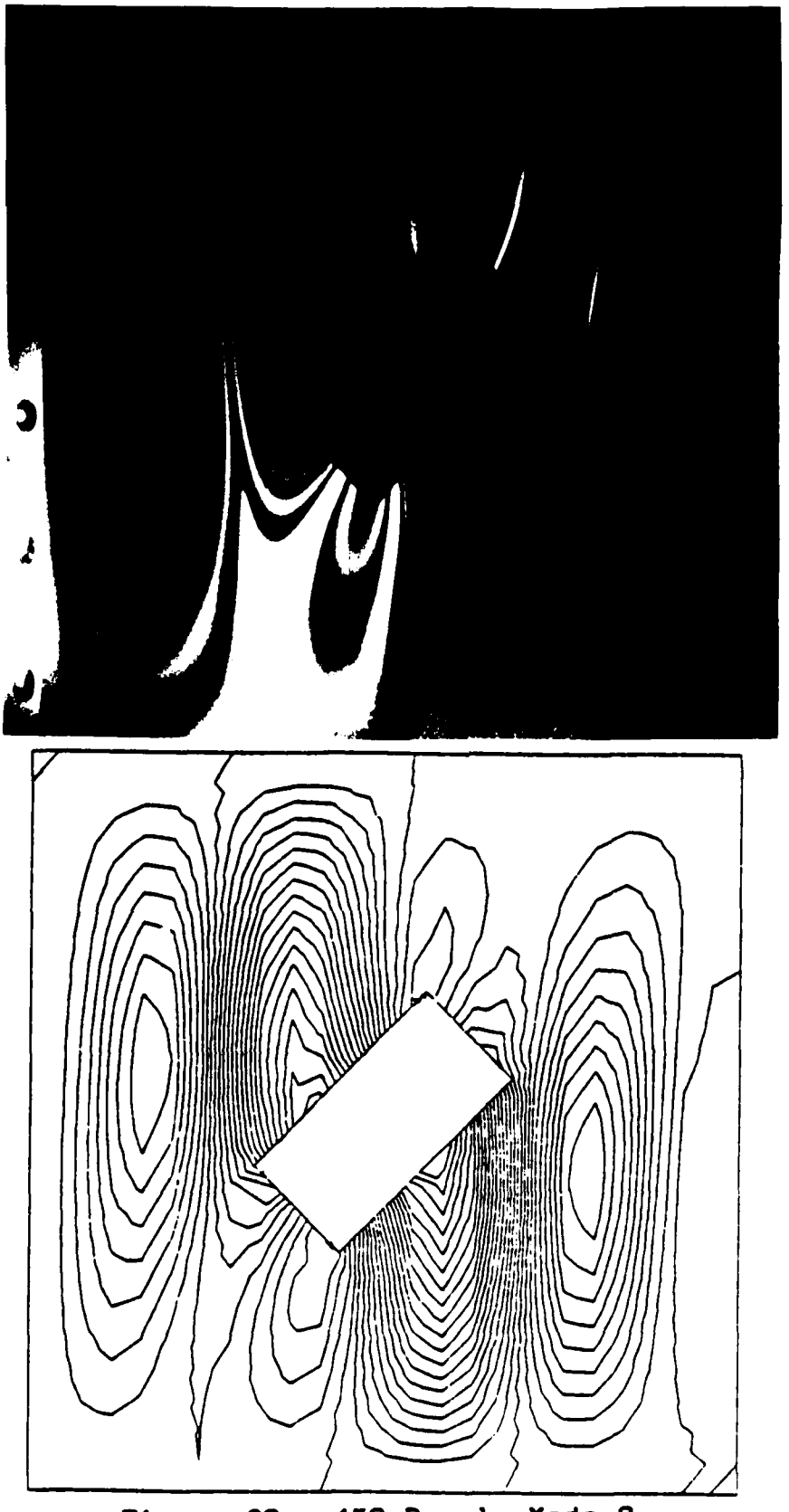

Figure 62 -45° Panel Mode 3

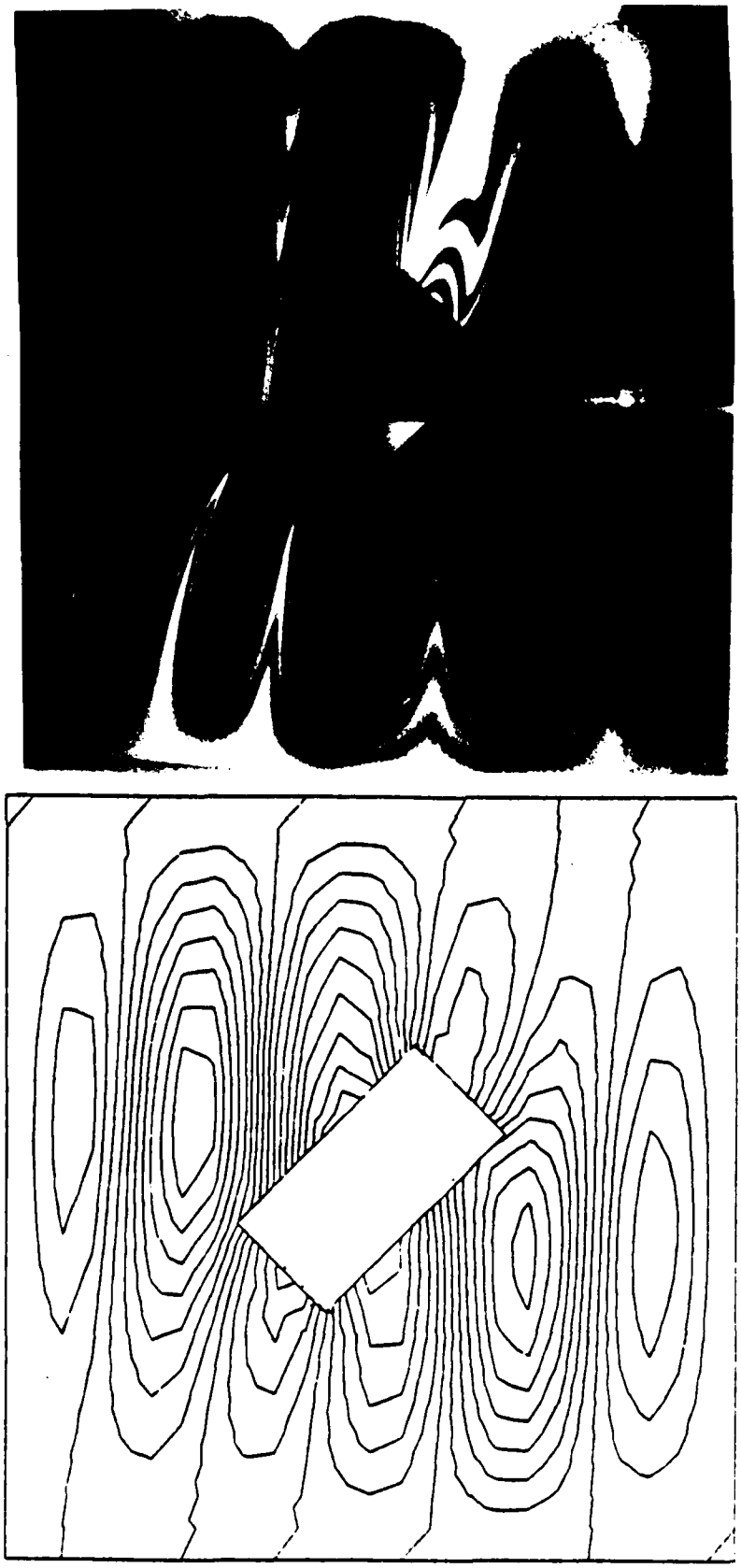

Figure 63 -45° Panel Mode 4

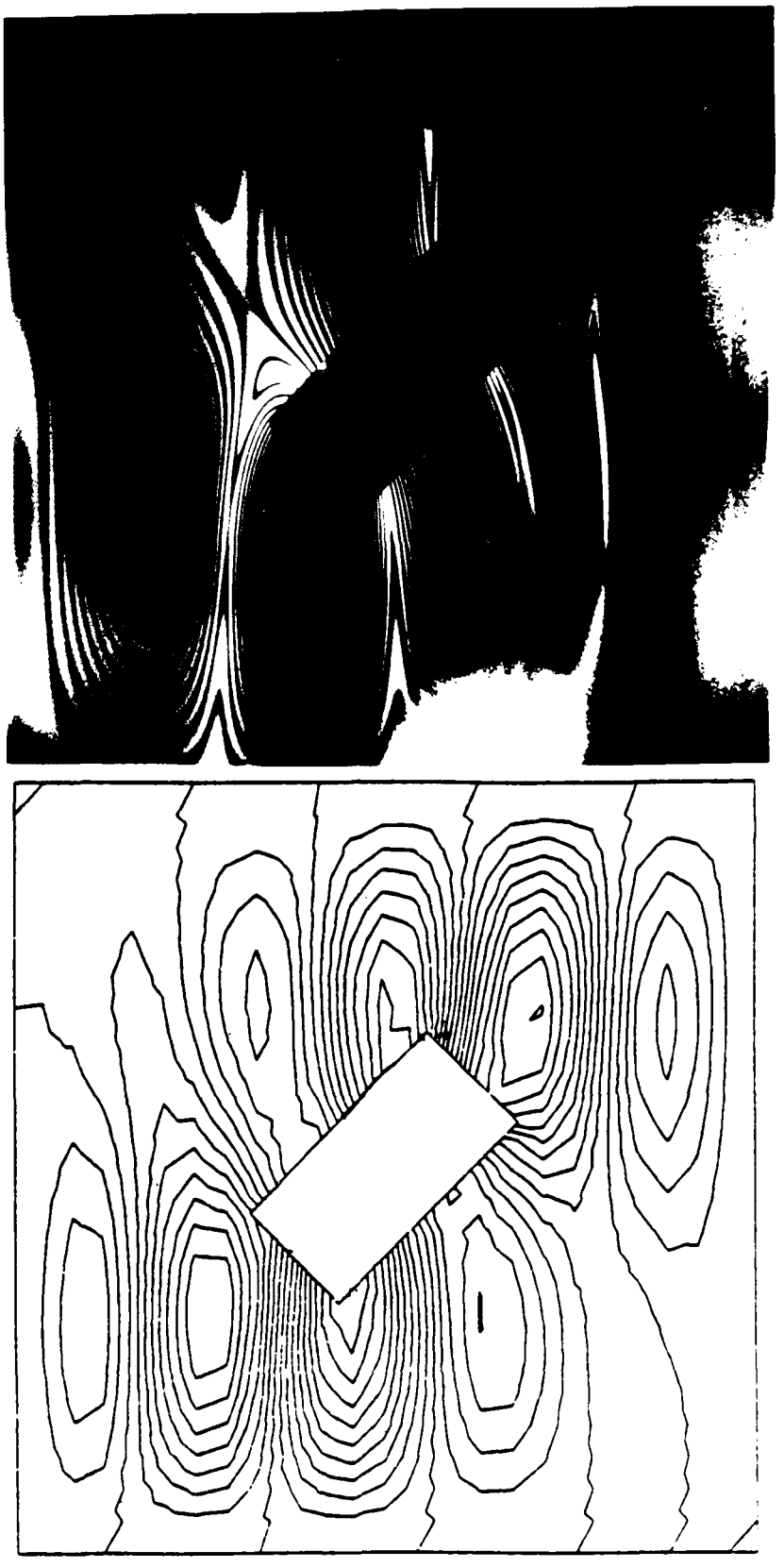

Figure 64 -45° Panel Mode 5

Cutout Effects

The effects of the cutout orientation can be best shown graphically in Figure 65. It is interesting to note that for the fundamental frequency there appears to be a significant decrease in the natural frequency for the 0° cutout. In order to determine if the dip in the fundamental frequency for the 0° cutout was a minimum, other STAGSC-1 runs were conducted at 27° and 14°. (The mesh used for these cutouts was similar to the mesh used in Figures 53 & 59). The 27° cutout orientation was selected because the diagonal of the 2x4 rectangle was oriented in the vertical direction (along the 0° fiber) and cut through the greatest number of 90° fibers. The hypothesis for doing this was that the 90° fiber provides the most stiffening properties to the panel (there is a 45° component present also from the ±45° fibers) since it is a circumferential fiber and if the circumferential fibers are cut, there is a larger corresponding reduction in the panel stiffness. There is approximately 5% more net circumferential fiber removed in the 0° cutout than the 45° cutout. As hypothesized, the 27° and 14° cutout orientations had natural frequencies that followed the curves in Figure 65, thereby supporting the validity that the 0° cutout orientation has the lowest fundamental natural frequency.

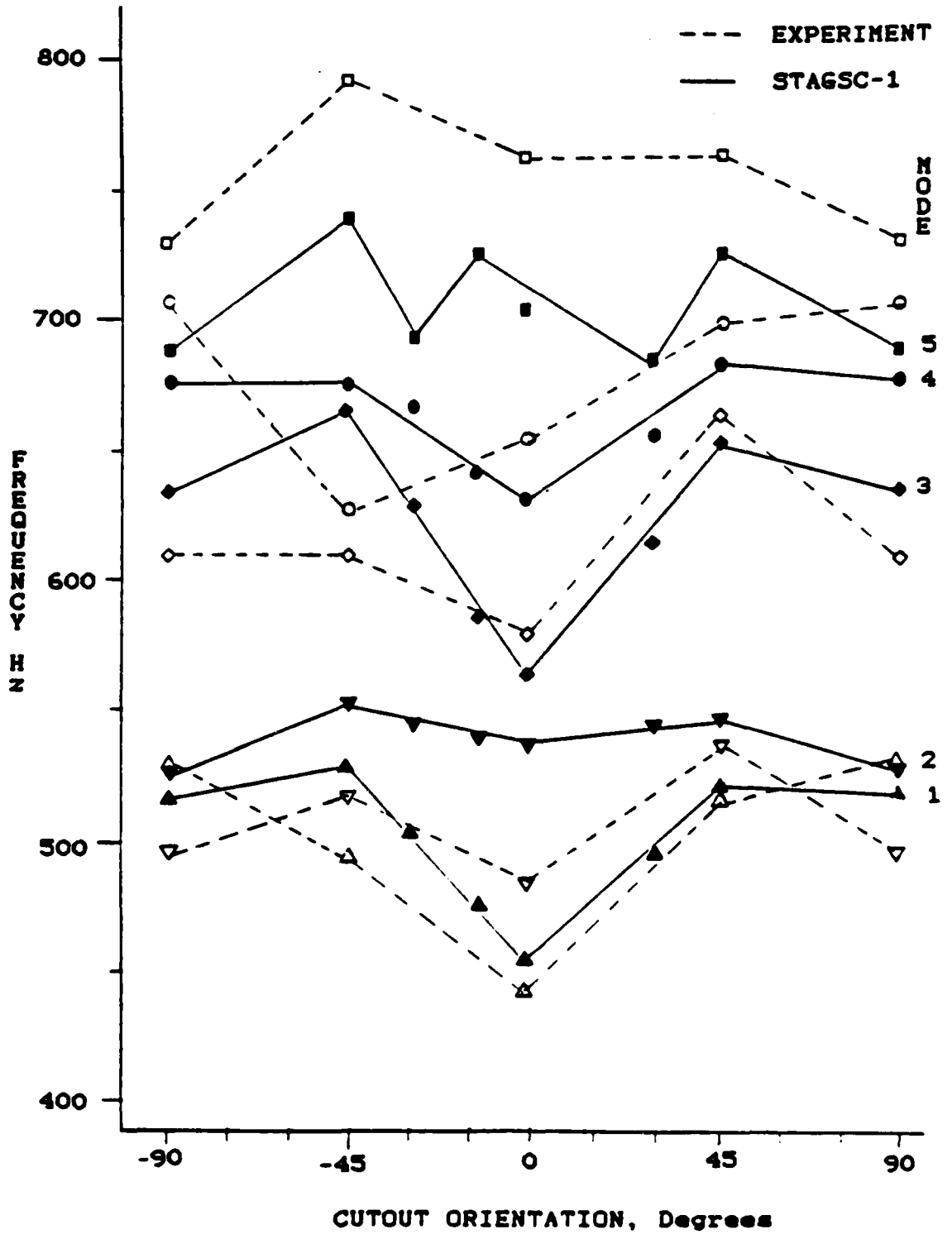


Figure 65 Cutout Orientation vs Frequency

As shown in Figure 65, the STAGSC-1 prediction was consistently higher than the experimental results for the fundamental frequency and the second natural frequency, as expected. The third natural frequency shows the experimental results to be lower than the analytical results for the -45° and 90° cutouts. The other cutout orientations are the opposite of this for the third mode. For the fourth and fifth natural frequencies the experimental results were consistently higher than what STAGSC-1 predicted. This suggests that STAGSC-1 is beginning to lose some accuracy at the higher natural frequencies. This was probably due to a combination of facts, the panel was modelled using flat elements, the shape functions were not of high enough order, and the mesh size was not fine enough.

It is interesting to note that the experimental results for the +45° cutout imply that for the first two natural frequencies, the +45° panel was stiffer than the -45° panel. This is exactly the opposite of what STAGSC-1 predicted. This is probably due to the fact that the test fixture did not provide perfect clamped-clamped boundary conditions as would STAGSC-1. Additionally, slight variations in the panel thickness (Figures 11-15) could cause the experimental results to vary from the numerical results. Also, the numerical results for the -45° cutout were probably influenced by the mesh design for that cutout.

Although the mesh for the -45° cutout is the mirror image of the mesh for the +45° cutout, the results are not symmetric as shown in Figure 65. This is due to the fact that the +45° cutout cuts through a larger number of -45° fibers than +45° fibers. (The -45° cutout cuts through a larger number of +45° fibers). The -45° fibers are the outer-most 45° fibers, thereby having a larger influence on the panel stiffness because of there distance from the midsurface. If this is a true statement, then if the ply layup is changed so that the +45° fiber is the outer most fiber, then the results would be as if the cutout orientation has changed to the mirror position (+45° to -45°). To support this hypothesis, the ply layup was changed for the -27° cutout. The STAGSC-1 results gave the same natural frequencies as the +27° cutout.

The results shown in Figure 65 would be quite valuable for a designer. If the designer was designing a shell with a cutout and the shell was operating near 450 Hz, the designer would not want to orient the cutout at 0° since that is very close to the fundamental frequency for that orientation.

In general, for the 2x4 cutout at any orientation there is no mode switching. Although for the 90° cutout a mode switch was observed experimentally for the fundamental and second natural frequency, this was probably an isolated case and only a property of that particular panel. Walley

[3] did observe this phenomena for the large cutout. As a result of his observations and the experimental results here, an analytical study using STAGSC-1 was conducted to determine what critical dimension would cause the modes to switch from antisymmetric to symmetric and vice versa. The results are summarized in Figures 66-69. The cutout orientations were not varied. The cutout sizes ranged from 1x1 to 1x5, 2x2 to 2x5, 3x3 to 3x5, 4x4 to 5x5 inch. As shown in Figure 66, the one inch high rectangles have very little effect on the first two modes. The higher modes show a sharp drop in frequency once the cutout is larger than 1x3 inch. In Figure 67, the same comments hold once the cutout is larger than 2x3 inch. For Figures 66 and 67 no mode switching occured between the first two natural frequencies. The first cutout to exhibit a mode switch was the 3x4 inch cutout. Every cutout larger than this exhibited mode switching. The critical dimension appears to be the circumferential dimension. In Figure 68, the equivalent stiffness for the panel was determined by assuming the panel was a one DOF spring-mass system. The mass of the cutout was determined and subtracted from the total mass of the panel. In Figure 68, the 3x5 inch cutout represents a local maximum in the equivalent stiffness and also when the first mode switch would occur for this particular set of data. As the cutout size increases, the equivalent stiffness decreases.

In order to define as close as possible when the mode switch will occur for a given dimension, STAGSC-1 output was generated for cutouts in dimensional increments of 0.33 inch near the region of the mode switch. In Figure 69, the region where the mode switch is occuring is evident and shows its dependence on the cutout width and height. It is interesting to note that the 2x4 cutout is bordering the mode switch region. This fact, coupled with the slight thickness variations present in the panel, could explain why a mode switch occurred in the 90° panel.

In summary, the cutout orientation does affect the natural frequency of the panel and mode switching appears to be a function of the cutout dimensions and not the orientations. Based on these observations, conclusions are presented in the following section.

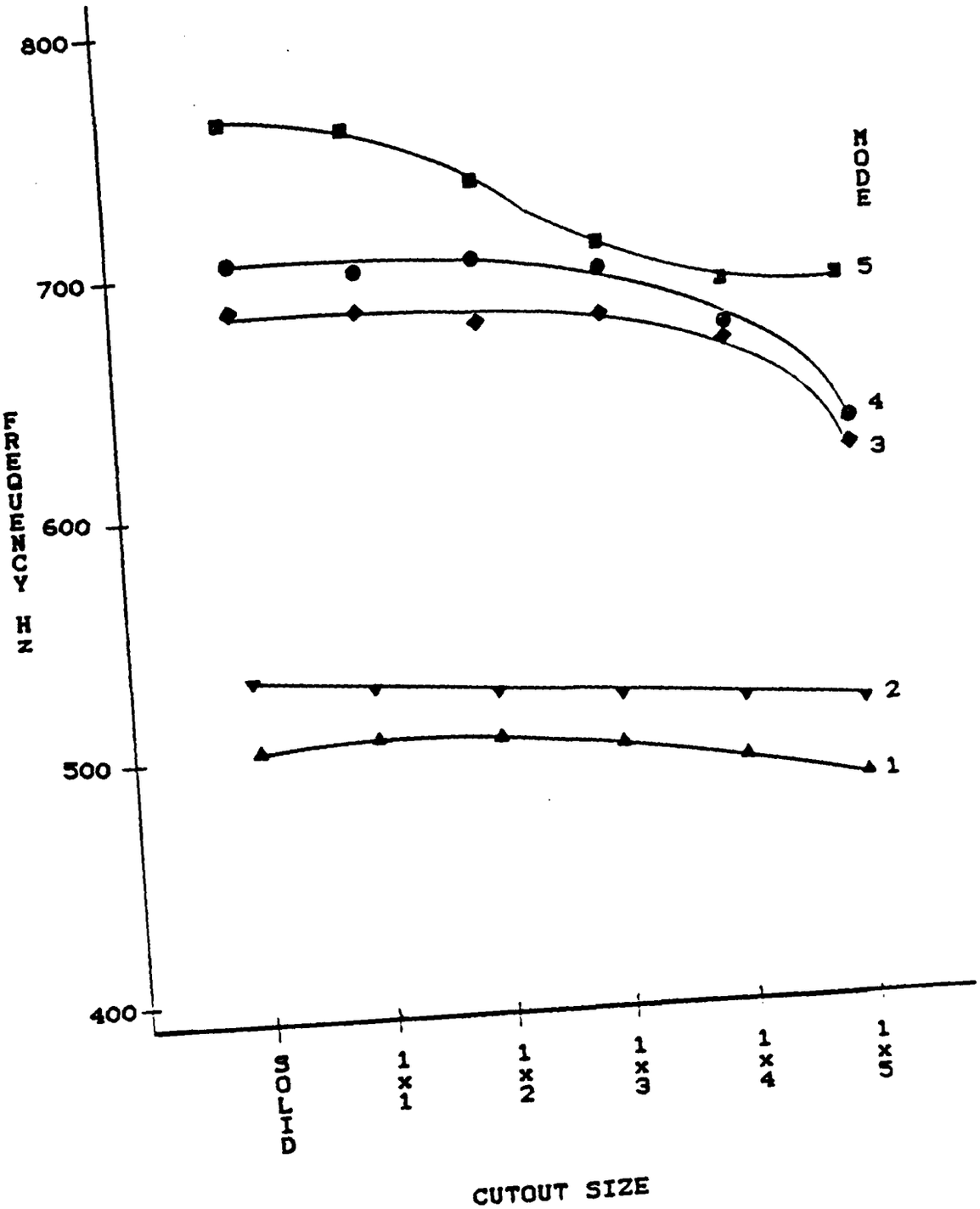


Figure 66 Cutout Size vs Frequency

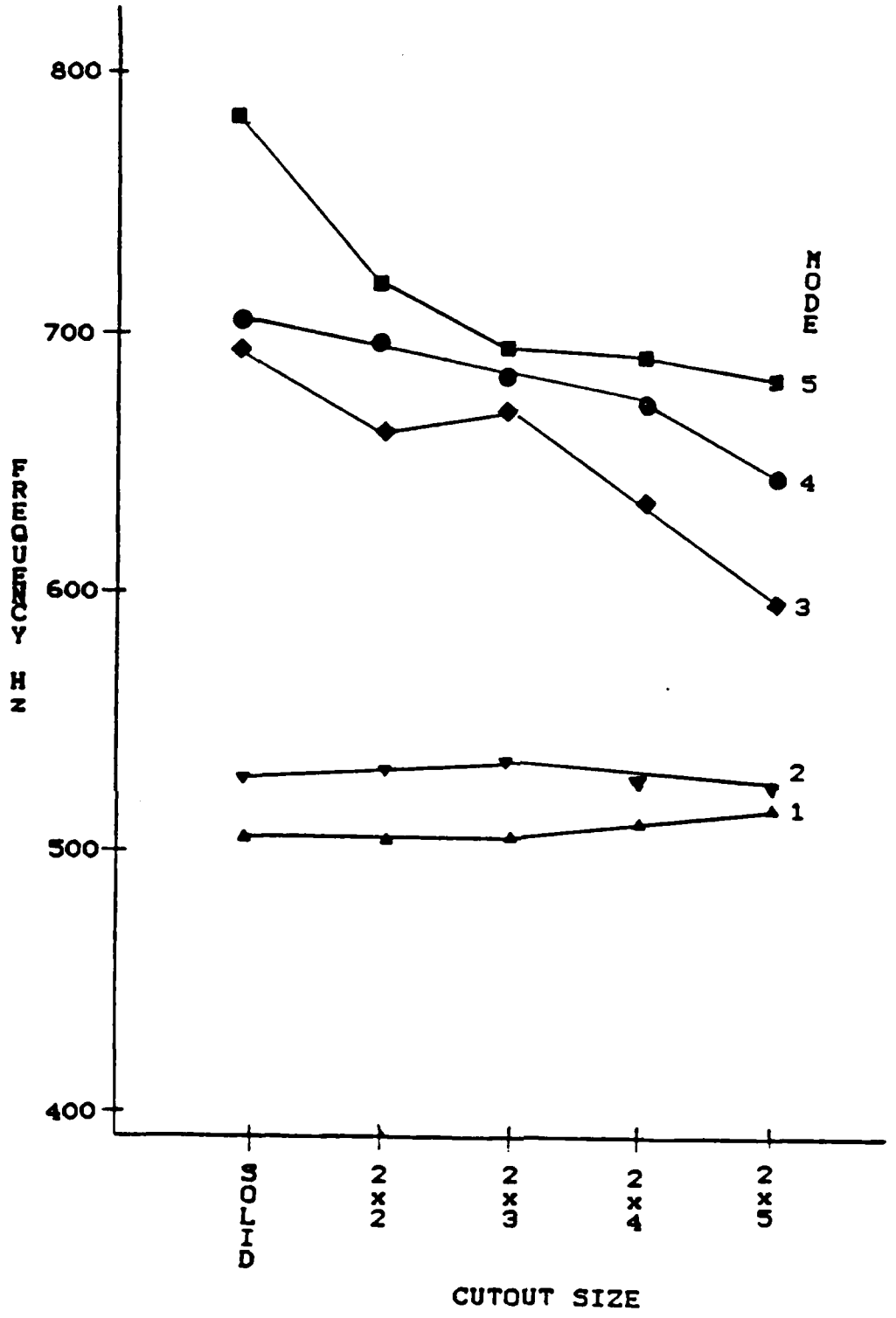


Figure 67 Cutout Size vs Frequency

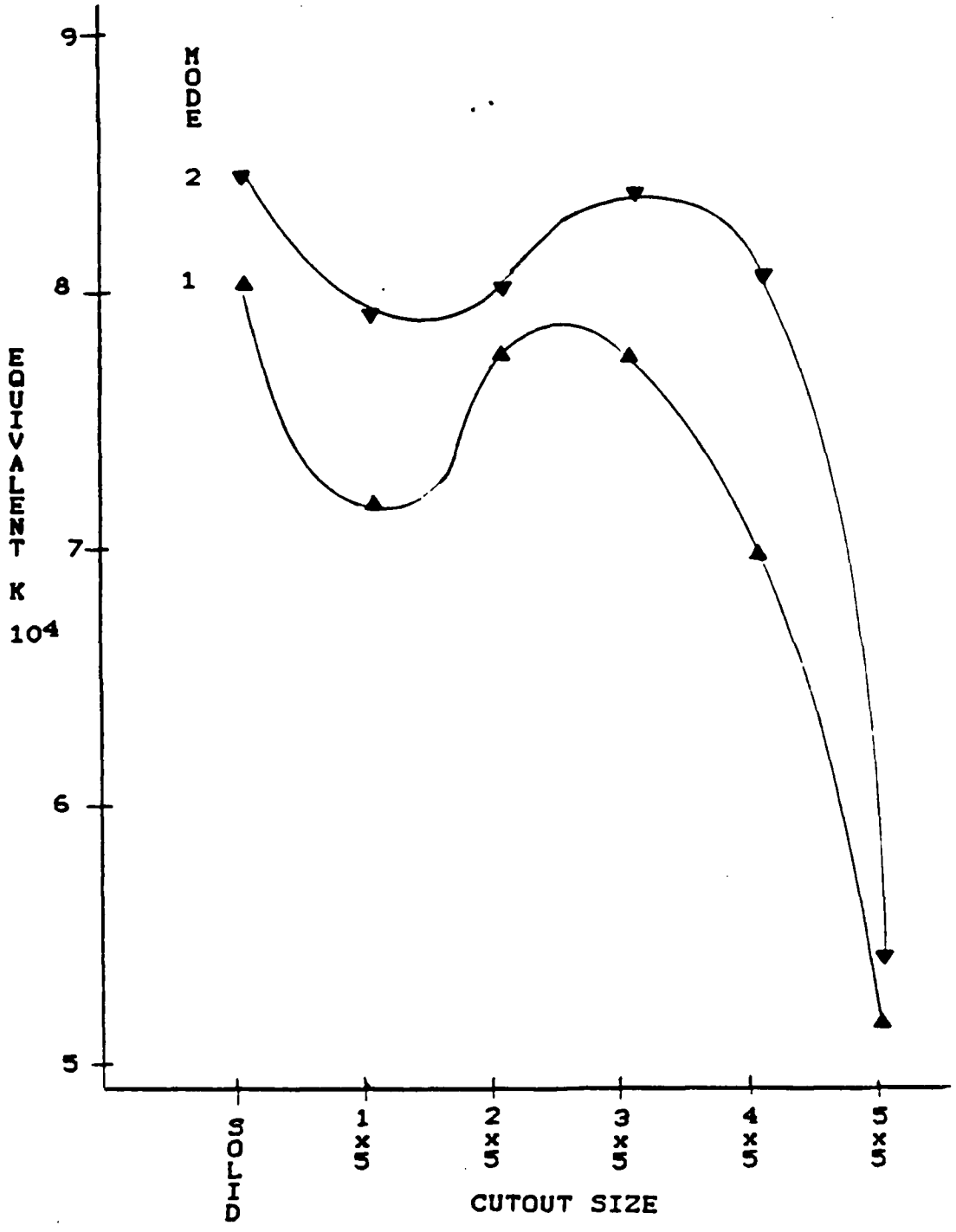


Figure 68 Equivalent Stiffness vs Cutout Size

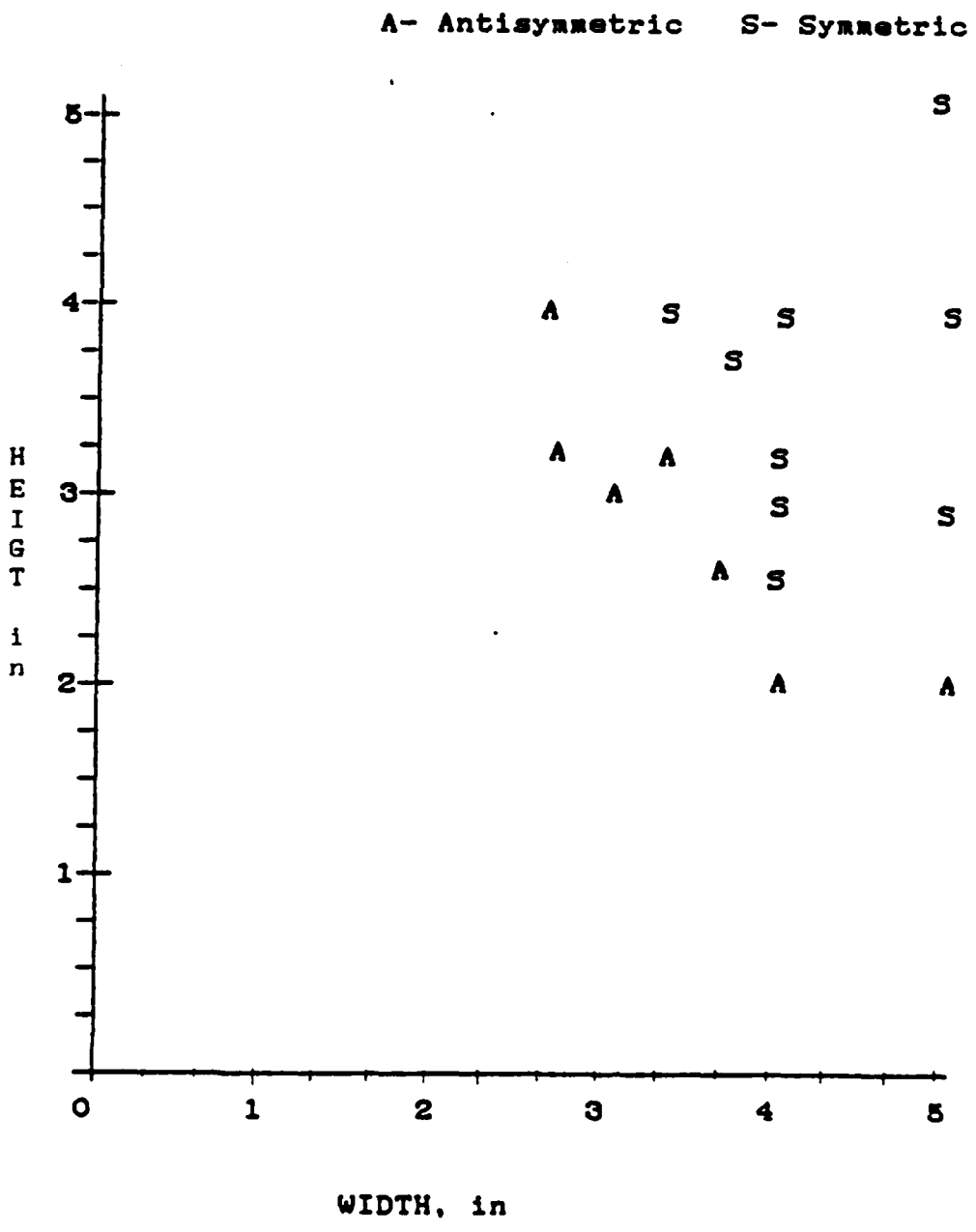


Figure 69 Mode Switch Region for Mode 1

# VII. CONCLUSIONS

In summary, this study investigated the effects of cutout orientations on the natural frequencies and mode shapes of curved Gr-Ep composite panels. Improved techniques for cutting the interior geometries of curved composite panels were employed in this study. During the course of the investigation, potential problem areas with the mesh design on curved shells were discussed.

Several conclusions can be drawn from the data that has been presented and are included here:

1. As a design tool, STAGSC-1 provides a good prediction for the natural frequencies and mode shapes for a curved composite panel. Care must be exercised in the mesh design when the cutout is at an orientation other than 0° and 90°.

2. For the out-of-plane displacement problem, elements without an out-of-plane rotation as a DOF give less accurate results.

3. STAGSC-1 artificially stiffens the model when a significant number of the element orientations are at angles other than 0° and 90°.

4. Cutout orientation does have an effect on panel stiffness and should be a design consideration for certain orientations. The $0^{o}$ cutout orientation had the largest effect on the fundamental frequency for the cutout sizes investigated here.

5. Mode switching is a function of the cutout height and width and is not a function of cutout orientation for the 2x4 cutout.

6. Ply layup will induce biasing for certain mode shapes of the solid panel. Any 2x4 inch cutout seems to reduce this dependence.

# VIII. RECOMMENDATIONS

1. A thorough investigation should be conducted into the effects of element orientation on the model stiffness in STAGSC-1.

2. Extend this study to determine the effects of randomly sized cutouts at different orientations. This would then lead into a study on the effects of damaged composites that have been repaired.

3. Different ply layups (to include both symmetric and non-symmetric layups) and different boundary conditions would help to build a higher confidence in the code.

4. The flat rod inserts, located in the vertical portion of the clamping fixture, should be machined to the proper radius to provide better clamped boundary conditions for the panel. The current configuration flattens the radius of curvature of the panel slightly (<0.01 inch) at the clamped surface.

## BIBLIOGRAPHY


1. Almroth, B. O., Brogan, F. A., and Stanley, G. M., Structural Analysis of General Shells Volume II. User Instructions for STAGSC-1., MSC-D673837. Applied Mechanics Laboratory, Lockheed Palo Alto Research Laboratory, January 1981.

2. Almroth, B. O., Brogan, F. A., and Stanley, G. M., STAGS Theory Manual, Cosmic Program No. HQN-10960 Applied Mechanics Laboratory, Lockheed Palo Alto Research Laboratory, April 1980.

3. Walley, R. A. Natural Frequencies and Mode Shapes of Curved Rectangular Composite Panels with Interior Cutouts. Masters Thesis GAE/AA/85D-16 School of Engineering, Air Force Institute of Technology (AU), Wright Patterson AFB, Oh. December 1985.

4. Jones, R. M. Mechanics of Composite Materials Washington D.C., Scripta Book Company, 1975.

5. Smith, H. M., Principles of Holography, New York, Wiley-Interscience, 1969.

6. Koch, W. E., Lasers and Holography: An Introduction to Coherent Optics, Dover Publication, New York, 1981.

7. Erf, R. K., Holographic Nondestructive Testing, New York, Academic Press, Inc, 1974.

8. Issue A/125A. Instruction Manual, Model 125A Helium-Neon Gas Laser, Spectra-Physics, Inc., Mountain View, California, 1969.

9. Rajamani, A. and Prabhakaran, R., Dynamic Response of Composite Plates with Cut-Outs, Part II Clamped-Clamped Plates, Journal of Sound and Vibration, Volume 54-4, pages 565-576, 1977.

10. Jenaise, Thomas C. A Parametric Study of Surface Imperfections and Small Cutouts in a Composite Panel. Master's Thesis, GAE/AA/82D-15. School of Engineering, Air Force Institute of Technology (AU), Wright-Patterson AFB, Oh, December 1982.

11. Timoshenko, S., Young, D. H., and Weaver, W. Jr., Vibration Problems in Engineering, 4th Edition, New York: John Wiley & Sons, 1974.

12. Monahan, Jon. Natural Frequencies and Mode Shapes of Plates with Interior Cutouts. Master's Thesis, GAM/MC/71-1. Schoool of Engineering, Air Force Institute of Technology (AU), Wright-Patterson AFB, OH September 1970.

13. Cook, R. D., Concepts and Applications of Finite Element Analysis, 2nd Edition, New York:John Wiley & Sons, 1981.

14. Carticate of Analysis, Hercules Aerospace Company, Aerospace Products Group, Bacchus Works, Magna Utah, Purchase Order Number 19568, 30 November 1985.

15. Walley, R. A., personal interviews, Wright Patterson AFB, Ohio, 10 January 1986 to 15 October 1986.

16. Almroth, B. O. and Brogan, F. A., Numerical Procedures for Analysis of Structural Shells, Technical Report, AFWAL-TR-80-3129. Flight Dynamics Laboratory, Wright Patterson AFB, Ohio, 1981.

17. Tisler, T. A., Collapse Analysis of Cylindrical Composite Panels with Large Cutouts Under Axial Loads Master's Thesis, GAE/AA/86D-18. School of Engineering, Air Force Institute of Technology (AU), Wright Patterson AFB, Ohio, December 1986.

## Appendix A

The following is the curing cycle steps used in the manufacture of the Graphite-Epoxy Panels. This cycle was last revised on 11 December 1984 and is still currently in use at the Flight Dynamics Laboratory. Figure A-1 shows the curing cycle temperature vs curing time.

The steps in the curing cycle are:

1. Apply full vacuum to bag, 25 in Hg per minute and increase air pressure to 85 psi.

2. Heat air to 240 F in 30±5 minutes using 90 kW heaters.

3. Hold part at 240±5 F for 60 minutes under 85 psi and full vacuum.

4. Increase pressure to 100 psi and vent vacuum.

5. Heat air to 350 F in 30±5 minutes using the 90 kW heaters.

6. Hold part at 350±5 F and 100 psi for 120 minutes.

7. Apply full cooling water and cool part below 150 F in

## Appendix B

The following computer listings consist of the control decks for the CYBER and VAX 11-875 that will execute STAGSC-1, the control deck for the CYBER that will execute the STAGSC-1 plot routine, and an example of the STAGSC-1 generated grid and a user generated grid.

### CYBER Control Deck

```
/JOB
CYR,P2,CM300000.
USER,D820090,STAGUL5.
CHARGE,*.
RFL=300000.
SETTL(*).
ATTACH,STAGS1/UN=D820090.
ATTACH,STAGS2/UN=D820090.
GET,GRID14.
STAGS1,GRID14.
RETURN,STAGS1.
RFL=300000.
STAGS2.
SWRITE,TAPE21,@CYR14PLOTT21@.
SWRITE,TAPE22,@CYR14PLOTT22@.
REWIND,OUTPUT.
COPY,OUTPUT,JUNK.
ROUTE,JUNK,DC=PR,UN=AF,UJN=CYR.
/EOR
END OF FILE
```

VAX 11-875 Control Deck

```
!
!       STAGS.COM     (Execute STAGS1 and STAGS2)
!
        assign isotrop.inp for005
        assign isotrop.OUT for006
!
        run stags$dir:stags1.exe
        run stags$dir:stags2.exe
!
!       End STAGS.COM
!
```

Cyber Control Deck for STAGSC-1 Plot

```
/JOB
CYR,P1.
/USER
CHARGE,*.
SETTL(*).
GET,STAPRUN,STAPLIB/UN=D820090.
ATTACH,CCLIB38/UN=LIBRARY.
LIBRARY,STAPLIB,CCLIB38.
GET,CYRPLOT/UN=D820090.
SREAD,TAPE21,$CYR14PLOTT21$.
SREAD,TAPE22,$CYR14PLOTT22$.
RFL,153000.
REDUCE,-.
STAPRUN,CYRPLOT.
REWIND,TAPE47.
ROUTE,TAPE47,DC=PU,UN=AF,UJN=CYR.
EXIT.
REWIND,TAPE47.
ROUTE,TAPE47,DC=PU,UN=AF,UJN=CYR.
/EOR
END OF FILE
```

## STAGSC-1 Generated Grid Input Deck

```
CASE --2X4 CUTOUT at 90 Degrees
2,1,1,0,0,0,0,0,0                                                    *B1
1,0,0                                                                *B2
1,0,1,0                                                              *B3
1                                                                    *C1
1,0,7000,1                                                           *D2
5,0,0,0                                                              *D3
25,25                                                                *F1
1,0                                                                  *I1
18.84E06,.021813,.9099E06,.055,.0216216,1.468E06,15.2                *I2
1,1,8                                                                *K1
1,.005,0.,0                                                          *K2
1,.005,45.0,0                                                        *K2
1,.005,-45.0,0                                                       *K2
1,.005,90.,0                                                         *K2
1,.005,90.0                                                          *K2
1,.005,-45.0,0                                                       *K2
1,.005,45.0,0                                                        *K2
1,.005,0.0,0                                                         *K2
5,0                                                                  *M1
0.0,12.0,-28.648,28.648,12.0                                         *M2A
1,0                                                                  *M5
410,0,0,1,0,0,0                                                      *N1
11,15,9,17                                                           *N8
2,2,2,2                                                              *P1
0                                                                    *Q1
1                                                                    *R1
```

## User Generated Grid Input Deck

```
CASE---SQUARE GRID WITH TRIS -30 CUTOUT
2,1,1,0,0,0,0,0,0                                                    *B1
0,1,0                                                                *B2
1,0,1,0                                                              *B3
1                                                                    *C1
1,0,7000,1                                                           *D2
5,0,0,0                                                              *D3
645,0,0,40,528,0,0                                                   *H1
1,0                                                                  *I1
18.84E06,.021813,.9099E06,.055,.0216216,1.468E06,15.2                *I2
1,1,8                                                                *K1
1,0.005,0.0,0                                                        *K2
1,0.005,-45.0,0                                                      *K2
1,0.005,45.0,0                                                       *K2
1,0.005,90.0,0                                                       *K2
1,0.005,90.0,0                                                       *K2
1,0.005,45.0,0                                                       *K2
1,0.005,-45.0,0                                                      *K2
1,0.005,0.0,0                                                        *K2
1,0,0,0,12.0000,-5.7531,10.5310,000,000,0                            *S1
2,0,0,0,12.0000,-5.3094,10.7615,000,000,0                            *S1
3,0,0,0,12.0000,-4.8566,10.9733,000,000,0                            *S1
                  *
                  *
      Do this for 645 nodal coordinates.
                  *
                  *
187,188,626,320,1,-90.0,0,1,0                                        *T3
188,189,626,320,1,-90.0,0,1,0                                        *T3
627,626,189,320,1,30.0,0,1,0                                         *T3
                  *
                  *
      Do this for 40 triangular elements.
                  *
                  *
1,2,27,26,410,1,-90.0,0,1,0,0                                        *T4
2,3,28,27,410,1,-90.0,0,1,0,0                                        *T4
3,4,29,28,410,1,-90.0,0,1,0,0                                        *T4
                  *
                  *
      Do this for 528 quadrilateral elements.
                  *
                  *
0,0,0                                                                *U1
1                                                                    *V1
```

## Appendix C

Holographic techniques vary slightly with the setup in use. These instructions will provide a step by step procedure for taking a hologram for this particular configuration. Hopefully, pitfalls can be avoided with these instructions. Prior to beginning, mount the panel in the mounting fixture and tighten all allen screws to 3 foot-pounds and bolt the mount to the table as indicated in Figure 28.

1. CAUTION: Do not use the laser until you have had a laser eye exam and have been checked out on its basic operations.

2. Clean all mirrors and lenses to ensure they are free of dust and dirt. Optical quality mirrors and lenses need to be treated with extreme care while cleaning and should not be rubbed with a lense tissue. Acetone or similiar cleaning fluid should be dripped lightly onto the mirror and brushed gently with lense tissue to absorb the fluid and dust.

3. Turn on Spectra-Physics 261 RF/DC Exciter. The laser requires 15-30 minutes for warmup. DO NOT adjust the controls during this time period, this will prevent any unnecessary misalignment of the laser.

4. Turn on NRC 800 Universal Shutter System.

5. Set NRC 800 to manual and trigger. This will keep the electric shutter in the open position for the following alignments.

6. Place the Spectra-Physics 401C Power Meter Sensor in the beam path. Set the sensitivity scale to 100 mW. The indicated power level should be 50+ mW. If the power level is lower than 50 mW, cleaning and/or alignment of the laser is necessary. See operations manual for the laser and have a qualified technician assist during the first alignment/cleaning session.

7. Remove the 401C from the beam path.

8. With the proper power level, the light intensity will be determined for the object and the reference beams, such that the reference beam has twice the intensity of the object beam. With a high quality, high resolution light meter, measure the reflectivity of panel surface and note

the number. (The panel should be fully illuminated, if not adjust diffuser). With the object beam fully blocked, position the light meter at the position of the photographic plate holder and measure the light level. The light level at the plate holder should be roughly twice the light level at the panel. If not, adjust the beam intensity level by rotating the beam splitter lense. Repeat measurements. Once the 2:1 ratio is obtained, note the degree number on the beam splitter.(Use a convienent reference point on the beam splitter mount to obtain number.) This setting will be used for the holograms.

9. The exposure time must be determined for the holographic plates. The exposure time is a direct function of the reflectivity of the panel, therefore the exposure time can change from panel to panel. Obtain and clean the exposure plate. The exposure plate is mounted on the panel side of the plate mounting fixture. Set the NRC 800 to auto and select a shutter time such as 120 ms. Turn lights off. Remove an unexposed photgraphic plate from the film box and mount to the backside of the plate holder with the chemical side of the film facing the panel. (The chemical side can be determined by moistening the finger slightly and gently touching a corner of one side of the plate. The chemical will feel sticky to the touch.) Trigger the shutter. Remove the film plate and mount in a portable metal holder.

Follow steps 10-14. Remove the exposure plate and set aside. Observe hologram and note the exposure numbers present on the hologram they will range from 5% to 100%. These numbers represent the amount of light transmitted through the plate. Select a number such as 40% if there is not good contrast then adjust the exposure time on the shutter and repeat these steps as necessary until the proper exposure time is obtained.

10. Develop in the developer for five minutes. This time can vary slightly with the age of the developing solution.

11. Insert into rapid fixer for two minutes. Light may be turned on after 1 1/2 minutes.

12. Rinse and allow to dry slightly (about 3 minutes).

13. While the plate is drying, set the shutter to manual and trigger. Rotate the beam splitter until the beam is blocked and most of it follows the reference beam path. Mount the black observation board over the panel fixture.

14. Mount the dried plate in the film holder and turn off the light. Observe hologram. If the hologram appears distorted remove plate and remount it, chances are the plate was inserted backwards or upside down.

15. Take a still of the panel. The still is necessary and will be used to find the natural frequencies of the panel by allowing you to visually observe the mode shapes. Once steps 10-14 are completed, remove the black observation board and set the beam splitter back to the original angle noted earlier. Observe the hologram. There should be fringe lines present in the hologram. The fewer and broader the fringe lines the better since a large number of fringe lines will be lost when the panel is excited. Turn on the signal generator at a low amplitude and turn on the horn amplifier an frequency counter. Adjust the frequency slowly while observing the hologram. As the natural frequency of the panel is reached the mode shapes will suddenly appear. Note the frequency and continue scanning until all natural frequencies desired are reached.

16. Holograms are taken repeating the basic procedures in step 9 and following the developing steps 10-14. Repeat as necessary.

17. Note: the still will probably only give good fringe lines for about 45 minutes because of changes in the room environmental conditions.

Appendix D

HERCULES

Hercules Aerospace Company
Aerospace Products Group
Bacchus Works
Magna, Utah 84044-0098
(801) 250-5911

CERTIFICATE OF ANALYSIS

30 November 1985

tomer: Beta Industries

chase Orc : No: 19568

erial: Graphite Fiber/Epoxy Material, AS4/3501-6, 12" Prepreg Tape

cificatic : BIW-1002, Rev. NC with Hercules Comments.

ntity: 501.00 lbs.

No: 3777-2
Manufactured: 12 November 1985

ol No: See Section V

in Lot Nc 422
Manufactured by Hercules Inc.

er Lot Nc 700-4A
Manufactured by Hercules Inc.

| Fiber P | operties | Spec Req | Lot Average |
|---|---|---|---|
| FLA Ten | le Str., ksi** | 325 minimum | 539 |
| FLA Ten | le Mod., msi** | 30 - 35 | 33 |
| Density | gm/cc | 1.80 nominal | 1.79 |

** Data normalized to 100% Fiber Volume.

| Prepreg | Physical Properties | Spec Req | Average/Individual |
|---|---|---|---|
| Spool N | | | |
| Flow, @ | 50°F, 90 psi, % | 16 - 30 | 16/16,16,16 |
| Volatil | s, @325°F, % | 1.0 maximum | 0.8/0.9,0.8,0.8 |

| Laminat | Mechanical Properties | Spec Req (min.avg) | Panel No. Spool 1 | Average/Individual |
|---|---|---|---|---|
| 0° Ten | le Str., RT, ksi | 190 | 38709 | 317/316,307,328 |
| 0° Ten | le Mod., RT, msi | 18.5 | 38709 | 21.2/21.6,20.3,21.7 |
| Short B | am Shear, RT, ksi | 12.5 | 38708 | 18.2/17.2,18.3,19.0 |

HERCULES

TIFICATE OF ANALYSIS
No: 3777-2
2

## Panel Physical Properties

| | Spec Req | Average/Individual |
|---|---|---|
| Spool No./Panel No. | | 1/38708 |
| Density, gm/cc | Report | 1.59/1.58,1.61,1.59 |
| Void Content, % | 2.0 maximum | 1.1/1.7,0.5,1.2 |
| Fiber Volume, % | 59 - 65 | 65/64,65,65 |
| Ply Thickness, inches | 0.0048-0.0056 | 0.0050 |
| | | |
| Spool No./Panel No. | | 1/38709 |
| Density, gm/cc | Report | 1.59/1.59,1.59,1.58 |
| Void Content, % | 2.0 maximum | 1.6/1.5,1.6,1.6 |
| Fiber Volume, % | 59 - 65 | 65/65,65,64 |
| Ply Thickness, inches | 0.0048-0.0056 | 0.0049 |

## Individual Spool Physical Properties

| | Resin Content,% | Fiber Areal Wt.,gm/m$^2$ |
|---|---|---|
| Spec Req (avg) | 32 - 38 | 138 - 150 |
| Spool No. | Average/Individual | Average/Individual |
| 2 | 35/35,35,35 | 148/147,151,145 |
| 3 | 36/35,38,34 | 146/149,141,147 |
| 4 | 36/37,35,36 | 146/145,148,146 |
| 6 | 36/34,37,37 | 147/150,146,145 |
| 7 | 34/32,35,36 | 146/150,143,144 |
| 8 | 35/34,35,36 | 146/149,148,142 |
| 9 | 35/33,36,36 | 147/150,146,144 |
| 10 | 36/34,36,38 | 148/150,148,146 |
| 11 | 35/34,35,35 | 147/148,147,145 |
| 12 | 34/32,35,35 | 147/151,146,145 |
| 13 | 36/34,36,37 | 148/150,147,146 |

C. J. Lovett

J. A. Rasmussen, Plant 3
QUALITY CONTROL

ed
4, Rev. C
q

## Appendix E

The following is a list of the equipment used to conduct the experimentation.

| | |
|---|---|
| Frequency Generator | HP Model 3310B |
| Frequency Counter | HP Model 5316A |
| Audio Amplifier | Bogen Model HTA125 |
| Light Displacement Meter | Mechanical Technology KD320 |
| Oscilliscope | Tektronix 7603 |
| HeNe Laser 50mW | Spectra Physics Model 125 |
| Horns | Atlas Sound 60 Watt |
| Assorted Optical Mirrors | |
| Kodak Holographic Plates | |

# VITA

Garry J. Cyr was born on 18 September 1955 in Great Lakes, Illinois. He graduated from Duncan U. Fletcher High School in 1973. He enlisted in the U.S. Air Force in 1974 where he worked as an Air Traffic Controller. In 1978, he was accepted into the Airman's Education and Commissioning Program and attended The Ohio State University in Columbus, Ohio where he graduated in 1981 with a Bachelor of Science in Mechanical Engineering. He was commissioned a Second Lieutenant through OTS and was assigned as a project engineer for the Air Force Armament Laboratory, Eglin AFB, Florida. Projects included the Advanced Aircraft Gun Design program and the Telescoped Ammunition Interior Ballistics Code. He was assigned as the Squadron Section Commander for the Armament Laboratory. He entered the School of Engineering, Air Force Institute of Technology in June 1985. He recieved his Master's Degree in Aeronautical Engineering with specialties in structural analysis and structural materials.

SECURITY CLASSIFICATION OF THIS PAGE

AD-A178 616

## REPORT DOCUMENTATION PAGE

| | |
|---|---|
| 1a. REPORT SECURITY CLASSIFICATION: UNCLASSIFIED | 1b. RESTRICTIVE MARKINGS |
| 2a. SECURITY CLASSIFICATION AUTHORITY | 3. DISTRIBUTION/AVAILABILITY OF REPORT: Approved for Public release; distribution unlimited. |
| 2b. DECLASSIFICATION/DOWNGRADING SCHEDULE | |
| 4. PERFORMING ORGANIZATION REPORT NUMBER(S): AFIT/GAE/AA/86D-3 | 5. MONITORING ORGANIZATION REPORT NUMBER(S) |
| 6a. NAME OF PERFORMING ORGANIZATION: SCHOOL OF ENGINEERING; 6b. OFFICE SYMBOL (If applicable): AFIT/EN | 7a. NAME OF MONITORING ORGANIZATION |
| 6c. ADDRESS (City, State and ZIP Code): Air Force Institute of Technology, Wright-Patterson AFB, Ohio 45433 | 7b. ADDRESS (City, State and ZIP Code) |
| 8a. NAME OF FUNDING/SPONSORING ORGANIZATION; 8b. OFFICE SYMBOL (If applicable) | 9. PROCUREMENT INSTRUMENT IDENTIFICATION NUMBER |
| 8c. ADDRESS (City, State and ZIP Code) | 10. SOURCE OF FUNDING NOS: PROGRAM ELEMENT NO; PROJECT NO; TASK NO; WORK UNIT NO |
| 11. TITLE (Include Security Classification): See Box 19 | |
| 12. PERSONAL AUTHOR(S): Garry J. Cyr, M.S., Capt., USAF | |
| 13a. TYPE OF REPORT: MS Thesis; 13b. TIME COVERED: FROM _____ TO _____; 14. DATE OF REPORT (Yr., Mo., Day): 1986 December; 15. PAGE COUNT: 141 | |
| 16. SUPPLEMENTARY NOTATION | |

| 17. COSATI CODES | | |
|---|---|---|
| FIELD | GROUP | SUB GR |
| 11 | 04 | |
| 20 | 11 | |

18. SUBJECT TERMS (Continue on reverse if necessary and identify by block number): Composites, Vibrations, Holography, ~~STAOSC-1~~ Finite Elements, Natural Frequencies, Mode Shapes

19. ABSTRACT (Continue on reverse if necessary and identify by block number)

11) Title: EFFECTS OF CUTOUT ORIENTATIONS ON NATURAL FREQUENCIES AND MODE SHAPES OF CURVED RECTANGULAR COMPOSITE PANELS

Thesis Advisor: Dr Ronald L. Hinrichsen

Approved for public release: IAW AFR 190-1.
LYNN E. WOLAVER 13 Mar 87
Dean for Research and Professional Development
Air Force Institute of Technology (AU)
Wright-Patterson AFB OH 45433

| 20. DISTRIBUTION/AVAILABILITY OF ABSTRACT | 21. ABSTRACT SECURITY CLASSIFICATION | |
|---|---|---|
| UNCLASSIFIED/UNLIMITED X SAME AS RPT ☐ DTIC USERS ☐ | UNCLASSIFIED | |
| 22a. NAME OF RESPONSIBLE INDIVIDUAL: Dr. Ronald L. Hinrichsen | 22b. TELEPHONE NUMBER (Include Area Code): (513)-255-3069 | 22c. OFFICE SYMBOL: AFIT/EN |

DD FORM 1473, 83 APR — EDITION OF 1 JAN 73 IS OBSOLETE

UNCLASSIFIED
SECURITY CLASSIFICATION OF THIS PAGE

STAGSC-1, a finite element code, and holographic interferometry were used to analyze the effects of cutout orientation (0°, +45°, -45° and 90°) on the first five natural frequencies and mode shapes of a curved Gr-Ep panel. The clamped-clamped panels had a quasi-isotropic layup $[0, -45, 45, 90]_S^n$ and measured 12 inch high with a 12 inch chord.

When the finite element code was compared to the time averaged holograms, the two techniques showed close correlation of both the natural frequencies and mode shapes. It was found that the 0° cutout orientation had a significant effect on the panel stiffness while the other cutout orientations did not adversely effect the stiffness. It was also found that if a large number of elements in the finite element mesh are oriented at an angle other than 0° or 90°, then the STAGSC-1 model is artificially stiffened. The phenomenon of mode switching was investigated analytically and determined to be a function of the cutout dimensions.

END

4-87

DTIC